2011

Theory of spin-fluctuation induced superconductivity in iron-based superconductors

Junhua Zhang
Iowa State University

Theory of spin-fluctuation induced superconductivity in iron-based superconductors

by

Junhua Zhang

A dissertation submitted to the graduate faculty

in partial fulfillment of the requirements for the degree of

DOCTOR OF PHILOSOPHY

Major: Condensed Matter Physics

Program of Study Committee:

Jörg Schmalian, Major Professor

Paul Canfield

Adam Kaminski

Kirill Tuchin

Gordon Miller

Iowa State University

Ames, Iowa

2011

DEDICATION

I would like to dedicate this thesis to my mother Yuzhen and to my brother Junfeng without whose support I would not have been able to complete this work and to my late father Baokui for his love and encouragement. I would also like to thank my friends for their loving guidance and help during the writing of this work.

TABLE OF CONTENTS

LIST OF FIGURES

ABSTRACT

In this dissertation we focus on the investigation of the pairing mechanism in the recently discovered high-temperature superconductor, iron pnictides. Due to the proximity to magnetic instability of the system, we considered short-range spin fluctuations as the major mediating source to induce superconductivity. Our calculation supports the magnetic fluctuations as a strong candidate that drives Cooper-pair formation in this material. We find the corresponding order parameter to be of the so-called sś-wave type and show its evolution with temperature as well as the capability of supporting high transition temperature up to several tens of Kelvin. On the other hand, our itinerant model calculation shows pronounced spin correlation at the observed antiferromagnetic ordering wave vector, indicating the underlying electronic structure in favor of antiferromagnetic state. Therefore, the electronic degrees of freedom could participate both in the magnetic and in the superconducting properties. Our work shows that the interplay between magnetism and superconductivity plays an important role to the understanding of the rich physics in this material.

The magnetic-excitation spectrum carries important information on the nature of magnetism and the characteristics of superconductivity. We analyze the spin excitation spectrum in the normal and superconducting states of iron pnictides in the magnetic scenario. As a consequence of the sign-reversed gap structure obtained in the above, a spin resonance mode appears below the superconducting transition temperature. The calculated resonance energy, scaled with the gap magnitude and the magnetic correlation length, agrees well with the inelastic neutron scattering (INS) measurements. More interestingly, we find a common feature of those short-range spin fluctuations that are capable of inducing a fully gapped sś state is the momentum anisotropy with elongated span along the direction transverse to the antiferromagnetic momentum transfer. This calculated intrinsic anisotropy exists both in the normal and in the superconducting state, which naturally explains the elliptically shaped magnetic responses

observed in INS experiments. Our detailed calculation further shows that the magnetic resonance mode exhibits an upward dispersion-relation pattern but anisotropic along the transverse and longitudinal directions. We also perform a qualitative analysis on the relationship between the anisotropic momentum structure of the magnetic fluctuations and the stability of superconducting phase by intraorbital but interband pair scattering to show the consistency of the magnetic mechanism for superconductivity.

As discussed for cuprates, an important identification of the mediating boson is from the fermionic spectrum. We study the spectral function in the normal and superconducting state. Not only do we extract the gap magnitude on the electron- and hole-pockets to show the momentum structure of the gap, but also find a peak-dip-hump feature in the electron spectrum, which reflects the feedback from the spin excitations on fermions. This serves as an interpretation of the kink structure observed in ARPES measurements.

CHAPTER 1. INTRODUCTION

1.1 Superconductivity: 100 Years Old

2011 is special in physics as it marks the 100th anniversary of the discovery of superconductivity. In April 1911, Onnes's group first observed the sudden vanishing of the electrical resistance in mercury at a finite temperature 4.2 K [Onnes (1911)], which opens a whole new chapter in physics: superconductivity. As a great success in theoretical physics, Bardeen, Cooper, and Schrieffer (BCS) developed a microscopic theory that contains the key ingredients of superconductivity: there appears an effective attraction between the charged quasiparticles such that two fermionic quasiparticles form a composite boson–Cooper pair [Cooper (1956); Bardeen et al. (1957)]. In the early 60 years, superconductivity was mostly discovered in metals and alloys that could be described by BCS theory in its generalized version by Eliashberg (1960); Schrieffer et al. (1963). A variation of this situation began when superconductivity was found in heary fermion system $CeCu_2Si_2$ by Steglich et al. (1979) and in organic compounds $(TMTSF)_2PF_6$ by Jerome et al. (1980) [Jerome (1994)]. Later the discovery of high-temperature cuprate superconductors [Bednorz and Muller (1986)] elevated this research field to an unprecedented heyday. 15 years after the searching for exotic superconducting mechanism, MgB_2 updated the understanding of conventional superconductors with a surprisingly high transition temperature $T_c = 39$ K [Nagamatsu et al. (2001)]. The thrilling moments in superconductivity never disappears over the 100 years. The discovery of Fe-based superconductors by Hosoto's group kicked off a new surfing in this field in early February 2008 [Kamihara et al. (2008)].

The antisymmetric property when exchanging two identical fermions in Cooper pair requires the coupled symmetry characters in spin and spacial wave functions: If the two members in a Cooper pair form a spin singlet, the spacial parity should be even, e.g., s-wave or d-wave; On

the other hand, the spin triplet pairing matches odd parity, e.g., p-wave or f-wave. Bardeen et al. (1957) specifically discussed the phonon-mediated pairing interaction that is typically negative at the relevant energy-momentum transfer, called "attractive", which induces an s-wave state without sign change in superconducting order parameter although it can have varying magnitude. We refer the phonon-mediated superconductors as "conventional" and consider the mediating degree of freedom other than phonons to be "unconventional". Phonon-induced superconductors are not necessarily low-T_c materials, as strong electron-phonon coupling can push the transition temperature above 30 K well demonstrated by strong-coupling calculations for MgB_2 [Kortus et al. (2001); Choi et al. (2001, 2002)], which also shows multiple gaps with different magnitude but still obeys s-wave symmetry. Non-phonon mechansim might be able to support other symmetries like p-wave, d-wave, f-wave et al. For example, the spin-spin interaction [Berk and Schrieffer (1966)] can be positive at the relevant energy-momentum transfer, called "repulsive", which is therefore capable to flip the phase of the Cooper-pair wave function as will be shown later. Experimentally, phase-sensitive measurements on Sr_2RuO_4 appear to show a spin-triplet p-wave pairing in this multiband layered transition oxide [Nelson et al. (2004)]. Experiments on cuprates, Ce 115 series, and organics exhibit evidence for d-wave symmetry. A recent phase-sensitive measurement using Josephson tunnel junctions on heavy-fermion UPt_3 indicates a possible f-wave pairing state in one of its superconducting phases [Strand et al. (2010)]. In the above mentioned p-, d- and f-wave states, the superconducting order parameter experiences sign change on the Fermi surface, has nodal lines or points where its magnitude vanishes, and exhibits directional π-phase shift. However, there could be another exotic symmetry: there is no sign change of the order parameter on each connected Fermi surface sheet under rotational operation, that is, belonging to s-wave symmetry, but there is relative π-phase difference of the order parameter between disconnected Fermi surface sheets, that is, the nodal line locating between disconneted Fermi surface sheets. It is also possible that the nodal line crosses one set of Fermi surface sheet but leaves the other set intact. These are the so-called extended s-wave, or, s$\pm$-wave states, which have the possibility to be realized in the newly-discovered iron-based superconductors.

1.2 Iron-based Superconductors

As the youngest (3-year-old) family of superconductors, facilitated by the almost-one-century study of superconductivity especially a broad spectrum of techniques developed for early unconventional superconductors [Sigrist and Ueda (1991); Dagotto (1994); Harlingen (1995)], a great amount of work has been carried out in a short time period on the likely unconventional iron-based superconductors [Ishida et al. (2009); Mazin and Schmalian (2009); Mazin (2010); Canfield and Bud'ko (2010); Paglione and Greene (2010); Johnston (2010); Wen and Li (2011); Wang and Lee (2011)]. The superconducting transition temperature was quickly promoted from 26 K [Kamihara et al. (2008)] to 55-56 K [Ren et al. (2008); Wang et al. (2008); Cheng et al. (2009)]. Significant understanding has been achieved with the material complexity in sight. And it remains to be an active and rapidly developing research field as there are still many puzzling aspects.

1.2.1 Materials and Structures

Thus far six different structures of iron pnictides and chalcogenides as shown in Fig. 1.1 have been fabricated [Wen and Li (2011)]. According to their chemical formulae, they are called 11, 111, 1111, 122, 21311/42622, and 32522. Five of them except the last one are found superconducting with the highest transition temperatures 55-56 K in the 1111 structure. A common feature associated with all the structure types is the existence of a tetrahedral Fe-pnictogen (P, As) or Fe-chalcogen (Se, Te) layer in which iron atoms form a plane with pnictogen or chalcogen residing alternatively above and below the plane. These tetrahedral layers are separated by alkali, alkaline-earth, or rare-earth and oxygen/fluorine layers. It is widely believed that this iron-based layer plays a major role to superconductivity in this family of materials.

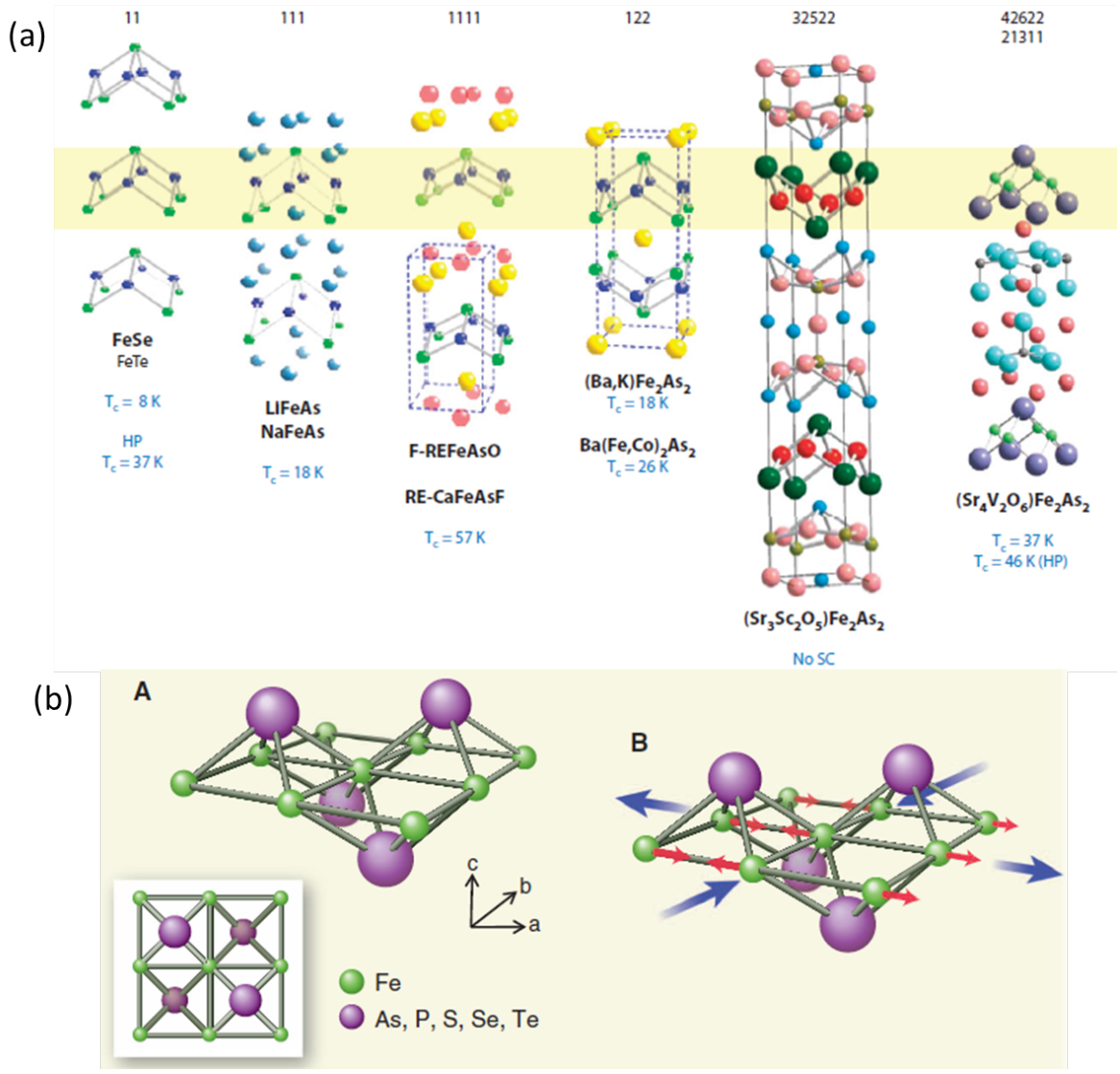

Figure 1.1 (a) Six structures of iron-based material ref.[Wen and Li (2011)]. (b) A The tetrahedral layer containing iron and pnictogen or chalcogen. (b)B shows the structural deformation direction with respect to the spin direction when the system under structural transition. Ref.[Wang and Lee 2011].

1.2.2 Phase Diagrams and Tuning Parameters

In the most studied structures 1111, 122, and 11, phase diagrams that show induced superconductivity have been produced. Figure 1.2 summarizes several available phase diagrams measured in the 1111 structure (the first row of Fig. 1.2) including F-doped LaOFeAs [Luetkens

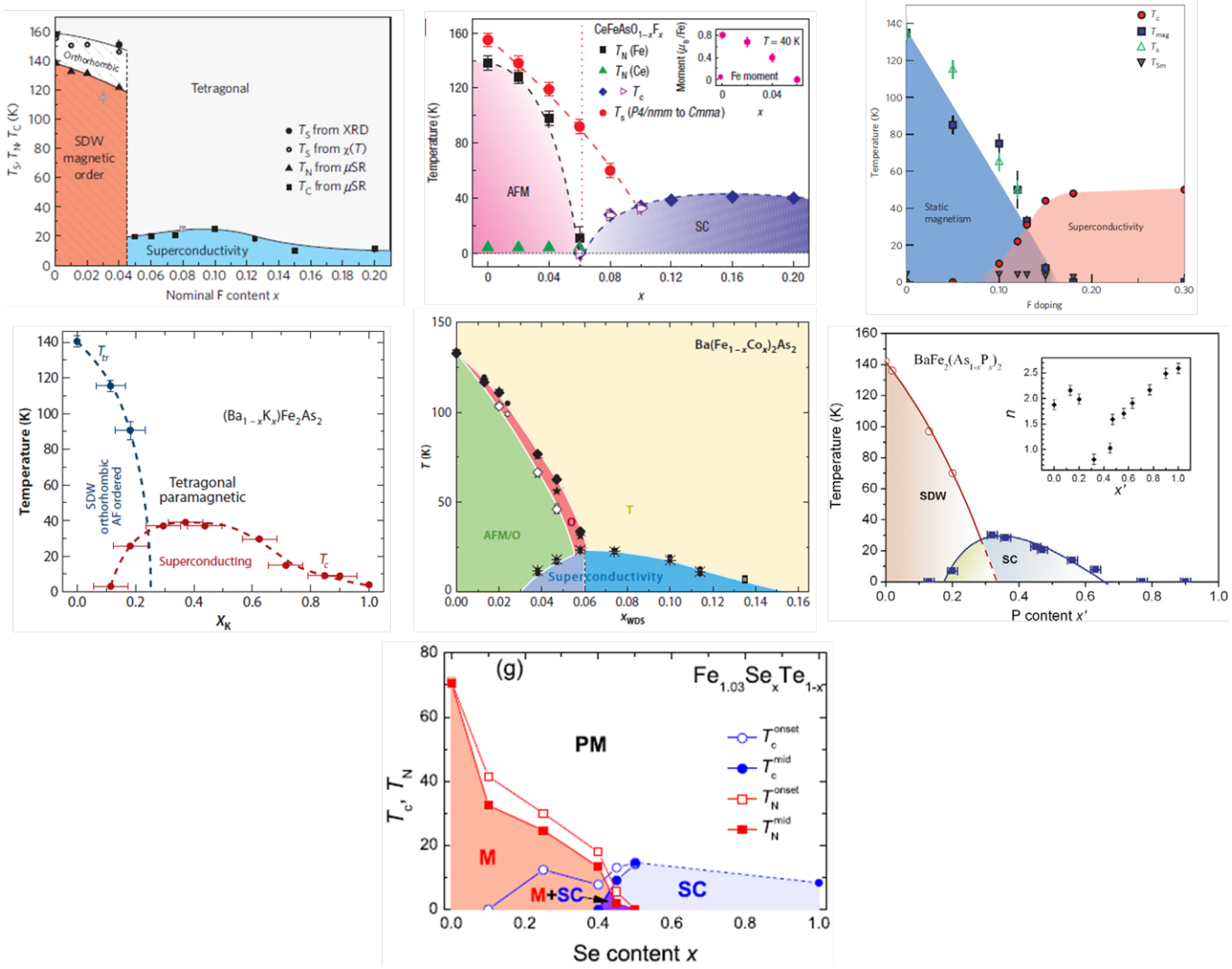

Figure 1.2 Phase diagrams for 1111 (first row), 122 (second row), and 11 (bottom row) systems. Refs are indicated in the text.

et al. (2009)] (left), F-doped CeFeAsO [Zhao et al. (2008)] (middle), and F-doped SmFeAsO [Drew et al. (2009)] (right), where fluorine substitutes oxygen in all cases, and in the 122 $BaFe_2As_2$ system (the second row) with K substitutes Ba [Wen and Li (2011)] (left), which is nominally hole doping, Co substitutes directly the active iron [Canfield and Bud'ko (2010)] (middle), which is nominally electron doping, and P substitutes As [Jiang et al. (2009)] (right), which is nominally isovalent doping, as well as in the 11 $Fe_{1.03}Te$ system with Se doping (the bottom row) [Khasanov et al. (2009)]. Also intercalating metal K in between FeSe layers promotes the transition temperature from 8 K to above 30 K [Guo et al. (2010)]. Besides the various chemical substitutions or intercalation, external presure is another tuning parameter that drives superconductivity. The inspection of the phase diagrams infers us the following information: most of the iron-based superconductors evolve from parent compounds that locate on a spin density wave (SDW) order; the SDW transition is often coupled with a structural transition from the high-temperature tetragonal to the low-temperature orthorhombic phase either simultaneously or separately; the SDW state and superconducting state are intimately related by either closely neighbouring (as in LaOFeAs and CeFeAsO systems), or interpenetrating to each other in a mesoscopic phase separation manner (as in K-doped $BaFe_2As_2$ system [Goko et al. (2009)] and possibly in SmFeAsOF [Drew et al. (2009)]) or even in a microscopic coexistence pattern as indicated by NMR [Laplace et al. (2009)] and neutron scattering measurement [Pratt et al. (2009)] on Co-doped $BaFe_2As_2$ system. This intimacy is taken into account by many experimental and theoretical study of the origin of superconducity.

1.2.3 Electronic Structure

Soon after Hosono group's discovery, density functional theory was applied to calculate the band structure and density of state [Singh and Du (2008); Mazin et al. (2008); Kuroki et al. (2008)]. They found that the parent compounds are semimetallic and the density of state near Fermi surface is mainly contributed by the Fe-3d electrons and all five of the 3d-electrons crosses Fermi surface. The electronic structure of this family of materials is characterized by two sets of disconnected Fermi surface sheets with two or three hole-pockets centered at the Brillouin zone (BZ) center (Γ-point) and two electron-pockets centered at $(0, \pm\pi)$ and $(\pm\pi, 0)$ (M-point)

in the tetragonal unit cell with one iron atom. The calculations show that 2 hole-pockets and 2 electron-pockets are likely more two dimensional with more or less cylindrical shape as shown in Fig. 1.3 [Singh and Du (2008); Mazin and Schmalian (2009)]. The quasi-2D feature in the electronic structure typically supports large fluctuation effect [Mermin and Wagner (1966)] when the system has the tendency to develop long-range order. Another important feature associated with the two well-separated sets of hole- and electron-pockets stems from fermiology: the nesting between matching hole and electron FS pieces, which can drive the system into certain particle-hole instabilities, e.g. the SDW instability. Angle-resolved photoemission spectroscopy (ARPES) [Ding et al. (2008); Kondo et al. (2008); Lu et al. (2008)] and quantum oscillation [Shishido et al. (2010)] measurements consistent with the predicted electronic structure. The nesting between hole and electron pockets in $Ba(Fe_{1-x}Co_x)_2As_2$ is observed by ARPES in a systematic study [Brouet et al. (2009); Terashima et al. (2010)]. No doubt that there appear three-dimensional pockets in the complicated band structure of the materials, which affect the physical properties and necessarily need to be taken into account to understand some experimental data. But the existence of quasi-2D structure may play a crucial role in the magnetic and superconducting phenomena.

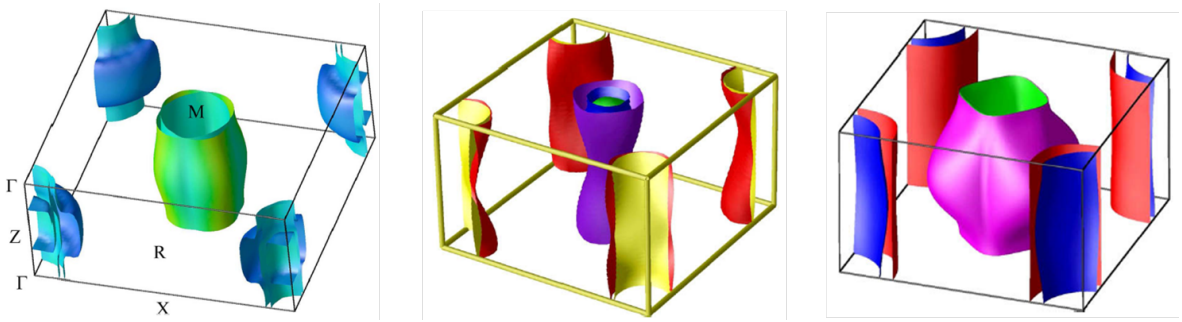

Figure 1.3 Fermi surface configuration calculated for 1111 system (left) ref.[Singh and Du (2008)], 122 system (middle), and 11 system (right) ref.[Mazin and Schmalian (2009)], respectively.

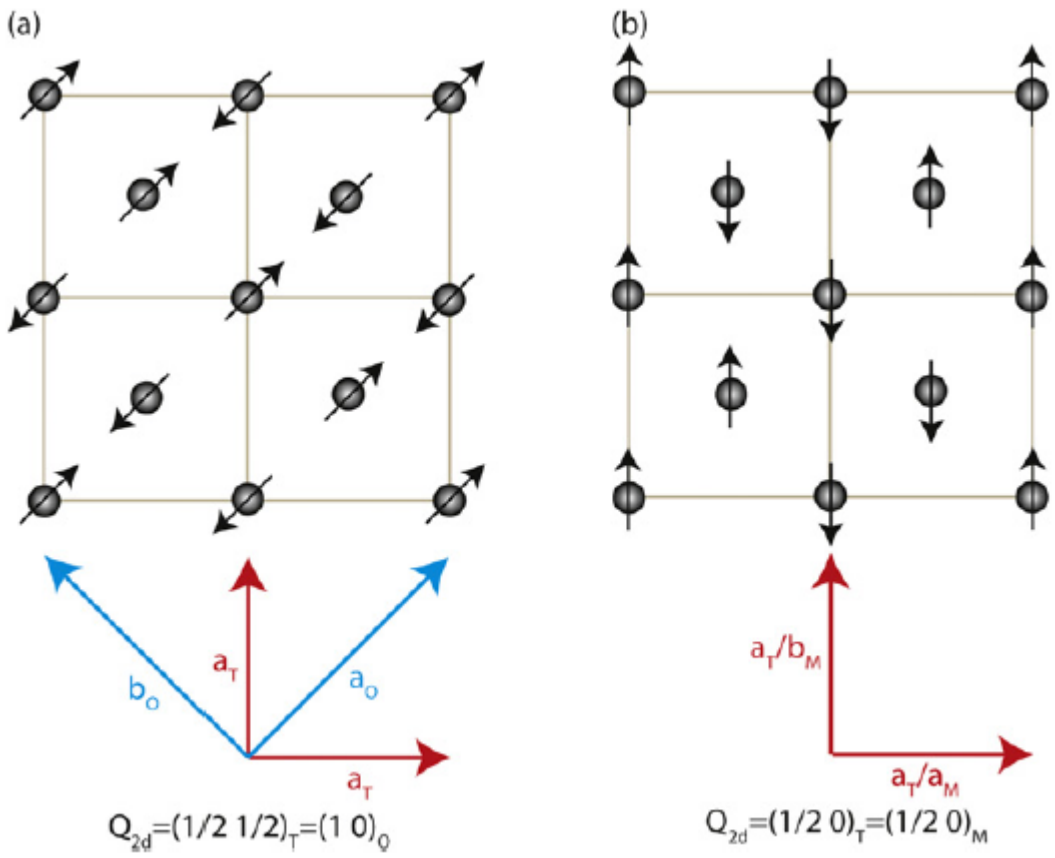

Figure 1.4 (a) The magnetic structure in 1111 and 122 systems. (b) The magnetic structure in 11 system. Ref. [Lumsden and Christianson (2010)].

1.2.4 Magnetic Structure

Neutron scattering quickly resolved the magnetic structures in these materials [de la Cruz et al. (2008); Lumsden and Christianson (2010)]. As illustrated in Fig. 1.4, most iron-based superconducting materials share an antiferromagnetic long-rangle order in the parent compounds with two interpenetrated Neel spin lattices such that antiferromagnetic stripes form along one direction which ferromagnetic stripes along the perpendicular direction as shown in Fig. 1.4 (a). This type of magetic order has an ordering wave vector at (π, π) that matches the nesting wave vector. Therefore it is a major opinion that this magnetic state is a SDW state arising from the particle-hole instability due to nesting, which is itinerant in nature. This point of view is supported by optical spectroscopy measurement on single crystals of $BaFe_2As_2$ and $SrFe_2As_2$ [Hu et al. (2008)], where they observed the formation of energy gaps when lowering the tem-

perature of the clearly metallic system down below the SDW transition temperature, and is also supported by a recent first-principle calculation combining density functional theory and dynamical mean-field theory (DFT+DMFT) [Yin et al. (2011)]. An interesting exception is the 11 system Fe(Se,Te), in which the nesting is still at (π, π) but the static magnetic ordering vector is rotated by 45°, i.e., different from the nesting vector [Bao et al. (2009); Qiu et al. (2009)]. However, the observation of magnetic resonance mode corresponds to the nesting wave vector instead of the long-range magnetic ordering vector [Qiu et al. (2009); Wen et al. (2010)]. This interesting discrepancy indicates that nesting might be directly related to superconductivity through dynamical magnetism (spin fluctuations) while there is other stronger source to dominate static magnetism.

1.2.5 Pairing Symmetry and Gap Structure

Next we discuss the superconducting properties. Scanning tunneling spectroscopy found a coherence length $\xi = 27.6 \pm 2.9$ Å for $Ba(Fe_{0.9}Co_{0.1})_2As_2$ [Yin et al. (2009)], while the measured London penetration depth at the same composition is $\lambda(0) = 1820$ Å [Gordon et al. (2010)]. Unlike in a conventional type I superconductor $\xi \approx 3000$ Å and $\lambda \approx 500$ Å [Tinkham (1996)], it is strongly type II with the Ginzburg-Landau parameter $\kappa = \frac{\lambda}{\xi} \approx 67 \gg \frac{1}{\sqrt{2}}$.

The pairing symmetry and gap structure are among the most interesting topics as they contain most relevant information on pairing mechanism. Nuclear magnetic resonance (NMR) measurements have been conducted on 1111 material $LaFeAsO_{0.9}F_{0.1}$ [Grafe et al. (2008)] and $PrFeAsO_{0.89}F_{0.11}$ [Matano et al. (2008)], 122 material $BaFe_{1.8}Co_{0.2}As_2$ [Ning et al. (2008)], and 11 structure $FeSe_{0.5}Te_{0.5}$ [Shimizu et al. (2009)]. All of them showed the Knight shift decreasing blow T_c, which indicates spin-singlet Cooper pairing, and no evidence for a Hebel-Slichter coherence peak [Hebel and Slichter (1959)] in the nuclear spin-lattice relaxation rate $1/T_1$, which is associated with traditional s-wave due to its constructive coherence factor in superconducting state. They confirm the singlet pairing therefore rule out odd-parity symmetries such as p-wave state. The lack of Hebel-Slichter coherence peak seems to against conventional s-wave symmetry. Therefore, s±-wave and d-wave are more likely according to NMR.

Both d-wave and s±-wave have internal π-phase shifts. The difference is if the π-phase

shift is direction-dependent or not. Also they belong to different symmetry classes. Scanning SQUID microscopy measurement on $NdFeAsO_{1-x}F_y$ did not observe π phase shifts between tunneling in different directions, which is against d-wave order [Hicks et al. (2009)]. Meanwhile, the observation of c-axis Josephson coupling in measurement on $Ba_{1-x}K_xFe_2As_2$ also rules out d-wave pairing symmetry [Zhang et al. (2009b)]. Chen et al. (2010) provided a phase-sensitive measurement through the observation of both integer and half-integer flux-quantum transitions in a composite $Nb - NdFeAsO_{0.88}F_{0.12}$ superconducting loop to establish a π-phase shift in the order parameter. This supports a sign change in the gap structure against conventional s-wave. These phase-sensitive experiments show strong evidence of the sign-reversed s-wave symmetry.

Another phase-sensitive measurement using scanning tunneling microscopy on the 11 structure Fe(Se,Te) to image the quasi-particle scattering interference patterns in the superconducting state was reported [Hanaguri et al. (2010); Hoffman (2010)]. By observing the magnetic-field dependence of the quasiparticle scattering strength, Hanaguri et al. (2010) found the sign of the gap is reversed between the hole and the electron pockets, favoring s±-wave. Zeng et al. (2010) measured the electronic specific heat in a rotating magnetic field on the same material and observed a fourfold oscillation of the specific heat as a function of the in-plane field direction, suggesting a significant gap anisotropy on the electron pockets. This seemingly discrepancy can be resolved by the nodal s±-wave which shows full gap on the hole pockets but nodal structure on the electron pockets.

An important experimental fact that closely relates to the sign-reverse feature in gap structure is the emergence of a magnetic resonance mode in the superconducting state which can be directly measured by inelastic neutron scattering (INS). This resonance mode is due to a constructive coherence factor different from but related to the coherence factor that responsible for the Hebel-Slichter peak in NMR $1/T_1$. We write down the two coherence factors in a simple version as $1 \mp \Delta_{\mathbf{k}}\Delta_{\mathbf{k}'}/E_{\mathbf{k}}E_{\mathbf{k}'}$ where the minus sign belong to the magnetic channel observed in INS and plus sign to the charge channel observed in NMR. If $\Delta_{\mathbf{k}}$ and $\Delta_{\mathbf{k}'}$ have opposite signs, the first coherence factor is constructive giving rise to the magnetic resonance mode while the second coherence factor is destructive resulting in the absence of Helbel-Slichter peak. If $\Delta_{\mathbf{k}}$ and $\Delta_{\mathbf{k}'}$ have the same signs, the opposite happens: there is no resonance mode but there is an

enhanced NMR peak, which are the observations for the conventional s-wave superconductors. As for iron superconductors, we have mentioned that no Hebel-Slichter peak observed in NMR. Meanwhile, the magnetic resonance mode is observed in 1111 material [Shamoto et al. (2010)], more in 122 material [Christianson et al. (2008); Chi et al. (2009); Lumsden et al. (2009)], and in 11 system [Qiu et al. (2009); Wen et al. (2010)]. The observation of magnetic resonance mode points to a sign-reversed gap structure.

ARPES experiments mostly observed fully gaped structure, but other techniques [Johnston (2010)] like penetration depth experiments, thermal conductivity measurements, et. al., showed evidence for the appearance of in-plane nodes in at least some members of the family. Also more evidence showed nodes along c-axis. Recently, ARPES reported the observation of three-dimensional gap [Xu et al. (2011)]. Therefore, the gap structure in iron superconductors is complex and diverse. Large amount of experiments are consistent with s±-wave symmetry, which can be fully gaped or nodal s±-wave. Therefore the observation of in-plane nodes does not conflict with this symmetry type. At the end of the discussion we need to keep in mind that the gap symmetry is not conclusive yet.

1.2.6 Pairing Mechanism

Phonons alone were quickly showed to be unable to explain the high transition temperature as the electron-phonon coupling constant is too small [Boeri et al. (2008)]. Even later Boeri et al. (2010) showed that the magnetism enhances the total electron-phonon coupling by $\sim 50\%$, up to $\lambda \leq 0.35$, still not enough to explain the transtion temperature, which suggests a non-phonon mechanism [Monthoux et al. (2007)]. NMR measurement reported a correlation between T_c and the strength of antiferromagnetic spin fluctuations [Ning et al. (2010)]. In light of the proximity to magnetic instabilities, strong spin fluctuations are active and might play a role in Cooper pair formation. Mazin et al. (2008) first proposed the spin-fluctuation-induced superconductivity scenario for iron pnictides and predicted s±-wave state in this material. If the gap symmetry is indeed s±-wave, it indicates the pairing interaction is repulsive. As shown in the follow

expression from Eliashberg equation,

$$\Delta_{\mathbf{k}} = -\sum_{\mathbf{k}'} V(\mathbf{k},\mathbf{k}')\frac{\Delta_{\mathbf{k}'}}{2E_{\mathbf{k}'}}\tanh\left(\frac{E_{\mathbf{k}'}}{2k_BT}\right),$$

a positive interaction $V(\mathbf{k},\mathbf{k}')$ would lead to a sign change in the gap Δ.

Many theoretical approaches have been used to address the pairing problem in iron-based superconductors, including random phase approximation (RPA) [Kuroki et al. (2008); Graser et al. (2009)], renormalization group (RG) analysis [Chubukov et al. (2008); Wang et al. (2009)], fluctuation exchange (FLEX) approximation [Yao et al. (2009); Sknepnek et al. (2009); Zhang et al. (2009a, 2010)], and variational Monte Carlo calculation [Yang et al. (2011)]. All of these theoretical calculations found that strong antiferromagnetic (AF) correlation (spin fluctuation) triggers s± pairing next to the antiferromagnetism. The match between spin fluctuation structure and fermiology might drive superconductivity in at least some of these materials. Therefore, antiferromagnetic spin fluctuations could possibly be the major mediating glue in the iron-based superconductors.

In this thesis, we consider the interactions between electrons by exchange of fluctuations to explore the pairing mechanism using fluctuation exchange approximation in the superconducting state as well as the interplay between magnetism and superconductivity.

CHAPTER 2. FLUCTUATION EXCHANGE APPROXIMATION

2.1 Cooper Pair due to Fluctuation Exchange

It was first proposed for the superfluidity of fermionic atom ^{3}He that Cooper pair can be formed by exchanging spin fluctuations. Unlike the Cooper pair of charged electrons that leads to superconductivity, ^{3}He is neutral and there is strong hard-core repulsion between the atoms which prevents s-wave pairing. The condensation of p-wave triplet Cooper pairs by exchanging ferromagnetic spin fluctuations gives rise to the well-known anisotropic superfluid phase in liquid ^{3}He [Nakajima (1973); Brinkman et al. (1974); Leggett (1975)]. This mechanism was considered later to be possibly relevant to superconductivity on the border of itinerant ferromagnetism [Fay and Appel (1980)].

Starting from late 1970s, superconductivity was found on the border of antiferromagnetism in a family of heavy electron compounds [Steglich et al. (1979)], organic charge transfer complexes [Jerome et al. (1980); Jerome (1994)], high-temperature cuprates, and iron-based superconductors. This motivated the proposal for Cooper pair mediated by antiferromagnetic spin fluctuations.

As one of the strong-coupling theories of superconductivity, fluctuation exchange approximation was first introduced by Bickers, Scalapino, and White [Bickers et al. (1988); Bickers and Scalapino (1989)] as one of the conserving approximations [Baym and Kadanoff (1961); Baym (1962)] with free energy functional is diagrammatically demonstrated in Fig. 2.1. In this work, they only considered approaching superconductivity in the normal state. Later, the FLEX calculation for superconducting state was performed by Pao and Bickers (1994); Monthoux and Scalapino (1994). Takimoto et al. (2004) generalized this method to multiorbital systems.

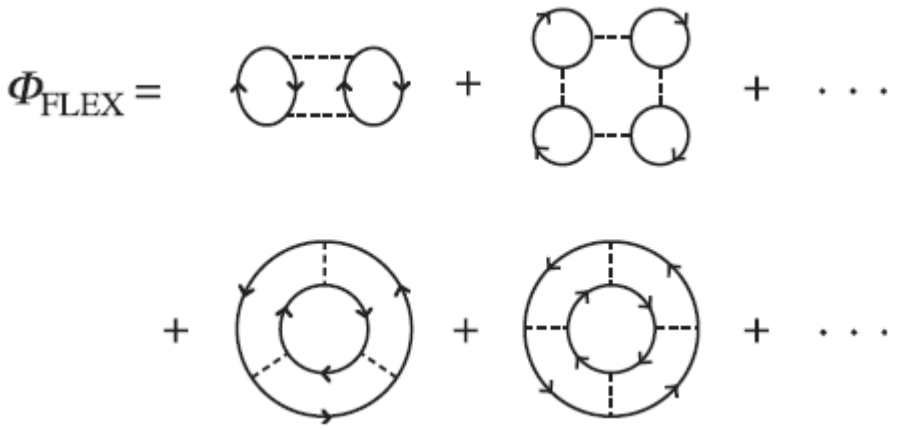

Figure 2.1 Diagrammatic demonstration of the free energy functional for the FLEX approximation.

2.2 Single-band FLEX Formalism

The conserving approximation formalism introduced by Baym and Kadanoff can be extended to treat exchange of the simplest particle-hole and particle-particle fluctuations. FLEX as such an extension is capable of treating possible competitions between superconductivity and charge or spin density ordering at low temperatures. And this is one of the simplest infinite-order conserving approximations that deal with competing normal-state instabilities in multiple channels, allowing the analysis of electronic charge- and spin-ordering transitions on the same footing.

2.2.1 Introduction

Now let us go through the self-consistent treatment of collective fluctuations by starting with a general interacting fermion system. Following Bickers and Scalapino (1989), we express the interaction theory in terms of an effective action and assume the action written as

$$\begin{aligned} S &= S_0 + S_{int} \\ S_0 &= \beta \sum_{xx'\sigma} \bar{c}_\sigma(x) \left(\frac{\partial}{\partial \tau} + H_0 \right) c_\sigma(x') \\ S_{int} &= \frac{1}{2}\beta \sum_{xx'\sigma\sigma'} v(x-x') \bar{c}_\sigma(x) \bar{c}_{\sigma'}(x') c_{\sigma'}(x') c_\sigma(x). \end{aligned}$$

The notations used here are $x = (\mathbf{x}, \tau)$ with $\mathbf{x}$ a discrete lattice point and τ the imaginary time, $\sum_x = \beta^{-1} \int_0^\beta \mathrm{d}\tau \sum_{\mathbf{x}}$ with $\beta = \frac{1}{k_B T}$ the inverse temperature, and σ (σ') refers to some internal degrees of freedom such as spin. The quantities c and $\bar{c}$ are anticommuting c-numbers, i.e., Grassmann numbers. H_0 represents the noninteracting Hamiltonian and v is a general interaction which depends only on the coordinate difference. For on-site interactions, such as Hubbard model, it can be expressed in terms of a coupling constant U as $v(x_1 - x_2) = U\delta_{x_1 x_2}$ or in abbreviated notation $v(1-2) = U\delta_{12}$.

For a simple lattice, i.e., a single-band model, the action may be rewritten using the Fourier-transformed quantities

$$\begin{aligned} c_\sigma(x) &= \frac{1}{\sqrt{N}} \sum_k c_\sigma(k) e^{ik\cdot x} \\ \bar{c}_\sigma(x) &= \frac{1}{\sqrt{N}} \sum_k \bar{c}_\sigma(k) e^{-ik\cdot x} \\ v(x) &= \sum_q v(q) e^{iq\cdot x}, \end{aligned}$$

where N is the number of lattice points. And sum over k contains the sum over $\mathbf{k}$ in momentum space restricted to the Brillouin zone and over the Matsubara frequencies ω_n, i.e.,

$$k = (\mathbf{k}, \omega_n), \quad \omega_n = \begin{cases} (2n+1)\pi T & \text{fermions} \\ 2n\pi T & \text{bosons} \end{cases}.$$

with n being an integer. The resulting expression in momentum space is

$$\begin{aligned} S_0 &= \beta \sum_{k\sigma} (-i\omega_n + \varepsilon_{\mathbf{k}}) \bar{c}_\sigma(k) c_\sigma(k) \\ S_{int} &= \frac{1}{2}\beta \sum_{kk'\sigma\sigma'} v(q) \bar{c}_\sigma(k+q) \bar{c}_{\sigma'}(k'-q) c_{\sigma'}(k') c_\sigma(k), \end{aligned}$$

with $\varepsilon_{\mathbf{k}}$ the single-particle energy determined by H_0. The prefactor $\frac{1}{2}$ in the interaction part removes a double counting from indistinguishability of particles.

When we self-consistently determine the single-particle Green's function, the interaction effect can be coded in an external field, the self-energy term Σ, by adopting certain approximations. In this way, the approximate interaction action becomes

$$S_{sc} = \beta \sum_{k\sigma} \Sigma_\sigma(k)\bar{c}_\sigma(k)c_\sigma(k) + \beta\bar{F}(G;v)$$

where $\bar{F}$ is a free energy term that does not depend on the fermion variables and the irreducible self-energy Σ is determined self-consistently through the dressed Green's function G: $\Sigma(G;v)$. By judiciouly choosing $\Sigma(G;v)$, we are able to treat the residual $\Delta S = S_{int} - S_{sc}$ as a perturbation.

The simplest self-consistently approximation is Hartree-Fock approximation. One can simply decouple the interaction term into quadratic forms

$$v(q)\bar{c}_\sigma(k+q)\bar{c}_{\sigma'}(k'-q)c_{\sigma'}(k')c_\sigma(k) = \left[v(0)\langle n(k')\rangle - v(k'-k)\langle n_\sigma(k')\rangle\right]\bar{c}_\sigma(k)c_\sigma(k),$$

where the density $\langle n_\sigma(k')\rangle = \langle \bar{c}_\sigma(k')c_\sigma(k')\rangle$ and $\langle n(k')\rangle = \sum_\sigma \langle n_\sigma(k')\rangle$. The first term is typically called the "direct" interaction and the second the "exchange" interaction. Then the Hartree-Fock self-energy can be analytically expressed as

$$\begin{aligned}\Sigma_\sigma(k) &= \sum_{k'}\left[v(0)\langle n(k')\rangle - v(k'-k)\langle n_\sigma(k')\rangle\right] \\ &= \sum_{k'}\left\{\left[v(0)-v(k'-k)\right]G_\sigma(k') + v(0)G_{-\sigma}(k')\right\}e^{i\omega'_n 0^+}\end{aligned}$$

with the self-consistent Green's function

$$G_\sigma(k) = -\langle c_\sigma(k)\bar{c}_\sigma(k)\rangle = \frac{T}{i\omega_n - \varepsilon_{\mathbf{k}} - \Sigma_\sigma(k)},$$

and we used the relation $\langle n_\sigma(k')\rangle = G_\sigma(k')e^{i\omega'_n 0^+}$. Note that for the Hubbard model, because $v(q) = U/N$ =constant, the equal-spin contribution to $\Sigma_\sigma(k)$ drops out.

Next, let us consider the scattering of collective fluctuations in the normal state. In a spin-rotationally invariant system, the possible particle-hole scattering channels are spin-singlet channel which corresponds to charge density ordering and spin-triplet channel which corresponds to spin density ordering. These channels can be further subdivided according to orbital symmetry. In order to write down the collective propagators, we discuss the decoupling of the interaction term in terms of charge density and spin density variables in two independent cases.

- Equal-spin particle-hole scattering. In this case, construct the equal-spin fluctuation variables

$$d(11') = \frac{1}{\sqrt{2}}\sum_{\sigma}\bar{c}_{\sigma}(1)c_{\sigma}(1') = \frac{1}{\sqrt{2}}\left[\bar{c}_{\uparrow}(1)c_{\uparrow}(1') + \bar{c}_{\downarrow}(1)c_{\downarrow}(1')\right] = \frac{1}{\sqrt{2}}\bar{c}_{\sigma}(1)\tau^{0}_{\sigma\sigma'}c_{\sigma'}(1'),$$
$$m_0(11') = \frac{1}{\sqrt{2}}\sum_{\sigma}\sigma\bar{c}_{\sigma}(1)c_{\sigma}(1') = \frac{1}{\sqrt{2}}\left[\bar{c}_{\uparrow}(1)c_{\uparrow}(1') - \bar{c}_{\downarrow}(1)c_{\downarrow}(1')\right] = \frac{1}{\sqrt{2}}\bar{c}_{\sigma}(1)\tau^{z}_{\sigma\sigma'}c_{\sigma'}(1'), \tag{2.1}$$

where τ^i is the Pauli matrix. The commuting variable d and m_0 represent normalized creation operators for charge density fluctuation and the zero-component of spin density fluctuation. Within a constant and with the convention of repeated index performing summation, the four fermion interaction term can be decoupled in terms of the above fluctuation variables as

$$\begin{aligned}
&v(x-x')\bar{c}_{\sigma}(x)\bar{c}_{\sigma'}(x')c_{\sigma'}(x')c_{\sigma}(x)\\
&\rightarrow v(x-x')\bar{c}_{\sigma}(x)c_{\sigma}(x)\bar{c}_{\sigma'}(x')c_{\sigma'}(x') - v(x-x')\bar{c}_{\sigma}(x)c_{\sigma}(x')\bar{c}_{\sigma'}(x')c_{\sigma}(x)\\
&= v(1-1')2d(11)d(1'1') - v(1-1')\left[d(11')d(1'1) + m_0(11')m_0(1'1)\right]\\
&= d(12)(v_d)_{12,34}d(34) + m_0(12)(v_m)_{12,34}m_0(34)
\end{aligned}$$

where the scattering vertices are

$$\begin{aligned}
(v_d)_{12,34} &= v(1-3)\left(2\delta_{12}\delta_{34} - \delta_{14}\delta_{23}\right)\\
(v_m)_{12,34} &= -v(1-3)\delta_{14}\delta_{23}.
\end{aligned}$$

- Opposite-spin particle-hole scattering. In this case, construct the opposite-spin fluctuation variables

$$\begin{aligned}
m_{+}(11') &= \bar{c}_{+}(1)c_{-}(1') = \bar{c}_{\sigma}(1)\frac{1}{2}\left[\tau^1 + i\tau^2\right]_{\sigma\sigma'}c_{\sigma'}(1') = \bar{c}_{\sigma}(1)S^{+}_{\sigma\sigma'}c_{\sigma'}(1'),\\
m_{-}(11') &= \bar{c}_{-}(1)c_{+}(1') = \bar{c}_{\sigma}(1)\frac{1}{2}\left[\tau^1 - i\tau^2\right]_{\sigma\sigma'}c_{\sigma'}(1') = \bar{c}_{\sigma}(1)S^{-}_{\sigma\sigma'}c_{\sigma'}(1').
\end{aligned} \tag{2.2}$$

These operators creat spin fluctuations with spin projection $S_z = \pm 1$. Again decouple the

interaction into fluctuation scattering form

$$
\begin{aligned}
&v(x-x')\bar{c}_\sigma(x)\bar{c}_{\sigma'}(x')c_{\sigma'}(x')c_\sigma(x) \\
&\to -v(x-x')\bar{c}_\sigma(x)c_{-\sigma}(x')\bar{c}_{-\sigma}(x')c_\sigma(x)+v(x-x')\bar{c}_\sigma(x)\bar{c}_\sigma(x')c_\sigma(x')c_\sigma(x) \\
&= -v(1-1')\left[m_+(11')m_-(1'1)+m_-(11')m_+(1'1)\right]+v(1-1')\bar{c}_\sigma(1)\bar{c}_\sigma(1')c_\sigma(1')c_\sigma(1) \\
&= [m_+(12)(v_m)_{12,34}m_-(34)+m_-(12)(v_m)_{12,34}m_+(34)]+v(1-1')\bar{c}_\sigma(1)\bar{c}_\sigma(1')c_\sigma(1')c_\sigma(1)
\end{aligned}
$$

where the last term is a residue.

In a summary, we can write down the charge and spin fluctuation scattering terms as

$$
d(12)(v_d)_{12,34}d(34)+m_0(12)(v_m)_{12,34}m_0(34)+m_+(12)(v_m)_{12,34}m_-(34)+m_-(12)(v_m)_{12,34}m_+(34) \tag{2.3}
$$

where in Hubbard model

$$
v_d = U, \quad v_m = -U.
$$

Alternatively, in the (S_x, S_y, S_z) reprentation, since

$$
m_0 = \sqrt{2}S_z, \quad m_0 v_m m_0 = 2S_z v_m S_z
$$

and

$$
m_+ + m_- = 2S_x, \quad m_+ - m_- = 2iS_y,
$$

$$
\begin{aligned}
m_+ v_m m_- + m_- v_m m_+ &= (S_x+iS_y)v_m(S_x-iS_y)+(S_x-iS_y)v_m(S_x+iS_y) \\
&= 2(S_x v_m S_x + S_y v_m S_y),
\end{aligned}
$$

combining with (2.1) (2.2) and (2.3), the four fermion interaction terms are more clearly decoupled in the spin and charge channels as

$$
\begin{aligned}
2v_m \mathbf{S}\cdot\mathbf{S} &= \frac{1}{2}v_m \boldsymbol{\tau}_{\sigma_1\sigma_4}\cdot\boldsymbol{\tau}_{\sigma_2\sigma_3}c^\dagger_{\sigma_1}c^\dagger_{\sigma_2}c_{\sigma_3}c_{\sigma_4}, \\
v_d d\cdot d &= \frac{1}{2}v_d\delta_{\sigma_1\sigma_4}\delta_{\sigma_2\sigma_3}c^\dagger_{\sigma_1}c^\dagger_{\sigma_2}c_{\sigma_3}c_{\sigma_4}.
\end{aligned} \tag{2.4}
$$

Therefore the vertices $v_m,\ v_d$ directly correspond to the spin-spin and charge-charge interaction. Later we will extend the represenation (2.4) to the multi-band case.

Prepared with the above fluctuation-interaction terms, we first derive the expressions for the collective propagators within a random phase approximation (RPA). Such an approximation is conserving when the single-particle Green's functions are treated within Hartree-Fock. For normal state, consider the particle-hole channels only. Let $r = d,\, m_0,\, m_\pm$, then $\bar{r} = r$ for $r = d$ or m_0. The RPA propagators take the form

$$\begin{aligned} R_{12,34} &= \langle r(12)\bar{r}(34)\rangle_{RPA}^{connected} = \langle r(12)\bar{r}(34)\rangle_{RPA} - \langle r(12)\rangle_{RPA}\langle \bar{r}(34)\rangle_{RPA} \\ &= \langle r(12)\bar{r}(34)\rangle_{sc}^{connected} - \beta \sum_{i'} \langle r(12)\bar{r}(1'2')\rangle_{sc}^{conn} (v_r)_{1'2',3'4'} \langle r(3'4')\bar{r}(34)\rangle_{sc}^{conn} + \cdots \end{aligned}$$

where the subscript "sc" indicates that the average is to be evaluated using the self-consistent single-particle action S_{sc} rather than the non-interacting action S_0 and the superscript "connected" requires the summation over only connected Feynman diagrams in the diagrammatic expansion. Define the irreducible correlation function

$$R^0_{12,34} = \langle r(12)\bar{r}(34)\rangle_{sc}^{connected} = \langle r(12)\bar{r}(34)\rangle_{sc} - \langle r(12)\rangle_{sc}\langle \bar{r}(34)\rangle_{sc},$$

then the RPA propagators become

$$R_{12,34} = R^0_{12,34} - \beta \sum_{i'} R^0_{12,1'2'}(v_r)_{1'2',3'4'} R^0_{3'4',34} + \cdots = \left[R^0(1+\beta v_r R^0)^{-1}\right]_{12,34},$$

where in the last step we took the sum over a geometric series of interaction vertices and irreducible propagators. As always, it is most convenient to work with Fourier-transformed propagators in a translational-invariant system. The bare interaction matrix may be written in a way which emphasizes the total momentum q carried by the particle-hole or particle-particle pair:

$$\begin{aligned} [v_d(q)]_{k_1k_2,k_3k_4} &= [2v(q) - v(k_1-k_4)]\,\delta_{k_1,k_2+q}\delta_{k_3+q,k_4} \\ [v_m(q)]_{k_1k_2,k_3k_4} &= -v(k_1-k_4)\delta_{k_1,k_2+q}\delta_{k_3+q,k_4}. \end{aligned}$$

Thus, the Fourier-transformed RPA propagators can be written as

$$R(q) = R^0(q)\left[1+\beta v_r(q)R^0(q)\right]^{-1}.$$

Specifically, the irreducible charge-fluctuation propagator is calculated through the single-particle Green's function

$$\begin{aligned}\left[D^0(q)\right]_{k_1k_2,k_3k_4} &= \langle d(k_1k_2)d(k_3k_4)\rangle_{sc}^{connected}\delta_{k_1,k_2+q} \\ &= -G(k_2+q)G(k_2)\delta_{k_1k_4}\delta_{k_2k_3}\delta_{k_1,k_2+q}\end{aligned}$$

in the normal state, and it can be shown that the spin-fluctuation part is the same in this case: $M^0(q) = D^0(q)$. Note that in the self-consistent approximation, the single-particle propagators in the irreducible fluctuation correlation function R^0 are those dressed, or say renormalized, rather than the bare ones.

In the normal state, the susceptibility corresponding to a perturbation which couples to operator r with momentum transfer q is just

$$\begin{aligned}\chi_r^0(q) &= -\frac{\beta}{N}\sum_k G(k+q)G(k), \quad r = d,\, m, \\ \chi_r(q) &= \frac{\chi_r^0(q)}{1+Nv_r(q)\chi_r^0(q)}.\end{aligned}$$

For example, Hubbard model gives

$$v_d(q) = U/N, \quad v_m(q) = -U/N,$$

thus

$$\chi_d(q) = \frac{\chi^0(q)}{1+U\chi^0(q)}, \quad \chi_m(q) = \frac{\chi^0(q)}{1-U\chi^0(q)}.$$

These are the RPA charge susceptibility $\chi_d = \chi^c$ and spin susceptibility $\chi_m = \chi^s$, respectively, for Hubbard model.

These susceptibilities are subsequently used to construct a Berk-Schrieffer-like interaction describing the exchange of spin and charge fluctuations [Berk and Schrieffer (1966)]. This interaction then provides the basis for calculating the single-particle self-energies in fluctuation exchange approximation. It is convenient to write the expression for self-energy as a sum of contributions

$$\Sigma_\sigma(11') = \Sigma_\sigma^{(2)}(11') + \Sigma_\sigma^{(p-h)}(11'),$$

where $\Sigma_\sigma^{(2)}$ is the full contribution of $O(v^2)$, $\Sigma_\sigma^{(p-h)}$ arises from exchange of collective particle-hole fluctuations of $O(v^3)$ and higher. The $O(v^2)$ contribution consists of one-bubble diagram

and vertex correction diagram which gives the analytical expression

$$\Sigma_\sigma^{(2)}(11') = -\beta \sum_{23} v(1-2)v(1'-3)\left[2G(1-1')G(2-3)G(3-2) - G(1-3)G(3-2)G(2-1')\right]$$

where the factor 2 in the first term comes from the sum over spin in the loop and the minus sign is due to the fermion loop in the first diagram. Accordingly, the momentum-space expression is

$$\Sigma_\sigma^{(2)}(k) = -\beta \sum_{k',q} v(q)\left[2v(q) - v(k-k'-q)\right] G(k-q)G(k'+q)G(k').$$

The contribution from particle-hole exchange after subtracting the $O(v^2)$ terms is given by

$$\Sigma_\sigma^{(p-h)}(k) = \beta \sum_q G(k-q)\left[\frac{1}{2}v_d(D-D^0)v_d + \frac{3}{2}v_m(M-M^0)v_m\right].$$

Note that the factor 3 in front of spin fluctuation part results from the three spin components: m_0, $m_\pm$. Thus we can express the fluctuation-exchange self-energy via an effective interaction V^n

$$\Sigma_\sigma^{(p-h)}(k) \quad = \quad \beta \sum_q G(k-q)V^n(k),$$

with the normal effective interaction contains charge-fluctuation exchange and spin-fluctuation exchange

$$V^n(k) = V^c(k) + V^s(k),$$

$$V^c = \frac{1}{2}v_d(D-D^0)v_d, \quad V^s = \frac{3}{2}v_m(M-M^0)v_m.$$

For instance, in the Hubbard model the self-energy contribution is simply as

$$\Sigma_\sigma(k) = \frac{1}{N}\sum_q G(k-q)\left[V^{(2)}(q) + V^{(p-h)}(q)\right],$$

where the vertices are in terms of the particle-hole susceptibility

$$\begin{aligned} V^{(2)}(q) &= U^2\chi^0(q), \\ V^{(p-h)}(q) &= \frac{1}{2}U^2\chi^0(q)\left[\frac{1}{1+U\chi^0(q)} - 1\right] + \frac{3}{2}U^2\chi^0(q)\left[\frac{1}{1-U\chi^0(q)} - 1\right], \end{aligned}$$

with the bare susceptibility defined as

$$\chi^0(q) = -\frac{\beta}{N}\sum_k G(k+q)G(k).$$

That is, we have the normal interaction vertex in the self-energy as

$$V^n(q) = \frac{1}{2}U^2\chi^0(q)\left[\frac{1}{1+U\chi^0(q)} + \frac{3}{1-U\chi^0(q)} - 2\right].$$

We can see that for $U > 0$, the spin fluctuation sector dominates the effective interaction.

In above we have introduced a general procedure to self-consistently determine the self-energy $\Sigma(G; v)$, single-particle propagator $G(\Sigma)$, and the irreducible fluctuation propagator $R^0(G)$ or susceptibility $\chi^0(G)$. Fluctuation exchange approximation takes into account a subset of Feynman diagrams including bubble and ladder series to describe the effective interaction by exchange of charge and spin fluctuations, which would play a major role when the system is close to a charge or spin instability. Thus far we only considered the non-superconducting state. To investigate the fluctuation-induced superconductivity, we need to extend our formalism to a charge condensate state. In order to perform a quantitative discussion, let us develop our formalism and carry out numerical evaluations for the two-dimensional Hubbard model on a square lattice.

2.2.2 2D Hubbard Model on a Square Lattice

Let us briefly introduce the single-band Hubbard model here. The two-dimensional Hubbard model is expressed as,

$$H = -\sum_{\langle i,j\rangle,\sigma} t_{ij}\left(c^\dagger_{i\sigma}c_{j\sigma} + h.c.\right) + U\sum_i n_{i\uparrow}n_{i\downarrow}.$$

Here we consider the square lattice and take into account the nearest neighboring hopping only, i.e.,

$$t_{ij} = \begin{cases} t, & \text{for nearest neighbors;} \\ 0, & \text{otherwise.} \end{cases}$$

Perform Fourier transform

$$c_{i\sigma} = \frac{1}{\sqrt{N}}\sum_{\mathbf{k}} e^{i\mathbf{k}\cdot\mathbf{r}_i}c_{\mathbf{k}\sigma},$$

where N is the number of lattice sites and we have chosen the lattice spacing to be unity. Then the kinetic part becomes

$$-\sum_{\langle i,j\rangle,\sigma} t_{ij}\left(c^{\dagger}_{i\sigma}c_{j\sigma}+h.c.\right)=-2t\sum_{\mathbf{k},\sigma}(\cos k_x+\cos k_y)c^{\dagger}_{\mathbf{k}\sigma}c_{\mathbf{k}\sigma},$$

which gives rise to the tight-binding dispersion,

$$\varepsilon(\mathbf{k})=-2t(\cos k_x+\cos k_y).$$

Then we can write the whole Hamiltonian as

$$H=\sum_{\mathbf{k},\sigma}\varepsilon(\mathbf{k})c^{\dagger}_{\mathbf{k}\sigma}c_{\mathbf{k}\sigma}+U\sum_{i}n_{i\uparrow}n_{i\downarrow}. \tag{2.5}$$

This is the so-called minimal Hubbard model, which serves as the starting point of the following analysis.

2.2.3 FLEX Formalism for Hubbard Model in the Superconducting State

Here the Dyson-Gor'kov equation and Éliashberg theory are used to discuss superconductivity. The formulation is suitable for applying diagrammatic quantum field theory. In this approach the superconducting state is described by introducing the normal and anomalous Green's functions, symbolically expressed as G and F, respectively. In the homogeneous system, they are well-defined in momentum space as

$$\begin{aligned}
G(\mathbf{k},i\omega_n) &= -\int_0^{\beta}\mathrm{d}\tau\, e^{i\omega_n\tau}\langle T_\tau c_{\mathbf{k}\sigma}(\tau)c^{\dagger}_{\mathbf{k}\sigma}\rangle,\\
F(\mathbf{k},i\omega_n) &= \int_0^{\beta}\mathrm{d}\tau\, e^{i\omega_n\tau}\langle T_\tau c_{\mathbf{k}\uparrow}(\tau)c_{-\mathbf{k}\downarrow}\rangle,\\
F^{\dagger}(\mathbf{k},i\omega_n) &= \int_0^{\beta}\mathrm{d}\tau\, e^{i\omega_n\tau}\langle T_\tau c^{\dagger}_{-\mathbf{k}\downarrow}(\tau)c^{\dagger}_{\mathbf{k}\uparrow}\rangle,
\end{aligned}$$

where $c_{\mathbf{k}\sigma}(\tau)=e^{\mathcal{H}\tau}c_{\mathbf{k}\sigma}e^{-\mathcal{H}\tau}$ with $\mathcal{H}$ being the grand canonical Hamiltonian $\mathcal{H}=H-\mu N$, $\beta=1/T$, and $\omega_n=(2n+1)\pi T$ with an integer n is the fermionic Matsubara frequency. $\langle ...\rangle$ refers to the statistical average and T_τ is the ordering operator with respect to τ. In the following, we use the four-momentum convention, i.e., $k=(\mathbf{k},\, i\omega_n)$ and $q=(\mathbf{q},\, i\nu_m)$, where $\omega_n=(2n+1)\pi T$ is the fermion frequency and $\nu_m=2m\pi T$ is the boson frequency.

The Green's functions are expressed by normal (Σ) and anomalous (Φ) self-energies through the Dyson-Gor'kov equation which is written in the matrix form as

$$\mathbb{G}(k) \equiv \begin{pmatrix} G(k) & F(k) \\ F^\dagger(k) & -G(-k) \end{pmatrix}, \quad \hat{\Sigma}(k) \equiv \begin{pmatrix} \Sigma(k) & \Phi(k) \\ \Phi^*(k) & -\Sigma(-k) \end{pmatrix}$$

$$\begin{aligned} \mathbb{G} &= \mathbb{G}_0 + \mathbb{G}_0\hat{\Sigma}\mathbb{G} \\ (1 - \mathbb{G}_0\hat{\Sigma})\mathbb{G} &= \mathbb{G}_0 \Longrightarrow \mathbb{G} = (\mathbb{G}_0^{-1} - \hat{\Sigma})^{-1} \end{aligned}$$

where the bare Green's function has only diagonal term $G_0(k) = \frac{1}{i\omega_n - \varepsilon(\mathbf{k}) + \mu}$. Explicitly Dyson-Gor'kov equation reads

$$\begin{aligned} \begin{pmatrix} G(k) & F(k) \\ F^\dagger(k) & -G(-k) \end{pmatrix} &= \begin{pmatrix} G_0(k)^{-1} - \Sigma(k) & -\Phi(k) \\ -\Phi^*(k) & -G_0(-k)^{-1} + \Sigma(-k) \end{pmatrix}^{-1} \\ &= \begin{pmatrix} \frac{i\omega_n + \varepsilon(\mathbf{k}) + \Sigma(-k)}{D(k)} & \frac{\Phi(k)}{D(k)} \\ \frac{\Phi^*(k)}{D(k)} & \frac{i\omega_n - \varepsilon(\mathbf{k}) - \Sigma(k)}{D(k)} \end{pmatrix} \end{aligned}$$

with

$$D(k) = \left(i\omega_n - \frac{\Sigma(k) - \Sigma(-k)}{2}\right)^2 - \left(\varepsilon(\mathbf{k}) + \frac{\Sigma(k) + \Sigma(-k)}{2}\right)^2 - |\Phi(k)|^2.$$

Now we parametrize the self-energy matrix $\hat{\Sigma}$ in the Nambu space as

$$\hat{\Sigma}(k) = \mathrm{Y}(k)\tau^0 + \mathrm{X}(k)\tau^z + \Phi(k)(\tau^x + i\tau^y)/2 + \Phi^*(k)(\tau^x - i\tau^y)/2$$

so that

$$\begin{pmatrix} G(k) & F(k) \\ F^\dagger(k) & -G(-k) \end{pmatrix} = \begin{pmatrix} \frac{i\omega_n + \varepsilon(\mathbf{k}) + (\mathrm{X}-\mathrm{Y})(k)}{D(k)} & \frac{\Phi(k)}{D(k)} \\ \frac{\Phi^*(k)}{D(k)} & \frac{i\omega_n - \varepsilon(\mathbf{k}) - (\mathrm{X}+\mathrm{Y})(k)}{D(k)} \end{pmatrix},$$

with

$$D(k) = (i\omega_n - \mathrm{Y}(k))^2 - (\varepsilon(\mathbf{k}) + \mathrm{X}(k))^2 - |\Phi(k)|^2.$$

Define a function $\mathrm{Z}(k)$ via $\mathrm{Y}(k) = i\omega_n(1 - \mathrm{Z}(k))$ so that

$$\begin{aligned} D(k) &= (i\omega_n \mathrm{Z}(k))^2 - (\varepsilon(\mathbf{k}) + \mathrm{X}(k))^2 - |\Phi(k)|^2, \\ \begin{pmatrix} G(k) & F(k) \\ F^*(k) & -G(-k) \end{pmatrix} &= \begin{pmatrix} \frac{i\omega_n \mathrm{Z}(k) + \varepsilon(\mathbf{k}) + \mathrm{X}(k)}{D(k)} & \frac{\Phi(k)}{D(k)} \\ \frac{\Phi^*(k)}{D(k)} & \frac{i\omega_n \mathrm{Z}(k) - \varepsilon(\mathbf{k}) - \mathrm{X}(k)}{D(k)} \end{pmatrix}. \end{aligned}$$

The renormalization parameter $\mathrm{Z}(k)$, the energy shift $\mathrm{X}(k)$, and the gap parameter $\Phi(k)$ will be determined by the effective interactions constructed from the irreducible spin and charge susceptibilities. From the parametrization we have the relations

$$\mathrm{Y}(k) = \frac{1}{2}\left[\Sigma(k) - \Sigma(-k)\right], \quad \mathrm{X}(k) = \frac{1}{2}\left[\Sigma(k) + \Sigma(-k)\right],$$

which yields the symmetry properties

$$\mathrm{Y}(-k) = -\mathrm{Y}(k), \quad \mathrm{X}(-k) = \mathrm{X}(k).$$

Note that in the superconducting state, the self-consistent action becomes

$$S_{sc} = \beta \sum_{k\sigma} \left[\Sigma_\sigma(k)\bar{c}_\sigma(k)c_\sigma(k) + \Phi_\sigma(k)c_\sigma(k)c_{-\sigma}(-k) + \Phi^*_\sigma(k)\bar{c}_{-\sigma}(-k)\bar{c}_\sigma(k)\right] + \beta\bar{F}(G;v),$$

where the off-diagonal terms result from the condensation of Cooper pairs. Therefore, the anomalous self-energy Φ can serve as the superconducting order parameter.

As shown in the last section, fluctuation exchange approximation can also be considered as one of the modifications of the RPA, in the sense that the renormalized Fermion Green's functions are used in the evaluation of the irreducible susceptibility, effective interactions and the normal and anomalous self-energies in a self-consistent way. We have obtained the general formula for the normal self-energy in FLEX

$$\Sigma(k) = \sum_q V_n(q)G(k-q),$$

Similarly, the anomalous self-energy is expressed as

$$\Phi(k) = \sum_q V_a(q)F(k-q).$$

Here the summation is defined as $\sum_q = (T/N)\sum_{\mathbf{q},m}$. In the case of superconductivity arising from electron correlations, the irreducible vertex $V_a(q)$ in the particle-particle channel is derived from the many-body effects. In analogy with the electron-phonon mechanism, this vertex is regarded as the effective interaction for the pairing. It is considered that the unconventional superconductivity arises from the momentum dependence in the effective interaction $V_a(q)$. The theoretical search for the pairing mechanism is then reduced to the identification of the effective interaction.

In the superconducting state, due to the existence of the anomalous Green's function, there are more terms contributing to the fluctuation propagators. First, we want to find the irreducible correlation $\chi_r^0 = \langle r(11')\bar{r}(22')\rangle_{sc}^{connected}$. The irreducible charge correlation is calculated as

$$\begin{aligned}
&\langle d(11')d(22')\rangle_{sc}^{connected} \\
&= \frac{1}{2}\sum_{\sigma_1,\sigma_2}\left[-\langle c_{\sigma_1}(1')\bar{c}_{\sigma_2}(2)\rangle_{sc}\langle c_{\sigma_2}(2')\bar{c}_{\sigma_1}(1)\rangle_{sc} + \langle \bar{c}_{\sigma_1}(1)\bar{c}_{\sigma_2}(2)\rangle_{sc}\langle c_{\sigma_2}(2')c_{\sigma_1}(1')\rangle_{sc}\right] \\
&= \frac{1}{2}\sum_{\sigma}\left[-\langle c_{\sigma}(1')\bar{c}_{\sigma}(2)\rangle_{sc}\langle c_{\sigma}(2')\bar{c}_{\sigma}(1)\rangle_{sc} + \langle \bar{c}_{\sigma}(1)\bar{c}_{-\sigma}(2)\rangle_{sc}\langle c_{-\sigma}(2')c_{\sigma}(1')\rangle_{sc}\right] \\
&= -G(1'-2)G(2'-1) + F^*(1-2)F(2'-1').
\end{aligned}$$

where we have considered all possible contractions. And for the zero-component magnetic correlation we have

$$\begin{aligned}
&\langle m_0(11')m_0(22')\rangle_{sc}^{connected} \\
&= \frac{1}{2}\sum_{\sigma_1,\sigma_2}\left[-\sigma_1\sigma_2\langle c_{\sigma_1}(1')\bar{c}_{\sigma_2}(2)\rangle_{sc}\langle c_{\sigma_2}(2')\bar{c}_{\sigma_1}(1)\rangle_{sc} + \sigma_1\sigma_2\langle \bar{c}_{\sigma_1}(1)\bar{c}_{\sigma_2}(2)\rangle_{sc}\langle c_{\sigma_2}(2')c_{\sigma_1}(1')\rangle_{sc}\right] \\
&= \frac{1}{2}\sum_{\sigma}\left[-\langle c_{\sigma}(1')\bar{c}_{\sigma}(2)\rangle_{sc}\langle c_{\sigma}(2')\bar{c}_{\sigma}(1)\rangle_{sc} - \langle \bar{c}_{\sigma}(1)\bar{c}_{-\sigma}(2)\rangle_{sc}\langle c_{-\sigma}(2')c_{\sigma}(1')\rangle_{sc}\right] \\
&= -G(1'-2)G(2'-1) - F^*(1-2)F(2'-1'),
\end{aligned}$$

as well as other magnetic correlations

$$\begin{aligned}
&\langle m_{\pm}(11')m_{\mp}(22')\rangle_{sc}^{connected} \\
&= -\langle c_{-\sigma}(1')\,\bar{c}_{-\sigma}(2)\rangle_{sc}\langle c_{\sigma}(2')\bar{c}_{\sigma}(1)\rangle_{sc} - \langle \bar{c}_{\sigma}(1)\bar{c}_{-\sigma}(2)\rangle_{sc}\langle c_{-\sigma}(1')c_{\sigma}(2')\rangle_{sc} \\
&= -G(1'-2)G(2'-1) - F^*(1-2)F(1'-2').
\end{aligned}$$

In this case, the three magnetic correlations are identical.

If $\Phi(k) = \Phi(-k)$, $F(k) = F(-k)$, and $\Phi = \Phi^*$, $F^* = F$, we have the irreducible charge and spin susceptibilities in momentum space

$$\begin{aligned}
\chi_c^0(q) &= -\sum_k \left(G(k+q)G(k) - F(k+q)F(k)\right), \\
\chi_s^0(q) &= -\sum_k \left(G(k+q)G(k) + F(k+q)F(k)\right).
\end{aligned}$$

Note that the different relative sign in the charge and spin channel corresponding to the coherence factor giving the Hebel-Slichter peak in NMR and the coherence factor that gives rise to the magnetic resonance mode in INS, respectively. And due to $v_d = U,\ v_m = -U$ the charge- and spin-fluctuation propagators are simply

$$\begin{aligned}\chi_c(q) &= \frac{\chi_c^0(q)}{1+U\chi_c^0(q)},\\ \chi_s(q) &= \frac{\chi_s^0(q)}{1-U\chi_s^0(q)}.\end{aligned}$$

Next let us consider the self-energies in the superconducting state:

$$\begin{aligned}\Sigma(k) &= \sum_q V_n(q)G(k-q),\\ \Phi(k) &= \sum_q V_a(q)F(k-q).\end{aligned}$$

Essentially we need to evaluate the contribution from charge- and spin-fluctuation exchange channels to V_n and V_a. First we calculate the normal self-energy owing to the charge fluctuations by evaluating the interacting effect on the single particle propagator

$$\begin{aligned}G_\sigma(1-1') &= -\langle T_\tau c_\sigma(1)\bar{c}_\sigma(1')\rangle\\ &= -\sum_n \frac{(-1)^n}{n!}(\frac{1}{2})^n\langle c_\sigma(1)\, d(23)v_d d(45)\cdots d(67)v_d d(89)\,\bar{c}_\sigma(1')\rangle.\end{aligned}$$

In terms of fluctuation propagator we obtain

$$\begin{aligned}G_\sigma(1-1') &= \frac{1}{2}\sum_{\sigma_1,\sigma_2}(-1)^3\langle c_\sigma(1)\bar{c}_{\sigma_1}(2)\rangle\langle c_{\sigma_1}(3)\bar{c}_{\sigma_2}(8)\rangle\langle c_{\sigma_2}(9)\bar{c}_\sigma(1')\rangle v_d^2\langle d(45)d(67)\rangle_{FLEX}\\ &= G_\sigma(1-2)\left[\frac{1}{2}G_\sigma(3-8)v_d^2\chi_c(45,67)\right]G_\sigma(9-1'),\end{aligned}$$

which gives rise to the charge-fluctuation contribution

$$V_n^c(q) = \frac{1}{2}U^2\left[\chi_c(q)-\chi_c^0(q)\right] \equiv V^c(q).$$

We have subtracted the lowest-order term in the above expression as a separate evaluation of the $O(U^2)$ terms will be performed later. Then that owing to the spin-fluctuation is derived in

the same way

$$\begin{aligned} G_\sigma(1-1') &= -\langle T_\tau c_\sigma(1)\bar{c}_\sigma(1')\rangle \\ &= -\sum_n \frac{(-1)^n}{n!}(\frac{1}{2})^n \langle c_\sigma(1)\, m_0(23)v_m m_0(45)\cdots m_0(67)v_m m_0(89)\, \bar{c}_\sigma(1')\rangle \\ &= G_\sigma(1-2)\left[\frac{1}{2}G_\sigma(3-8)v_m^2\chi_s(45,67)\right] G_\sigma(9-1') \end{aligned}$$

which yields

$$V_n^{m_0}(q) = \frac{1}{2}U^2\left[\chi_s(q) - \chi_s^0(q)\right].$$

And

$$\begin{aligned} G_\sigma(1-1') &= -\langle T_\tau c_\sigma(1)\bar{c}_\sigma(1')\rangle \\ &= -\sum_n \frac{(-1)^n}{n!}(\frac{1}{2})^n \langle c_\sigma(1)\, m_\pm(23)v_m m_\mp(45)\cdots m_\pm(67)v_m m_\mp(89)\, \bar{c}_\sigma(1')\rangle \\ &= G_\sigma(1-2)\left[G_{-\sigma}(3-8)v_m^2\chi_s(45,67)\right] G_\sigma(9-1') \end{aligned}$$

yields

$$V_n^{m_\pm}(q) = U^2\left[\chi_s(q) - \chi_s^0(q)\right].$$

Therefore the total contribution from spin fluctuations is

$$V_n^s(q) = \frac{3}{2}U^2\left[\chi_s(q) - \chi_s^0(q)\right] \equiv V^s(q).$$

Again we have subtracted the lowest-order terms in the above expressions. Thus

$$V_n(q) = V_n^c + V_n^s = V^s(q) + V^c(q).$$

Note that we have not included the $O(U^2)$ terms here.

Now let us consider the anomalous interaction vertex V_n. Following the similar strategy, we consider the interaction effect of the charge-fluctuation exchange on the anomalous Green's function

$$\begin{aligned} F_\sigma(1-1') &= -\langle T_\tau c_\sigma(1)c_{-\sigma}(1')\rangle \\ &= -\sum_n \frac{(-1)^n}{n!}(\frac{1}{2})^n \langle c_\sigma(1)\, d(23)v_d d(45)\cdots d(67)v_d d(89)\, c_{-\sigma}(1')\rangle \end{aligned}$$

Similarly we have the contraction as

$$F_\sigma(1-1') = (-1)^3\frac{1}{2}\sum_{\sigma_1\sigma_2} -\langle c_\sigma(1)\bar{c}_{\sigma_1}(2)\rangle\langle c_{\sigma_1}(3)c_{\sigma_2}(9)\rangle\langle\bar{c}_{\sigma_2}(8)c_{-\sigma}(1')\rangle v_d^2\langle d(45)d(67)\rangle_{FLEX}$$
$$= G_\sigma(1-2)\left[-\frac{1}{2}F_\sigma(3-9)v_d^2\chi_c(45,67)\right]G^\dagger_{-\sigma}(8-1')$$

It indicates the charge-fluctuation contribution to the anomalous vertex

$$V_a^c(q) = -\frac{1}{2}U^2\left[\chi_c(q)-\chi_c^0(q)\right] = -V^c(q),$$

where the lowest order term has been subtracted. And the interaction effect of spin-fluctuation exchange is given by

$$F_\sigma(1-1') = -\langle T_\tau c_\sigma(1)c_{-\sigma}(1')\rangle$$
$$= -\sum_n \frac{(-1)^n}{n!}(\frac{1}{2})^n\langle c_\sigma(1)\, m_0(23)v_m m_0(45)\cdots m_0(67)v_m m_0(89)\, c_{-\sigma}(1')\rangle$$
$$= G_\sigma(1-2)\left[\frac{1}{2}F_\sigma(3-9)v_m^2\chi_s(45,67)\right]G^\dagger_{-\sigma}(8-1'),$$

which yields

$$V_a^{m_0}(q) = \frac{1}{2}U^2\left[\chi_s(q)-\chi_s^0(q)\right].$$

As well as

$$F_\sigma(1-1') = -\langle T_\tau c_\sigma(1)c_{-\sigma}(1')\rangle$$
$$= -\sum_n \frac{(-1)^n}{n!}(\frac{1}{2})^n\langle c_\sigma(1)\, m_\pm(23)v_m m_\mp(45)\cdots m_\pm(67)v_m m_\mp(89)\, c_{-\sigma}(1')\rangle$$
$$= G_\sigma(1-2)\left[F_\sigma(9-3)v_m^2\chi_s(45,67)\right]G^\dagger_{-\sigma}(8-1')$$

indicates

$$V_a^{m_\pm}(q) = U^2\left[\chi_s(q)-\chi_s^0(q)\right].$$

Therefore the total contribution from spin-fluctuation exchange is

$$V_a^s(q) = \frac{3}{2}U^2\left[\chi_s(q)-\chi_s^0(q)\right] = V^s(q).$$

Thus we have

$$V_a(q) = V^s(q) - V^c(q).$$

Note that here we have subtracted the lowest order out, which will be evaluated separately. The subtracted terms remove a double counting that occurs in second order.

The above expressions contain the order of $O(U^3)$ and higher-order contributions. What left are the two lowest order parts including the order of $O(U)$, the Hartree-Fock self-energy, and the second order diagrams. Since the Hartree-Fock term is momentum and frequency independent, it can be treated as a renormalization of the chemical potential μ.

On the order of $O(U^2)$, the related terms are

$$U^2\bar{c}_{\sigma_1}(1)\bar{c}_{\sigma_1'}(1)c_{\sigma_1'}(1)c_{\sigma_1}(1)\bar{c}_{\sigma_2}(2)\bar{c}_{\sigma_2'}(2)c_{\sigma_2'}(2)c_{\sigma_2}(2) = U^2\bar{c}_{\sigma}(1)\langle\bar{c}_{\sigma_1'}(1)c_{\sigma_1'}(1)c_{\sigma}(1)\bar{c}_{\sigma}(2)\bar{c}_{\sigma_2'}(2)c_{\sigma_2'}(2)\rangle c_{\sigma}(2),$$

where the three-particle correlation can be decoupled in the normal propagator channel

$$\begin{aligned}
&\langle\bar{c}_{\sigma_1'}(1)c_{\sigma_1'}(1)c_{\sigma}(1)\bar{c}_{\sigma}(2)\bar{c}_{\sigma_2'}(2)c_{\sigma_2'}(2)\rangle \\
&= -\langle c_{\sigma_2'}(2)\bar{c}_{\sigma_1'}(1)\rangle\left[\langle c_{\sigma}(1)\bar{c}_{\sigma}(2)\rangle\langle c_{\sigma_1'}(1)\bar{c}_{\sigma_2'}(2)\rangle - \langle c_{\sigma_1'}(1)\bar{c}_{\sigma}(2)\rangle\langle c_{\sigma}(1)\bar{c}_{\sigma_2'}(2)\rangle\right] \\
&= G(1-2)\left[-G(2-1)G(1-2)\right]
\end{aligned}$$

and in the anomalous channel

$$\begin{aligned}
&\langle\bar{c}_{\sigma_1'}(1)c_{\sigma_1'}(1)c_{\sigma}(1)\bar{c}_{\sigma}(2)\bar{c}_{\sigma_2'}(2)c_{\sigma_2'}(2)\rangle \\
&= \langle\bar{c}_{\sigma_1'}(1)\bar{c}_{\sigma_2'}(2)\rangle\langle c_{\sigma}(1)\bar{c}_{\sigma}(2)\rangle\langle c_{\sigma_2'}(2)c_{\sigma_1'}(1)\rangle - \langle\bar{c}_{\sigma_1'}(1)\bar{c}_{\sigma_2'}(2)\rangle\langle c_{\sigma_1'}(1)\bar{c}_{\sigma}(2)\rangle\langle c_{\sigma_2'}(2)c_{\sigma}(1)\rangle \\
&- \langle\bar{c}_{\sigma}(2)\bar{c}_{\sigma_1'}(1)\rangle\langle c_{\sigma}(1)\bar{c}_{\sigma_2'}(2)\rangle\langle c_{\sigma_1'}(1)c_{\sigma_2'}(2)\rangle - \langle\bar{c}_{\sigma}(2)\bar{c}_{\sigma_1'}(1)\rangle\langle c_{\sigma_1'}(1)\bar{c}_{\sigma_2'}(2)\rangle\langle c_{\sigma_2'}(2)c_{\sigma}(1)\rangle \\
&= G(1-2)\left[-F^*(1-2)F(2-1)\right].
\end{aligned}$$

Therefore we obtain the second-order normal self-energy

$$\Sigma^{(2)}(k) = \sum_q\left[U^2\left(-\sum_{k'}\left[G(k'+q)G(k') + F(k'+q)F(k')\right]\right)\right]G(k-q).$$

This gives the second-order contribution to the normal effective interaction

$$V_n^{(2)}(q) = U^2\chi_s^0(q).$$

In similar procedure, it can be shown that the second-order contribution to the anomalous effective interaction takes the same form

$$V_a^{(2)}(q) = U^2\chi_s^0(q).$$

Finally we have all-order contributions, with the $O(U^3)$ and higher-order contribution under FLEX approximation in mind, to the normal and anomalous effective interaction vertices as

$$\begin{aligned} V_n(q) &= V_s(q) + V_c(q), \\ V_a(q) &= V_s(q) - V_c(q). \end{aligned}$$

Here the spin- and charge-interaction vertices are redefined to include the $O(U^2)$ parts as

$$\begin{aligned} V_s(q) &\equiv \frac{3}{2}U^2 \frac{\chi_s^0(q)}{1 - U\chi_s^0(q)} - \frac{1}{2}U^2\chi_s^0(q), \\ V_c(q) &\equiv \frac{1}{2}U^2 \frac{\chi_c^0(q)}{1 + U\chi_c^0(q)} - \frac{1}{2}U^2\chi_c^0(q). \end{aligned}$$

Note that if we approach the superconducting transition from the normal state: $\chi_s^0 = \chi_c^0 = \chi^0$, we see that

$$\begin{aligned} V_n(q) &= \frac{3}{2}U^2 \frac{\chi_s^0(q)}{1 - U\chi_s^0(q)} - \frac{1}{2}U^2\chi_s^0(q) + \frac{1}{2}U^2 \frac{\chi_c^0(q)}{1 + U\chi_c^0(q)} - \frac{1}{2}U^2\chi_c^0(q) \\ &\to \frac{3}{2}U^2 \frac{\chi^0(q)}{1 - U\chi^0(q)} + \frac{1}{2}U^2 \frac{\chi^0(q)}{1 + U\chi^0(q)} - U^2\chi^0(q) \end{aligned}$$

and

$$\begin{aligned} V_a(q) &= \frac{3}{2}U^2 \frac{\chi_s^0(q)}{1 - U\chi_s^0(q)} - \frac{1}{2}U^2\chi_s^0(q) - \frac{1}{2}U^2 \frac{\chi_c^0(q)}{1 + U\chi_c^0(q)} + \frac{1}{2}U^2\chi_c^0(q) \\ &\to \frac{3}{2}U^2 \frac{\chi^0(q)}{1 - U\chi^0(q)} - \frac{1}{2}U^2 \frac{\chi^0(q)}{1 + U\chi^0(q)} \end{aligned}$$

Those are the expressions in the normal state. Clearly the second-order subtraction is cancelled in the anomalous interaction. However, if we approach the transition from the superconducting state: $\chi_s^0 \neq \chi_c^0$, we have

$$\begin{aligned} V_n(q) &= \frac{3}{2}U^2 \frac{\chi_s^0(q)}{1 - U\chi_s^0(q)} + \frac{1}{2}U^2 \frac{\chi_c^0(q)}{1 + U\chi_c^0(q)} - \frac{1}{2}U^2 \left[\chi_s^0(q) + \chi_c^0(q)\right], \\ V_a(q) &= \frac{3}{2}U^2 \frac{\chi_s^0(q)}{1 - U\chi_s^0(q)} - \frac{1}{2}U^2 \frac{\chi_c^0(q)}{1 + U\chi_c^0(q)} - \frac{1}{2}U^2 \left[\chi_s^0(q) - \chi_c^0(q)\right]. \end{aligned}$$

In this case the second-order subtraction is not cancelled due to the non-vanishing $F(k)$, since

$$\begin{aligned} \frac{1}{2}U^2 \left[\chi_s^0(q) + \chi_c^0(q)\right] &= -U^2 \sum_k G(k+q)G(k), \\ \frac{1}{2}U^2 \left[\chi_s^0(q) - \chi_c^0(q)\right] &= -U^2 \sum_k F(k+q)F(k). \end{aligned}$$

In the above, we have derived all the analytical expressions for the many-body quantities in the superconducting state under FLEX approximation in the single-band Hubbard model on a square lattice. The next step is to numerically evaluate these quantities and to study the characteristics of the magnetic and superconducting properties when the microscopic parameters are varied. Our numerical work found the well-known d-wave solution for the single-band Hubbard model.

2.2.4 Numerical Solution: d-wave Superconductivity

We briefly list the numerical steps in below. Please refer to Appendix B.1 for the relevant numerical tricks.

1. Choose the parameters t, U, T, and n.

2. Set a starting value for the normal self-energy, e.g., $\Sigma_{\mathbf{k}}(\omega_n) = -i\Gamma sign(\omega_n)$. It is even possible to start with $\Sigma_{\mathbf{k}}(\omega_n) = 0$ as the Green's function on the imaginary axis is always well defined. And set the trial anomalous self-energy $\Phi_{\mathbf{k}}(\omega_n)$ according to a certain symmetry, e.g., s-wave or d-wave.

3. Determine the Green's functions $G_{\mathbf{k}}(\omega_n)$ and $F_{\mathbf{k}}(\omega_n)$.

4. Using $n = 1 + \frac{1}{N^2}\sum_{\mathbf{k}} G_{\mathbf{k}}(\tau^+) = 1 + \frac{T}{N^2}\sum_{\mathbf{k},n} G_{\mathbf{k}}(\omega_n)$ determine the chemical potential μ to obtain the correct particle number n. Start with an initial value of the chemical potential chosen such that the corresponding Green's function $G_{\mathbf{k}}(\omega_n;\mu)$ yields the desired number of carries at each stage of the iteration.

5. Determine $G_{\mathbf{i}}(\tau)$ and $F_{\mathbf{i}}(\tau)$ via Fourier transform and determine $\chi^s_{\mathbf{i}}(\tau) = -G_{\mathbf{i}}(\tau)G_{\mathbf{i}}(-\tau) - F_{\mathbf{i}}(\tau)F_{\mathbf{i}}(\tau)$ and $\chi^c_{\mathbf{i}}(\tau) = -G_{\mathbf{i}}(\tau)G_{\mathbf{i}}(-\tau) + F_{\mathbf{i}}(\tau)F_{\mathbf{i}}(\tau)$.

6. Fourier transform $\chi^{s,c}_{\mathbf{i}}(\tau)$ back to momentum and energy space to obtain $\chi^{s,c}_{\mathbf{q}}(\nu_m)$.

7. Determine $V_n(\mathbf{q},\nu_m)$ and $V_a(\mathbf{q},\nu_m)$.

8. Fourier transform $V_{n,a}(\mathbf{q},\nu_m)$ to obtain $V_{n,a}(\mathbf{i},\tau)$ and determine the self-energies $\Sigma(\mathbf{i},\tau) = G(\mathbf{i},\tau)V_n(\mathbf{i},\tau)$ and $\Phi(\mathbf{i},\tau) = F(\mathbf{i},\tau)V_a(\mathbf{i},\tau)$.

9. Fourier transform $\Sigma(\mathbf{i},\tau)$, $\Phi(\mathbf{i},\tau)$ back to $\Sigma(\mathbf{k},\omega_n)$, $\Phi(\mathbf{k},\omega_n)$ and check whether they are indentical to the results of the previous iteration. If yes, finish the calculation. If not, go to item 3.

The above loop is iterated until the relative difference between the new self-energy matrix element and the old one is less than 10^{-6}. Then the convergence is considered to be achieved. The form of the survival anomalous self-energy indicates the allowed superconducting order parameter symmetry and by observing its decay with rising temperature we can identify the corresponding transition temperature. Meanwhile, the resultant susceptibility delivers the information of the fluctuation type that drives the superconductivity.

Now we show the numerical solution solved for the superconducting state of single-band Hubbard model on square lattice. It turns out that the system develops strong antiferromagnetic spin correlation at (π, π) and supports a d-wave superconducting state with sign change between different pieces of the Fermi surface. The effective pairing interaction V_a is dominated by spin-fluctuation exchange. Figure 2.2 shows the static spin susceptibility $\chi^s(\mathbf{q}, 0)$ in the superconducting state, which is peaked at (π, π) in the normal state but becomes incommensurate in the superconducting state. The finite order parameter $\Phi(\mathbf{q}, \pi T)$ is shown in Fig. 2.3 with an intraband sign-reverse feature.

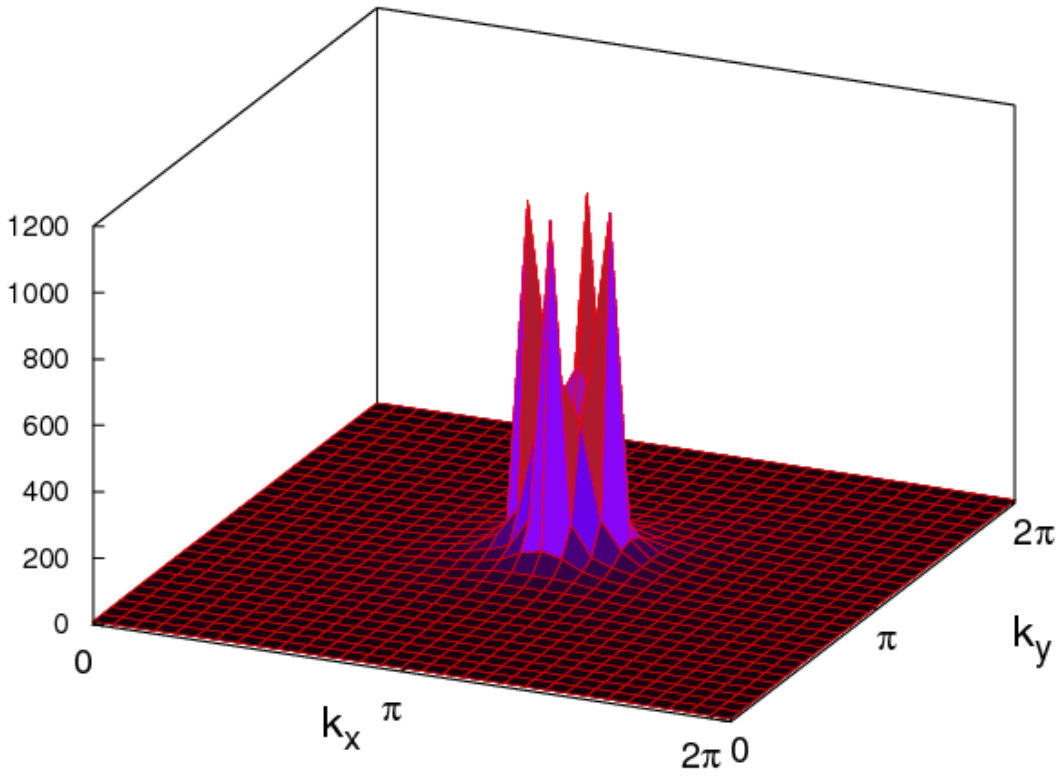

Figure 2.2 Plot of $\chi(\mathbf{q}, 0)$ in the superconducting state of the single-band Hubbard model on a square lattice. The antiferromagnetic spin fluctuation centered at (π, π) in the normal state becomes incommensurate below T_c.

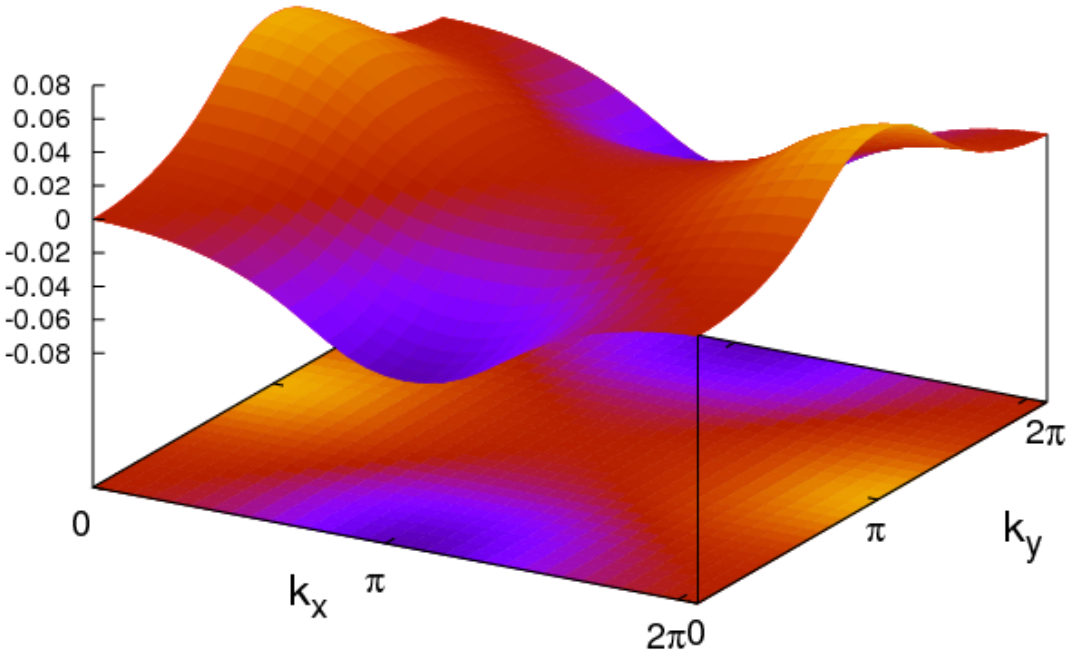

Figure 2.3 The superconducting order parameter in the single-band Hubbard model on a square lattice. It exhibits d-wave symmetry with sign change by 90 degree rotation.

CHAPTER 3. MULTIORBITAL FLEX FORMALISM: THE SUPERCONDUCTING STATE

In this chapter we present a detailed derivation of the FLEX formula in 2D multi-orbital Hubbard model and apply it to explore the possibility of fluctuation-induced superconductivity in FeAs-based superconductors. It can easily be extended to other multi-band Hubbard superconductors. The appearance of orbital degrees of freedom requires more careful treatment since all the quantities and expressions have complicated structures now due to orbital dependence. And accordingly, the physics becomes richer with the additional orbital-fluctuation channel and more types of microscopic interactions.

3.1 Unperturbed Hamiltonian

In the multi-orbital Hubbard model, the quadratic Hamiltonian is expressed through a tight-binding description

$$H_0 = \sum_{ij,ab,\sigma} (-t_{ij}^{ab} - \mu\delta_{ij}\delta^{ab}) d_{ia\sigma}^{\dagger} d_{jb\sigma},$$

where $d_{i,a,\sigma}$ is the annihilation operator of electrons in orbital a with spin σ on site i, t_{ij}^{ab} represents the hopping of electron with spin σ from obital b on site j to obital a on site i, and the chemical potential is μ. This yields in momentum space

$$H_0 = \sum_{\mathbf{k},ab,\sigma} \left(\varepsilon_{\mathbf{k}}^{ab} - \mu\delta^{ab}\right) d_{\mathbf{k}a\sigma}^{\dagger} d_{\mathbf{k}b\sigma}.$$

For a two-orbital problem, which is the simplest multi-orbital model, diagonalizing the Hamiltonian gives the dispersions of two bands, if $\varepsilon^{12} = \varepsilon^{21}$, as

$$E_{\mathbf{k}}^{\pm} = \varepsilon_{\mathbf{k}}^{+} \pm \sqrt{\left(\varepsilon_{\mathbf{k}}^{-}\right)^2 + \left(\varepsilon_{\mathbf{k}}^{12}\right)^2} - \mu$$

where

$$\varepsilon_{\mathbf{k}}^{+}=\frac{1}{2}\left(\varepsilon_{\mathbf{k}}^{11}+\varepsilon_{\mathbf{k}}^{22}\right),\quad \varepsilon_{\mathbf{k}}^{-}=\frac{1}{2}\left(\varepsilon_{\mathbf{k}}^{11}-\varepsilon_{\mathbf{k}}^{22}\right).$$

The quadratic coefficient of the Hamiltonian determines the inverse of the bare single-particle Green's function,

$$\tilde{G}^{0}(\mathbf{k},i\omega_n)^{-1}=i\omega_n\tilde{\mathbf{1}}-\left(\tilde{\varepsilon}_{\mathbf{k}}-\mu\tilde{\mathbf{1}}\right).$$

where $det\left(G^{0}\right)^{-1}=(i\omega_n-E^{+})(i\omega_n-E^{-})$. Thus the Green's function can be explicitly written as a matrix in the orbital space

$$\mathbb{G}^{0}(\mathbf{k},i\omega_n)=\begin{bmatrix} \frac{i\omega_n-(\varepsilon_{\mathbf{k}}^{11}-\mu)}{(i\omega_n-E_{\mathbf{k}}^{+})(i\omega_n-E_{\mathbf{k}}^{-})} & \frac{-\varepsilon_{\mathbf{k}}^{12}}{(i\omega_n-E_{\mathbf{k}}^{+})(i\omega_n-E_{\mathbf{k}}^{-})} \\ \\ \frac{-\varepsilon_{\mathbf{k}}^{21}}{(i\omega_n-E_{\mathbf{k}}^{+})(i\omega_n-E_{\mathbf{k}}^{-})} & \frac{i\omega_n-(\varepsilon_{\mathbf{k}}^{22}-\mu)}{(i\omega_n-E_{\mathbf{k}}^{+})(i\omega_n-E_{\mathbf{k}}^{-})} \end{bmatrix}.$$

Since $\varepsilon^{12}=\varepsilon^{21}$, the non-interacting Green's function is symmetric in orbital space $G_0^{ab}=G_0^{ba}$. In the compact form we can write the non-interacting Green's function as

$$\tilde{G}^{0}(\mathbf{k},i\omega_n)=\frac{\left(i\omega_n-(\varepsilon_{\mathbf{k}}^{+}-\mu)\right)\tilde{\mathbf{1}}-\varepsilon_{\mathbf{k}}^{-}\tilde{\tau}_3-\varepsilon_{\mathbf{k}}^{12}\tilde{\tau}_1}{\left(i\omega_n-E_{\mathbf{k}}^{+}\right)\left(i\omega_n-E_{\mathbf{k}}^{-}\right)}.$$

3.2 Interaction Hamiltonian

We start with a general multi-orbital Hubbard interaction,

$$H_{int}=\frac{1}{4}\sum_{i;a_1a_2a_3a_4;\sigma_1\sigma_2\sigma_3\sigma_4}U_{\sigma_1\sigma_2\sigma_3\sigma_4}^{a_1a_2a_3a_4}d_{i,a_1\sigma_1}^{\dagger}d_{i,a_2\sigma_2}^{\dagger}d_{i,a_3\sigma_3}d_{i,a_4\sigma_4}.$$

The prefactor $\frac{1}{4}$ is to eliminate the symmetry of $1\longleftrightarrow 2$ and $3\longleftrightarrow 4$. Due to the SU(2) symmetry in spin space, the interaction potential can be typically parametrized as

$$U_{\sigma_1\sigma_2\sigma_3\sigma_4}^{a_1a_2a_3a_4}=-\frac{1}{2}U_s^{a_1a_4,a_2a_3}\boldsymbol{\tau}_{\sigma_1\sigma_4}\cdot\boldsymbol{\tau}_{\sigma_2\sigma_3}+\frac{1}{2}U_c^{a_1a_4,a_2a_3}\delta_{\sigma_1\sigma_4}\delta_{\sigma_2\sigma_3}$$

where U_s and U_c are two scalar potentials, which, if ignoring spin-orbit coupling, are defined as

$$U_s^{a_1a_4,a_2a_3}=\begin{cases} U & \text{if } a_1=a_2=a_3=a_4 \\ U' & \text{if } a_1=a_3\neq a_2=a_4 \\ J_H & \text{if } a_1=a_4\neq a_2=a_3 \\ J' & \text{if } a_1=a_2\neq a_3=a_4 \end{cases}$$

and

$$U_c^{a_1a_4,a_2a_3} = \begin{cases} U & \text{if } a_1 = a_2 = a_3 = a_4 \\ -U' + 2J_H & \text{if } a_1 = a_3 \neq a_2 = a_4 \\ 2U' - J_H & \text{if } a_1 = a_4 \neq a_2 = a_3 \\ J' & \text{if } a_1 = a_2 \neq a_3 = a_4 \end{cases}$$

Notice that $U_{s,c}^{a_1a_4,a_2a_3}$ are invariant under the exchange of any two set of indices such as $1 \longleftrightarrow 2\bigcap 3 \longleftrightarrow 4$, $1 \longleftrightarrow 3\bigcap 2 \longleftrightarrow 4$ and $1 \longleftrightarrow 4\bigcap 2 \longleftrightarrow 3$, that is, in group language, they are invariant under the following permutations of indices (12)(34), (13)(24) and (14)(23). Also $1 \longleftrightarrow 2$ is equivalent to $3 \longleftrightarrow 4$, etc, and the following equalities hold

$$\begin{aligned} \frac{1}{2}(3U_s - U_c)^{1234} &= U_c^{2134} = U_c^{1243}, \\ \frac{1}{2}(U_s + U_c)^{1234} &= U_s^{2134} = U_s^{1243}, \\ 2U_s^{1234} - U_s^{1243} &= U_c^{1243} = \frac{1}{2}(3U_s - U_c)^{1234}. \end{aligned}$$

By making use of the SU(2) identity

$$\boldsymbol{\tau}_{\sigma_1\sigma_4} \cdot \boldsymbol{\tau}_{\sigma_2\sigma_3} = 2\delta_{\sigma_1\sigma_3}\delta_{\sigma_2\sigma_4} - \delta_{\sigma_1\sigma_4}\delta_{\sigma_2\sigma_3},$$

the interaction potential becomes

$$U_{\sigma_1\sigma_2\sigma_3\sigma_4}^{a_1a_2a_3a_4} = -U_s^{a_1a_4,a_2a_3}\delta_{\sigma_1\sigma_3}\delta_{\sigma_2\sigma_4} + \frac{1}{2}\left(U_s^{a_1a_4,a_2a_3} + U_c^{a_1a_4,a_2a_3}\right)\delta_{\sigma_1\sigma_4}\delta_{\sigma_2\sigma_3}.$$

Then the Hamiltonian can be expressed as

$$\begin{aligned} H_{int} &= \frac{1}{4}\sum\left[-U_s^{a_1a_2a_3a_4} d_{i,a_1\sigma}^\dagger d_{i,a_2\sigma'}^\dagger d_{i,a_3\sigma} d_{i,a_4\sigma'} + \frac{1}{2}\left(U_s^{a_1a_2a_3a_4} + U_c^{a_1a_2a_3a_4}\right) d_{i,a_1\sigma}^\dagger d_{i,a_2\sigma'}^\dagger d_{i,a_3\sigma'} d_{i,a_4\sigma}\right] \\ &= \frac{1}{2}\sum U_s^{a_1a_2a_3a_4} d_{i,a_1\sigma}^\dagger d_{i,a_3\sigma} d_{i,a_2\sigma'}^\dagger d_{i,a_4\sigma'} \end{aligned}$$

where we used the identity

$$\frac{1}{2}\left(U_s + U_c\right)^{a_1a_2a_3a_4} = U_s^{a_1a_2a_4a_3}.$$

Or more physically we can express it as

$$\begin{aligned} H_{int} &= \frac{1}{2}\sum_{i,a\neq b,\sigma\sigma'}\left[U\, n_{ia\sigma}n_{ia\sigma'} + U' n_{ia\sigma}n_{ib\sigma'} - J_H d_{i,a\sigma}^\dagger d_{i,a\sigma'} d_{i,b\sigma'}^\dagger d_{i,b\sigma} + J' d_{i,a\sigma}^\dagger d_{i,a\sigma'}^\dagger d_{i,b\sigma'} d_{i,b\sigma}\right] \\ &= U\sum_{i,a} n_{ia\uparrow}n_{ia\downarrow} + U'\sum_{i,a>b} n_{ia}n_{ib} - J_H\sum_{i,a>b}\left(2\mathbf{S}_{ia}\cdot\mathbf{S}_{ib} + \frac{1}{2}n_{ia}n_{ib}\right) + J'\sum_{i,a\neq b} d_{i,a\uparrow}^\dagger d_{i,a\downarrow}^\dagger d_{i,b\downarrow} d_{i,b\uparrow} \end{aligned}$$

through the relations

$$\begin{aligned}\frac{1}{2}n_a n_b + 2S_a^z S_b^z &= \frac{1}{2}\sum_{\sigma\sigma'}(1+\sigma\sigma')d^\dagger_{a\sigma}d_{a\sigma}d^\dagger_{b\sigma'}d_{b\sigma'} \\ &= \sum_{\sigma} d^\dagger_{a\sigma}d_{a\sigma}d^\dagger_{b\sigma}d_{b\sigma},\end{aligned}$$

and

$$\begin{aligned}2\left(S_a^x S_b^x + S_a^y S_b^y\right) &= \frac{1}{2}\sum_{\sigma\sigma'}(1-\sigma\sigma')d^\dagger_{a\sigma}d_{a\bar{\sigma}}d^\dagger_{b\sigma'}d_{b\bar{\sigma'}} \\ &= \sum_{\sigma} d^\dagger_{a\sigma}d_{a\bar{\sigma}}d^\dagger_{b\bar{\sigma}}d_{b\sigma}.\end{aligned}$$

Then the physical Hamiltonian is writen as

$$H_{int} = U\sum_{i,a} n_{ia\uparrow}n_{ia\downarrow} + U'\sum_{i,a>b} n_{ia}n_{ib} - J_H\sum_{i,a>b}\left(2\mathbf{S}_{ia}\cdot\mathbf{S}_{ib} + \frac{1}{2}n_{ia}n_{ib}\right) + J'\sum_{i,a\neq b} d^\dagger_{i,a\uparrow}d^\dagger_{i,a\downarrow}d_{i,b\downarrow}d_{i,b\uparrow}. \tag{3.1}$$

Clearly, the on-site interactions contain intra-orbital and inter-orbital Coulomb repulsions U, U', Hund's rule coupling J_H, and the inter-orbital pair hopping term J'. Besides the usual intra-orbital interaction, the last three terms are all between different orbitals.

But in order to simplify the calculation we use different equivalent form of the interaction Hamiltonian for different derivations later. To evaluate the low-order diagrams in perturbation theory, we adopt the form

$$H_{int} = \frac{1}{2}\sum_{i,a_i,\sigma\sigma'} U_s^{a_1a_2a_3a_4} d^\dagger_{i,a_1\sigma}d_{i,a_3\sigma}d^\dagger_{i,a_2\sigma'}d_{i,a_4\sigma'} \tag{3.2}$$

and to derive the FLEX interaction vertices we apply the following form

$$H_{int} = \frac{1}{2}\sum_{\mathbf{q},a_i,\alpha}\left[b_{a_1a_4}(\mathbf{q})U_c^{a_1a_4,a_2a_3}b_{a_2a_3}(-\mathbf{q}) + m^\alpha_{a_1a_4}(\mathbf{q})\left(-U_s^{a_1a_4,a_2a_3}\right)m^\alpha_{a_2a_3}(-\mathbf{q})\right] \tag{3.3}$$

where $\alpha = x,\ y,\ z$, $b_{ab}(\mathbf{q})$ and $m^\alpha_{ab}(\mathbf{q})$ are charge- and spin-fluctuation type operators which are defined as

$$b_{ab}(\mathbf{q}) = \frac{1}{\sqrt{2}}\sum_{\mathbf{k},\sigma} d^\dagger_{\mathbf{k},a\sigma}d_{\mathbf{k}+\mathbf{q},b\sigma},$$

and

$$m^z_{ab}(\mathbf{q}) = \frac{1}{\sqrt{2}}\sum_{\mathbf{k},\sigma} \sigma d^\dagger_{\mathbf{k},a\sigma}d_{\mathbf{k}+\mathbf{q},b\sigma},$$

$$m^x_{ab}(\mathbf{q}) = \frac{1}{\sqrt{2}}\sum_{\mathbf{k},\sigma} d^\dagger_{\mathbf{k},a\sigma} d_{\mathbf{k}+\mathbf{q},b\bar{\sigma}},$$

$$m^y_{ab}(\mathbf{q}) = \frac{1}{\sqrt{2}}\sum_{\mathbf{k},\sigma} (-i\sigma) d^\dagger_{\mathbf{k},a\sigma} d_{\mathbf{k}+\mathbf{q},b\bar{\sigma}}.$$

Note that since the orbital a, b in the fluctuation variable could be different, the above definitions are generalized charge- and spin-fluctuation variables. b_{ab} is sometimes called orbital fluctuation in the literature and m_{ab} for $a \neq b$ sometimes called higher-order moment fluctuations.

Here we show how we can achieve the effective interaction Hamiltonian in terms of fluctuations (3.3). The interaction may be rewritten in four different ways to simplify perturbation theory in the various channels. (1) For equal-spin particle-hole scattering, considering all the contributions from the Hamiltonian, effectively we have

$$\begin{aligned} H_{int} &= \frac{1}{2}\sum_{i,a_i,\sigma\sigma'} U_s^{a_1a_2a_3a_4} d^\dagger_{i,a_1\sigma} d_{i,a_3\sigma} d^\dagger_{i,a_2\sigma'} d_{i,a_4\sigma'} \\ &= \frac{1}{2}\sum_{i,a_i} U_s^{a_1a_2a_3a_4} \left(2b_{i,a_1a_3} b_{i,a_2a_4} - \sum_\sigma d^\dagger_{i,a_1\sigma} d_{i,a_4\sigma} d^\dagger_{i,a_2\sigma} d_{i,a_3\sigma} \right) \\ &= \frac{1}{2}\sum_{i,a_i} \left(2U_s^{a_1a_2a_4a_3} - U_s^{a_1a_2a_3a_4}\right) b_{i,a_1a_4} b_{i,a_2a_3} + m^z_{i,a_1a_4}(-U_s^{a_1a_2a_3a_4}) m^z_{i,a_2a_3}. \end{aligned}$$

Since the relation $2U_s^{1243} - U_s^{1234} = U_c^{1234}$ holds it becomes

$$H_{int} == \frac{1}{2}\sum_{i,a_i} b_{i,a_1a_4} \left(U_c^{a_1a_2a_3a_4}\right) b_{i,a_2a_3} + m^z_{i,a_1a_4} \left(-U_s^{a_1a_2a_3a_4}\right) m^z_{i,a_2a_3}.$$

(2) For opposite-spin particle-hole scattering we have

$$\begin{aligned} H_{int} &= \frac{1}{2}\sum_{i,a_i,\sigma\sigma'} U_s^{a_1a_2a_3a_4} d^\dagger_{i,a_1\sigma} d_{i,a_3\sigma} d^\dagger_{i,a_2\sigma'} d_{i,a_4\sigma'} \\ &= \frac{1}{2}\sum_{i,a_i,\sigma} -U_s^{a_1a_2a_3a_4} d^\dagger_{i,a_1\sigma} d_{i,a_4\bar{\sigma}} d^\dagger_{i,a_2\bar{\sigma}} d_{i,a_3\sigma} + (\text{residual}) \\ &= \frac{1}{2}\sum_{i,a_i} m^+_{i,a_1a_4} \left(-U_s^{a_1a_2a_3a_4}\right) m^-_{i,a_2a_3} + m^-_{i,a_1a_4} \left(-U_s^{a_1a_2a_3a_4}\right) m^+_{i,a_2a_3} + (\text{residual}) \end{aligned}$$

where

$$m^+_{i,ab} = d^\dagger_{i,a\uparrow} d_{i,b\downarrow}, \quad m^-_{i,ab} = d^\dagger_{i,a\downarrow} d_{i,b\uparrow}.$$

Thus in momentum space we have the following effective interaction Hamiltonian

$$H_{int} = \frac{1}{2}\sum_{\mathbf{q},a_i}[b_{a_1a_4}(\mathbf{q})\,(U_c^{a_1a_4,a_2a_3})\,b_{a_2a_3}(-\mathbf{q}) + m^z_{a_1a_4}(\mathbf{q})\,(-U_s^{a_1a_4,a_2a_3})\,m^z_{a_2a_3}(-\mathbf{q}) + m^+_{a_1a_4}(\mathbf{q})\,(-U_s^{a_1a_4,a_2a_3})\,m^-_{a_2a_3}(-\mathbf{q}) + m^-_{a_1a_4}(\mathbf{q})\,(-U_s^{a_1a_4,a_2a_3})\,m^+_{a_2a_3}(-\mathbf{q})]$$

Here and later we group the orbital indices as $14, 23$ in $U_{s,c}^{a_1a_2a_3a_4}$.

3.3 Fluctuation Variables

In order to evaluate the interaction mediated by fluctuation exchange, we define two types of electronic fluctuations, density or charge and spin fluctuations, in momentum space. There are two equivalent set of definitions, either in the $\pm$ representation for the transverse spin fluctuations

$$b_{ab}(\mathbf{q},\tau) = \frac{1}{\sqrt{2}}\sum_{\mathbf{k},\sigma} d^\dagger_{\mathbf{k},a\sigma}(\tau)d_{\mathbf{k}+\mathbf{q},b\sigma}(\tau),$$

$$m^0_{ab}(\mathbf{q},\tau) = \frac{1}{\sqrt{2}}\sum_{\mathbf{k},\sigma} \sigma d^\dagger_{\mathbf{k},a\sigma}(\tau)d_{\mathbf{k}+\mathbf{q},b\sigma}(\tau),$$

$$m^+_{ab}(\mathbf{q},\tau) = \sum_{\mathbf{k}} d^\dagger_{\mathbf{k},a\uparrow}(\tau)d_{\mathbf{k}+\mathbf{q},b\downarrow}(\tau),$$

$$m^-_{ab}(\mathbf{q},\tau) = \sum_{\mathbf{k}} d^\dagger_{\mathbf{k},a\downarrow}(\tau)d_{\mathbf{k}+\mathbf{q},b\uparrow}(\tau),$$

or in the (x, y) representation for the transverse part

$$b_{ab}(\mathbf{q},\tau) = \frac{1}{\sqrt{2}}\sum_{\mathbf{k},\sigma} d^\dagger_{\mathbf{k},a\sigma}(\tau)d_{\mathbf{k}+\mathbf{q},b\sigma}(\tau),$$

$$m^z_{ab}(\mathbf{q},\tau) = \frac{1}{\sqrt{2}}\sum_{\mathbf{k},\sigma} \sigma d^\dagger_{\mathbf{k},a\sigma}(\tau)d_{\mathbf{k}+\mathbf{q},b\sigma}(\tau),$$

$$m^x_{ab}(\mathbf{q},\tau) = \frac{1}{\sqrt{2}}\sum_{\mathbf{k},\sigma} d^\dagger_{\mathbf{k},a\sigma}(\tau)d_{\mathbf{k}+\mathbf{q},b\bar{\sigma}}(\tau),$$

$$m^y_{ab}(\mathbf{q},\tau) = \frac{1}{\sqrt{2}}\sum_{\mathbf{k},\sigma} (-i\sigma) d^\dagger_{\mathbf{k},a\sigma}(\tau)d_{\mathbf{k}+\mathbf{q},b\bar{\sigma}}(\tau),$$

where $b_{ab}(\mathbf{q},\tau)$ is the annihilation operator of density fluctuation and $m^\alpha_{ab}(\mathbf{q},\tau)$ is the annihilation operator of spin fluctuations. We will use the second set of notation in the following calculation.

3.4 Properties of Green's Functions

To simplify formula derived later, we need to first study the symmetry properties of normal and anomalous Green's functions under various transformations. Let us define the following orbtial-dependent Green's functions: the normal Greens' function

$$\begin{aligned} G^{\sigma}_{ab}(\mathbf{k},\tau) &= -\langle T_\tau d_{\mathbf{k}a\sigma}(\tau) d^{\dagger}_{\mathbf{k}b\sigma}(0)\rangle, \\ \overline{G}^{\sigma}_{ab}(\mathbf{k},\tau) &= -\langle T_\tau d^{\dagger}_{\mathbf{k}a\sigma}(\tau) d_{\mathbf{k}b\sigma}(0)\rangle, \end{aligned}$$

where

$$\overline{G}^{\sigma}_{ab}(\mathbf{k},\tau) = -G^{\sigma}_{ba}(\mathbf{k},-\tau),$$

and the anomalous Green's functions

$$\begin{aligned} F^{\sigma\sigma'}_{ab}(\mathbf{k},\tau) &= -\langle T_\tau d_{\mathbf{k}a\sigma}(\tau) d_{-\mathbf{k}b\sigma'}(0)\rangle, \\ \overline{F}^{\sigma\sigma'}_{ab}(\mathbf{k},\tau) &= -\langle T_\tau d^{\dagger}_{-\mathbf{k}a\sigma}(\tau) d^{\dagger}_{\mathbf{k}b\sigma'}(0)\rangle. \end{aligned}$$

First, performing complex conjugate results in

$$\begin{aligned} G^{\sigma}_{ab}(\mathbf{k},\tau) &= -\langle T_\tau d_{\mathbf{k}a\sigma}(\tau) d^{\dagger}_{\mathbf{k}b\sigma}(0)\rangle \\ &= -\Theta(\tau)\mathrm{Tr}\left[e^{-\beta(K-\Omega)} e^{K\tau} d_{\mathbf{k}a\sigma} e^{-K\tau} d^{\dagger}_{\mathbf{k}b\sigma}\right] + \Theta(-\tau)\mathrm{Tr}\left[e^{-\beta(K-\Omega)} d^{\dagger}_{\mathbf{k}b\sigma} e^{K\tau} d_{\mathbf{k}a\sigma} e^{-K\tau}\right] \\ &= \left(-\Theta(\tau)\mathrm{Tr}\left[e^{-\beta(K-\Omega)} e^{K\tau} d_{\mathbf{k}a\sigma} e^{-K\tau} d^{\dagger}_{\mathbf{k}b\sigma}\right]^{\dagger} + \Theta(-\tau)\mathrm{Tr}\left[e^{-\beta(K-\Omega)} d^{\dagger}_{\mathbf{k}b\sigma} e^{K\tau} d_{\mathbf{k}a\sigma} e^{-K\tau}\right]^{\dagger}\right)^{*} \\ &= \left(-\Theta(\tau)\mathrm{Tr}\left[d_{\mathbf{k}b\sigma} e^{-K\tau} d^{\dagger}_{\mathbf{k}a\sigma} e^{K\tau} e^{-\beta(K-\Omega)}\right] + \Theta(-\tau)\mathrm{Tr}\left[e^{-K\tau} d^{\dagger}_{\mathbf{k}a\sigma} e^{K\tau} d_{\mathbf{k}b\sigma} e^{-\beta(K-\Omega)}\right]\right)^{*} \end{aligned}$$

where $K = H - \mu N,\ e^{-\beta\Omega} = \mathrm{Tr} e^{-\beta K}$. Upon permution in the trace it becomes

$$\begin{aligned} G^{\sigma}_{ab}(\mathbf{k},\tau) &= \left(-\Theta(\tau)\mathrm{Tr}\left[e^{-\beta(K-\Omega)} e^{K\tau} d_{\mathbf{k}b\sigma} e^{-K\tau} d^{\dagger}_{\mathbf{k}a\sigma}\right] + \Theta(-\tau)\mathrm{Tr}\left[e^{-\beta(K-\Omega)} d^{\dagger}_{\mathbf{k}a\sigma} e^{K\tau} d_{\mathbf{k}b\sigma} e^{-K\tau}\right]\right)^{*} \\ &= -\langle T_\tau d_{\mathbf{k}b\sigma}(\tau) d^{\dagger}_{\mathbf{k}a\sigma}\rangle^{*} = G^{\sigma}_{ba}(\mathbf{k},\tau)^{*}. \end{aligned}$$

and similarly we find

$$\begin{aligned} & F^{\sigma\sigma'}_{ab}(\mathbf{k},\tau) \\ &= -\langle T_\tau d_{\mathbf{k}a\sigma}(\tau) d_{-\mathbf{k}b\sigma'}(0)\rangle \\ &= \left(-\Theta(\tau)\mathrm{Tr}\left[d^{\dagger}_{-\mathbf{k}b\sigma'} e^{-K\tau} d^{\dagger}_{\mathbf{k}a\sigma} e^{K\tau} e^{-\beta(K-\Omega)}\right] + \Theta(-\tau)\mathrm{Tr}\left[e^{-K\tau} d^{\dagger}_{\mathbf{k}a\sigma} e^{K\tau} d^{\dagger}_{-\mathbf{k}b\sigma'} e^{-\beta(K-\Omega)}\right]\right)^{*} \end{aligned}$$

gives

$$
\begin{aligned}
&F_{ab}^{\sigma\sigma'}(\mathbf{k},\tau) \\
&= \left(-\Theta(\tau)\mathrm{Tr}\left[e^{-\beta(K-\Omega)}e^{K\tau}d^{\dagger}_{-\mathbf{k}b\sigma'}e^{-K\tau}d^{\dagger}_{\mathbf{k}a\sigma}\right] + \Theta(-\tau)\mathrm{Tr}\left[e^{-\beta(K-\Omega)}d^{\dagger}_{\mathbf{k}a\sigma}e^{K\tau}d^{\dagger}_{-\mathbf{k}b\sigma'}e^{-K\tau}\right]\right)^{*} \\
&= -\langle T_\tau d^{\dagger}_{-\mathbf{k}b\sigma'}(\tau)d^{\dagger}_{\mathbf{k}a\sigma}\rangle^{*} = \overline{F}_{ba}^{\sigma'\sigma}(\mathbf{k},\tau)^{*}.
\end{aligned}
$$

Also we have for the simultaneous exchange of spin and orbital indices

$$
\begin{aligned}
&- F_{ba}^{\sigma'\sigma}(-\mathbf{k},-\tau) \\
&= \Theta(-\tau)\mathrm{Tr}\left[e^{-\beta(K-\Omega)}e^{-K\tau}d_{-\mathbf{k}b\sigma'}e^{K\tau}d_{\mathbf{k}a\sigma}\right] - \Theta(\tau)\mathrm{Tr}\left[e^{-\beta(K-\Omega)}d_{\mathbf{k}a\sigma}e^{-K\tau}d_{-\mathbf{k}b\sigma'}e^{K\tau}\right] \\
&= -\Theta(\tau)\mathrm{Tr}\left[e^{-\beta(K-\Omega)}e^{K\tau}d_{\mathbf{k}a\sigma}e^{-K\tau}d_{-\mathbf{k}b\sigma'}\right] + \Theta(-\tau)\mathrm{Tr}\left[e^{-\beta(K-\Omega)}d_{-\mathbf{k}b\sigma'}e^{K\tau}d_{\mathbf{k}a\sigma}e^{-K\tau}\right]
\end{aligned}
$$

which yields

$$
-F_{ba}^{\sigma'\sigma}(-\mathbf{k},-\tau) = -\langle T_\tau d_{\mathbf{k}a\sigma}(\tau)d_{-\mathbf{k}b\sigma'}\rangle = F_{ab}^{\sigma\sigma'}(\mathbf{k},\tau).
$$

Under the rotation of π degree about y axis in spin space, $U^{y}(\pi) = -i\sigma^{y}$, the relation holds

$$
F_{ab}^{\sigma\sigma'}(\mathbf{k},\tau) \quad = \quad \sigma\sigma' F_{ab}^{\overline{\sigma\sigma'}}(\mathbf{k},\tau).
$$

Transforming to Mastubara frequency, the above equalities are expressed in frequency space as

$$
G_{ab}^{\sigma}(\mathbf{k},i\omega_n) = G_{ba}^{\sigma}(\mathbf{k},-i\omega_n)^{*} \Longrightarrow \tilde{G}(\mathbf{k},i\omega_n)^{T} = \tilde{G}(\mathbf{k},-i\omega_n)^{*}
$$

where T refers to the transpose operation, and

$$
F_{ab}^{\sigma\sigma'}(\mathbf{k},i\omega_n) = \overline{F}_{ba}^{\sigma'\sigma}(\mathbf{k},-i\omega_n)^{*},
$$

$$
F_{ab}^{\sigma\sigma'}(\mathbf{k},i\omega_n) = -F_{ba}^{\sigma'\sigma}(-\mathbf{k},-i\omega_n),
$$

as well as

$$
F_{ab}^{\sigma\sigma'}(\mathbf{k},i\omega_n) = \sigma\sigma' F_{ab}^{\overline{\sigma\sigma'}}(\mathbf{k},i\omega_n).
$$

Then the following equalities hold for the anomalous Green's function

$$
F_{ab}^{\sigma\bar{\sigma}}(\mathbf{k},i\omega_n) = -F_{ab}^{\bar{\sigma}\sigma}(\mathbf{k},i\omega_n) = -F_{ba}^{\bar{\sigma}\sigma}(-\mathbf{k},-i\omega_n) = F_{ba}^{\sigma\bar{\sigma}}(-\mathbf{k},-i\omega_n)
$$

$$
\overline{F}_{ab}^{\sigma\sigma'}(\mathbf{k},i\omega_n) = F_{ba}^{\sigma'\sigma}(\mathbf{k},-i\omega_n)^{*} = -F_{ab}^{\sigma\sigma'}(-\mathbf{k},i\omega_n)^{*} = -\sigma\sigma' F_{ab}^{\overline{\sigma\sigma'}}(-\mathbf{k},i\omega_n)^{*}
$$

Among them the most important equalities we are going to use later are

$$\tilde{G}(\mathbf{k}, i\omega_n)^T = \tilde{G}(\mathbf{k}, -i\omega_n)^*,$$

and

$$F_{ab}^{\sigma\bar{\sigma}}(\mathbf{k}, i\omega_n) = -F_{ab}^{\bar{\sigma}\sigma}(\mathbf{k}, i\omega_n),$$

$$\overline{F}_{ab}^{\sigma\bar{\sigma}}(\mathbf{k}, i\omega_n) = F_{ab}^{\bar{\sigma}\sigma}(-\mathbf{k}, i\omega_n)^*.$$

For singlet pairing, F is time-reversal invariant, when performing time-reversal transformation, it becomes

$$\begin{aligned}
&F_{ab}^{\sigma\sigma'}(\mathbf{k}, \tau) = -\langle T_\tau d_{\mathbf{k}a\sigma}(\tau) d_{-\mathbf{k}b\sigma'}(0)\rangle \\
&\xrightarrow{\mathcal{T}} -\Theta(\tau)\mathrm{Tr}\left[\sigma\sigma' d^\dagger_{\mathbf{k}b\overline{\sigma'}} e^{-K\tau} d^\dagger_{-\mathbf{k}a\bar{\sigma}} e^{K\tau} e^{-\beta(K-\Omega)}\right] + \Theta(-\tau)\mathrm{Tr}\left[\sigma\sigma' e^{-K\tau} d^\dagger_{-\mathbf{k}a\bar{\sigma}} e^{K\tau} d^\dagger_{\mathbf{k}b\overline{\sigma'}} e^{-\beta(K-\Omega)}\right] \\
&= \sigma\sigma'\left(-\Theta(\tau)\mathrm{Tr}\left[e^{-\beta(K-\Omega)} e^{K\tau} d^\dagger_{\mathbf{k}b\overline{\sigma'}} e^{-K\tau} d^\dagger_{-\mathbf{k}a\bar{\sigma}}\right] + \Theta(-\tau)\mathrm{Tr}\left[e^{-\beta(K-\Omega)} d^\dagger_{-\mathbf{k}a\bar{\sigma}} e^{K\tau} d^\dagger_{\mathbf{k}b\overline{\sigma'}} e^{-K\tau}\right]\right)
\end{aligned}$$

yields

$$F_{ab}^{\sigma\sigma'}(\mathbf{k}, \tau) = -\sigma\sigma'\langle T_\tau d^\dagger_{\mathbf{k}b\overline{\sigma'}}(\tau) d^\dagger_{-\mathbf{k}a\bar{\sigma}}\rangle = \sigma\sigma'\overline{F}_{ba}^{\overline{\sigma'\sigma}}(-\mathbf{k}, \tau).$$

Then in frequency representation

$$F_{ab}^{\sigma\sigma'}(\mathbf{k}, i\omega_n) = \sigma\sigma'\overline{F}_{ba}^{\overline{\sigma'\sigma}}(-\mathbf{k}, i\omega_n).$$

Similarly for G

$$\begin{aligned}
G_{ab}^{\sigma}(\mathbf{k}, \tau) &= -\langle T_\tau d_{\mathbf{k}a\sigma}(\tau) d^\dagger_{\mathbf{k}b\sigma}(0)\rangle \\
&\xrightarrow{\mathcal{T}} -\langle T_\tau d_{-\mathbf{k}b\bar{\sigma}}(\tau) d^\dagger_{-\mathbf{k}a\bar{\sigma}}(0) \\
&= G_{ba}^{\bar{\sigma}}(-\mathbf{k}, \tau)
\end{aligned}$$

which yields

$$G_{ab}^{\sigma}(\mathbf{k}, i\omega_n) = G_{ba}^{\bar{\sigma}}(-\mathbf{k}, i\omega_n).$$

The above time-reversal transformation properties gives rise to

$$F_{ab}^{\sigma\bar{\sigma}}(\mathbf{k}, i\omega_n) = -\overline{F}_{ba}^{\sigma\bar{\sigma}}(-\mathbf{k}, i\omega_n) = \overline{F}_{ab}^{\bar{\sigma}\sigma}(\mathbf{k}, -i\omega_n)$$

$$\Longrightarrow \overline{F}_{ab}^{\sigma\bar{\sigma}}(\mathbf{k}, i\omega_n) = F_{ab}^{\bar{\sigma}\sigma}(\mathbf{k}, -i\omega_n),$$

and

$$G^{\sigma}_{ab}(\mathbf{k}, i\omega_n) = G^{\bar{\sigma}}_{ba}(-\mathbf{k}, i\omega_n).$$

Combining with the earlier results under complex conjugate and spin rotation,

$$\overline{F}^{\sigma\bar{\sigma}}_{ab}(\mathbf{k}, i\omega_n) = F^{\bar{\sigma}\sigma}_{ab}(-\mathbf{k}, i\omega_n)^*,$$

$$G^{\sigma}_{ab}(\mathbf{k}, i\omega_n) = G^{\sigma}_{ba}(\mathbf{k}, -i\omega_n)^*,$$

we obtain the following identities

$$F^{\sigma\bar{\sigma}}_{ab}(\mathbf{k}, i\omega_n) = F^{\sigma\bar{\sigma}}_{ab}(-\mathbf{k}, -i\omega_n)^*$$

$$G^{\sigma}_{ab}(\mathbf{k}, i\omega_n) = G^{\bar{\sigma}}_{ab}(-\mathbf{k}, -i\omega_n)^*.$$

If we further assume inversion invariant, G and F are both even functions of $\mathbf{k}$. Then $F_{ab}(\tau),\ G_{ab}(\tau)$ are both real and

$$\begin{aligned} G_{ab}(\tau) &= G_{ba}(\tau), \\ F_{ab}(\tau) &= F_{ba}(-\tau). \end{aligned}$$

That is

$$\begin{aligned} G_{ab} &= G_{ba} \Longrightarrow \tilde{G}^T = \tilde{G}, \\ F_{ab}(\mathbf{k}, i\omega_n) &= F_{ba}(-\mathbf{k}, -i\omega_n) = F_{ba}(\mathbf{k}, i\omega_n)^* \Longrightarrow F^T = F^*,\ F = F^\dagger. \end{aligned}$$

G is symmetric matrix and F is Hermitian matrix under the above assumptions.

Here the phase convention for Fourier transformation of the Green's functions to imaginary frequency space is defined as

$$\begin{aligned} G^{\sigma}_{ab}(\mathbf{k}, i\omega_n) &= \int_0^\beta \mathrm{d}\tau G^{\sigma}_{ab}(\mathbf{k}, \tau) e^{i\omega_n \tau} \\ F^{\sigma\sigma'}_{ab}(\mathbf{k}, i\omega_n) &= \int_0^\beta \mathrm{d}\tau F^{\sigma\sigma'}_{ab}(\mathbf{k}, \tau) e^{i\omega_n \tau} \\ \overline{F}^{\sigma\sigma'}_{ab}(\mathbf{k}, i\omega_n) &= \int_0^\beta \mathrm{d}\tau \overline{F}^{\sigma\sigma'}_{ab}(\mathbf{k}, \tau) e^{i\omega_n \tau}, \end{aligned}$$

with the inverse transformation

$$\begin{aligned} G^{\sigma}_{ab}(\mathbf{k},\tau) &= T\sum_{n} G^{\sigma}_{ab}(\mathbf{k},i\omega_n)e^{-i\omega_n\tau} \\ F^{\sigma\sigma'}_{ab}(\mathbf{k},\tau) &= T\sum_{n} F^{\sigma\sigma'}_{ab}(\mathbf{k},i\omega_n)e^{-i\omega_n\tau} \\ \overline{F}^{\sigma\sigma'}_{ab}(\mathbf{k},\tau) &= T\sum_{n} \overline{F}^{\sigma\sigma'}_{ab}(\mathbf{k},i\omega_n)e^{-i\omega_n\tau}. \end{aligned}$$

3.5 Susceptibilities

3.5.1 Irreducible Susceptibilities

As in single-band case, the irreducible density-fluctuation correlation can be evaluated straightforwardly

$$\begin{aligned} \chi^{c,0}_{ab,a'b'}(\mathbf{q},\tau) &= \langle T_\tau b_{ab}(\mathbf{q},\tau) b_{a'b'}(-\mathbf{q},0)\rangle \\ &= \frac{1}{2}\sum_{\mathbf{k}\mathbf{k}',\sigma\sigma'} \langle T_\tau d^{\dagger}_{\mathbf{k},a\sigma}(\tau) d_{\mathbf{k}+\mathbf{q},b\sigma}(\tau) d^{\dagger}_{\mathbf{k}'+\mathbf{q},a'\sigma'}(0) d_{\mathbf{k}',b'\sigma'}(0)\rangle \\ &= \frac{1}{2}\sum_{\mathbf{k}\mathbf{k}',\sigma\sigma'} [-\langle T_\tau d_{\mathbf{k}+\mathbf{q},b\sigma}(\tau) d^{\dagger}_{\mathbf{k}'+\mathbf{q},a'\sigma'}(0)\rangle \langle T_\tau d_{\mathbf{k}',b'\sigma'}(0) d^{\dagger}_{\mathbf{k},a\sigma}(\tau)\rangle \\ &\qquad + \langle T_\tau d_{\mathbf{k}+\mathbf{q},b\sigma}(\tau) d_{\mathbf{k}',b'\sigma'}(0)\rangle \langle T_\tau d^{\dagger}_{\mathbf{k}'+\mathbf{q},a'\sigma'}(0) d^{\dagger}_{\mathbf{k},a\sigma}(\tau)\rangle] \\ &= \frac{1}{2}\sum_{\mathbf{k}\mathbf{k}',\sigma\sigma'} \left[-G^{\sigma}_{ba'}(\mathbf{k}+\mathbf{q},\tau) G^{\sigma}_{b'a}(\mathbf{k},-\tau)\delta_{\mathbf{k},\mathbf{k}'}\delta_{\sigma,\sigma'} + F^{\sigma\sigma'}_{bb'}(\mathbf{k}+\mathbf{q},\tau)\overline{F}^{\sigma'\sigma}_{a'a}(\mathbf{k},-\tau)\delta_{-\mathbf{k}-\mathbf{q},\mathbf{k}'}\right]. \end{aligned}$$

Transforming to frequency space, we have

$$\begin{aligned} &\chi^{c,0}_{ab,a'b'}(\mathbf{q},i\Omega_n) \\ &= -\frac{T}{N}\sum_{\mathbf{k},i\omega_n}\left[G_{ba'}(\mathbf{k}+\mathbf{q},i\omega_n+i\Omega_n)G_{b'a}(\mathbf{k},i\omega_n) - \frac{1}{2}\sum_{\sigma\sigma'} F^{\sigma\sigma'}_{bb'}(\mathbf{k}+\mathbf{q},i\omega_n+i\Omega_n)\overline{F}^{\sigma'\sigma}_{a'a}(\mathbf{k},i\omega_n)\right] \end{aligned}$$

where $\Omega_n = 2n\pi T$ and $\omega_n = (2n+1)\pi T$, N is the number of sites on the lattice.

Similarly the irreducible longitudinal spin-fluctuation propagator is given by

$$\begin{aligned} &\chi^{m^z,0}_{ab,a'b'}(\mathbf{q},\tau) \\ =&\langle T_\tau m^z_{ab}(\mathbf{q},\tau) m^z_{a'b'}(-\mathbf{q},0)\rangle \\ =&\frac{1}{2}\sum_{\mathbf{k}\mathbf{k}',\sigma\sigma'}\left[-G^{\sigma}_{ba'}(\mathbf{k}+\mathbf{q},\tau)G^{\sigma}_{b'a}(\mathbf{k},-\tau)\delta_{\mathbf{k},\mathbf{k}'}\delta_{\sigma,\sigma'} + \sigma\sigma' F^{\sigma\sigma'}_{bb'}(\mathbf{k}+\mathbf{q},\tau)\overline{F}^{\sigma'\sigma}_{a'a}(\mathbf{k},-\tau)\delta_{-\mathbf{k}-\mathbf{q},\mathbf{k}'}\right] \\ =&-\frac{1}{2}\sum_{\mathbf{k},\sigma} G^{\sigma}_{ba'}(\mathbf{k}+\mathbf{q},\tau)G^{\sigma}_{b'a}(\mathbf{k},-\tau) + \frac{1}{2}\sum_{\mathbf{k},\sigma\sigma'}\sigma\sigma' F^{\sigma\sigma'}_{bb'}(\mathbf{k}+\mathbf{q},\tau)\overline{F}^{\sigma'\sigma}_{a'a}(\mathbf{k},-\tau). \end{aligned}$$

Then the frequency form becomes

$$\chi^{m^z,0}_{ab,a'b'}(\mathbf{q},i\Omega_n) = -\frac{T}{N}\sum_{\mathbf{k},i\omega_n}\left[G_{ba'}(\mathbf{k}+\mathbf{q},i\omega_n+i\Omega_n)G_{b'a}(\mathbf{k},i\omega_n) - \frac{1}{2}\sum_{\sigma\sigma'}\sigma\sigma' F^{\sigma\sigma'}_{bb'}(\mathbf{k}+\mathbf{q},i\omega_n+i\Omega_n)\overline{F}^{\sigma'\sigma}_{a'a}(\mathbf{k},i\omega_n)\right].$$

Similarly we find the transverse form for the x-component is

$$\chi^{m^x,0}_{ab,a'b'}(\mathbf{q},i\Omega_n) = -\frac{T}{N}\sum_{\mathbf{k},i\omega_n}\left[G_{ba'}(\mathbf{k}+\mathbf{q},i\omega_n+i\Omega_n)G_{b'a}(\mathbf{k},i\omega_n) - \frac{1}{2}\sum_{\sigma\sigma'} F^{\overline{\sigma\sigma'}}_{bb'}(\mathbf{k}+\mathbf{q},i\omega_n+i\Omega_n)\overline{F}^{\sigma'\sigma}_{a'a}(\mathbf{k},i\omega_n)\right]$$

The same procedure for y-component propagator gives

$$\chi^{m^y,0}_{ab,a'b'}(\mathbf{q},i\Omega_n) = -\frac{T}{N}\sum_{\mathbf{k},i\omega_n}\left[G_{ba'}(\mathbf{k}+\mathbf{q},i\omega_n+i\Omega_n)G_{b'a}(\mathbf{k},i\omega_n) + \frac{1}{2}\sum_{\sigma\sigma'}(\sigma\sigma') F^{\overline{\sigma\sigma'}}_{bb'}(\mathbf{k}+\mathbf{q},i\omega_n+i\Omega_n)\overline{F}^{\sigma'\sigma}_{a'a}(\mathbf{k},i\omega_n)\right].$$

It can be shown that

$$\langle T_\tau b_{ab}(\mathbf{q},\tau)m^\alpha_{a'b'}(-\mathbf{q},0)\rangle = \langle T_\tau m^\alpha_{ab}(\mathbf{q},\tau)m^\beta_{a'b'}(-\mathbf{q},0)\rangle = 0, \quad \alpha\neq\beta$$

that is, there is no mix of different fluctuations in the propagators. For example

$$\begin{aligned}&\langle T_\tau m^x_{ab}m^y_{a'b'}\rangle \\ &= \frac{-i}{2}\langle T_\tau\left(d^\dagger_{\mathbf{k},a\downarrow}(\tau)d_{\mathbf{k}+\mathbf{q},b\uparrow}(\tau)d^\dagger_{\mathbf{k}',a'\uparrow}(0)d_{\mathbf{k}'+\mathbf{q},b'\downarrow}(0) - d^\dagger_{\mathbf{k},a\uparrow}(\tau)d_{\mathbf{k}+\mathbf{q},b\downarrow}(\tau)d^\dagger_{\mathbf{k}',a'\downarrow}(0)d_{\mathbf{k}'+\mathbf{q},b'\uparrow}(0)\right)\rangle \\ &= \frac{-i}{2}\left[F^{\uparrow\downarrow}_{bb'}(\mathbf{k}+\mathbf{q},\tau)\overline{F}^{\uparrow\downarrow}_{a'a}(\mathbf{k},-\tau) - F^{\downarrow\uparrow}_{bb'}(\mathbf{k}+\mathbf{q},\tau)\overline{F}^{\downarrow\uparrow}_{a'a}(\mathbf{k},-\tau)\right],\end{aligned}$$

Since $F^{\sigma\bar\sigma}_{ab}(\mathbf{k},i\omega_n) = -F^{\bar\sigma\sigma}_{ab}(\mathbf{k},i\omega_n)$, we have $\langle T_\tau m^x_{ab}m^y_{a'b'}\rangle = 0$.

For singlet pairing, $\sigma' = \bar\sigma$, the above expressions become

$$\begin{aligned}&\chi^{c,0}_{ab,a'b'}(\mathbf{q},i\Omega_n) \\ &= -\frac{T}{N}\sum_{\mathbf{k},i\omega_n}\left[G_{ba'}(\mathbf{k}+\mathbf{q},i\omega_n+i\Omega_n)G_{b'a}(\mathbf{k},i\omega_n) - \frac{1}{2}\sum_{\sigma} F^{\sigma\bar\sigma}_{bb'}(\mathbf{k}+\mathbf{q},i\omega_n+i\Omega_n)\overline{F}^{\bar\sigma\sigma}_{a'a}(\mathbf{k},i\omega_n)\right]\end{aligned}$$

for the irreducible charge susceptibility and the longitudinal irreducible spin susceptibility beomes

$$\begin{aligned}&\chi^{m^z,0}_{ab,a'b'}(\mathbf{q},i\Omega_n) \\ &= -\frac{T}{N}\sum_{\mathbf{k},i\omega_n}\left[G_{ba'}(\mathbf{k}+\mathbf{q},i\omega_n+i\Omega_n)G_{b'a}(\mathbf{k},i\omega_n) + \frac{1}{2}\sum_{\sigma} F^{\sigma\bar\sigma}_{bb'}(\mathbf{k}+\mathbf{q},i\omega_n+i\Omega_n)\overline{F}^{\bar\sigma\sigma}_{a'a}(\mathbf{k},i\omega_n)\right],\end{aligned}$$

as well as the transverse ones

$$\chi^{m^x,0}_{ab,a'b'}(\mathbf{q},i\Omega_n)$$
$$=-\frac{T}{N}\sum_{\mathbf{k},i\omega_n}\left[G_{ba'}(\mathbf{k}+\mathbf{q},i\omega_n+i\Omega_n)G_{b'a}(\mathbf{k},i\omega_n)-\frac{1}{2}\sum_{\sigma}F^{\bar{\sigma}\sigma}_{bb'}(\mathbf{k}+\mathbf{q},i\omega_n+i\Omega_n)\overline{F}^{\bar{\sigma}\sigma}_{a'a}(\mathbf{k},i\omega_n)\right]$$

and

$$\chi^{m^y,0}_{ab,a'b'}(\mathbf{q},i\Omega_n)$$
$$=-\frac{T}{N}\sum_{\mathbf{k},i\omega_n}\left[G_{ba'}(\mathbf{k}+\mathbf{q},i\omega_n+i\Omega_n)G_{b'a}(\mathbf{k},i\omega_n)-\frac{1}{2}\sum_{\sigma}F^{\bar{\sigma}\sigma}_{bb'}(\mathbf{k}+\mathbf{q},i\omega_n+i\Omega_n)\overline{F}^{\bar{\sigma}\sigma}_{a'a}(\mathbf{k},i\omega_n)\right].$$

As derived in the last section, the following relation holds

$$F^{\sigma\bar{\sigma}}_{ab}(\mathbf{k},i\omega_n)=-F^{\bar{\sigma}\sigma}_{ab}(\mathbf{k},i\omega_n)$$

$$\overline{F}^{\sigma\bar{\sigma}}_{ab}(\mathbf{k},i\omega_n)=F^{\bar{\sigma}\sigma}_{ab}(\mathbf{k},-i\omega_n)$$

which yields $\chi^{m^z}=\chi^{m^x}=\chi^{m^y}$. Therefore, we simply have two types of irreducible susceptibilities: the charge irreducible bubble

$$\chi^{c,0}_{ab,a'b'}(\mathbf{q},i\Omega_n)$$
$$=-\frac{T}{N}\sum_{\mathbf{k},i\omega_n}\left[G_{ba'}(\mathbf{k}+\mathbf{q},i\omega_n+i\Omega_n)G_{b'a}(\mathbf{k},i\omega_n)-\frac{1}{2}\sum_{\sigma}F^{\sigma\bar{\sigma}}_{bb'}(\mathbf{k}+\mathbf{q},i\omega_n+i\Omega_n)F^{\sigma\bar{\sigma}}_{a'a}(\mathbf{k},-i\omega_n)\right] \tag{3.4}$$

and the spin irreducible bubble

$$\chi^{s,0}_{ab,a'b'}(\mathbf{q},i\Omega_n)$$
$$=-\frac{T}{N}\sum_{\mathbf{k},i\omega_n}\left[G_{ba'}(\mathbf{k}+\mathbf{q},i\omega_n+i\Omega_n)G_{b'a}(\mathbf{k},i\omega_n)+\frac{1}{2}\sum_{\sigma}F^{\sigma\bar{\sigma}}_{bb'}(\mathbf{k}+\mathbf{q},i\omega_n+i\Omega_n)F^{\sigma\bar{\sigma}}_{a'a}(\mathbf{k},-i\omega_n)\right]. \tag{3.5}$$

Again we notice the relative sign is different in the two channels indicating the constructive effect in one channel whileas destructive in the other.

3.5.2 FLEX Susceptibilities

Next we need to evaluate the renormalized fluctuation propagator in FLEX approximation, in which we take into account all the bubble and ladder diagrams as demonstrated in Fig. 3.1.

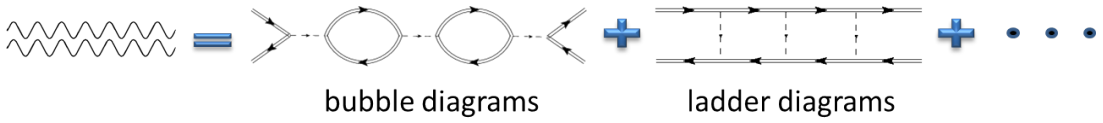

Figure 3.1 Diagrammatic demonstration of the renormalized fluctuation propagator. The higher-order diagrams contain bubble and ladder series with the double line refering to the renormalized single-particle propagator and the dashed line indicates the bare interaction, here is the Hubbard U-matrix.

Recall that the interaction Hamiltonian can be expressed as

$$H_{int} = \frac{1}{2} \sum_{\mathbf{q},a_i,\alpha} \left[b_{a_1 a_4}(-\mathbf{q}) U_c^{a_1 a_4, a_2 a_3} b_{a_2 a_3}(\mathbf{q}) + m^{\alpha}_{a_1 a_4}(-\mathbf{q}) \left(-U_s^{a_1 a_4, a_2 a_3}\right) m^{\alpha}_{a_2 a_3}(\mathbf{q}) \right].$$

Note that the prefactor $\frac{1}{2}$ eliminates the symmetry between $b(m)_{14}$ and $b(m)_{23}$, that is the exchange between the two fluctuation legs. The renormalized propagator can be obtained in the standard perturbation theory

$$\chi^{c,FLEX}_{ab,a'b'}(\mathbf{q},\tau) = \langle T_\tau b_{ab}(\mathbf{q},\tau) b_{a'b'}(-\mathbf{q},0) \rangle_{FLEX}$$

$$= \sum_n \frac{(-1)^n}{n!} \left(\frac{1}{2}\right)^n \int_0^\beta d\tau_1 \cdots \int_0^\beta d\tau_n$$
$$\langle T_\tau b_{ab}(\mathbf{q},\tau) \sum_{\mathbf{q}_1,a_i} \left(b_{a_1 a_4}(-\mathbf{q}_1,\tau_1) U_c^{a_1 a_4, a_2 a_3} b_{a_2 a_3}(\mathbf{q}_1,\tau_1) \right)$$
$$\cdots \sum_{\mathbf{q}_n,b_i} \left(b_{b_1 b_4}(-\mathbf{q}_n,\tau_n) U_c^{b_1 b_4, b_2 b_3} b_{b_2 b_3}(\mathbf{q}_n,\tau_n) \right) b_{a'b'}(-\mathbf{q},0) \rangle$$

in terms of fluctuation correlators it becomes

$$\begin{aligned}
&\chi^{c,FLEX}_{ab,a'b'}(\mathbf{q},\tau) \\
&= \langle T_\tau b_{ab}(\mathbf{q},\tau) b_{a'b'}(-\mathbf{q},0)\rangle + \\
&+ (-1)\int_0^\beta d\tau_1 \sum_{\mathbf{q}_1,a_i} \langle T_\tau b_{ab}(\mathbf{q},\tau) b_{a_1a_4}(-\mathbf{q}_1,\tau_1)\rangle U_c^{a_1a_4,a_2a_3} \left[\langle T_\tau b_{a_2a_3}(\mathbf{q}_1,\tau_1) b_{a'b'}(-\mathbf{q},0)\rangle_{FLEX}\right]
\end{aligned}$$

that is

$$\chi^{c,FLEX}_{ab,a'b'}(\mathbf{q},\tau) = \chi^{c,0}_{ab,a'b'}(\mathbf{q},\tau) - \int_0^\beta d\tau_1 \sum_{\mathbf{q},a_i} \chi^{c,0}_{ab,a_1a_4}(\mathbf{q},\tau-\tau_1) U_c^{a_1a_4,a_2a_3} \chi^{c,FLEX}_{a_2a_3,a'b'}(\mathbf{q},\tau_1).$$

Then we obtain the Dyson series

$$\chi^{c}_{ab,a'b'}(\mathbf{q},i\nu_n) \;=\; \chi^{c,0}_{ab,a'b'}(\mathbf{q},i\nu_n) - \chi^{c,0}_{ab,a_1a_4}(\mathbf{q},i\nu_n) U_c^{a_1a_4,a_2a_3} \chi^{c}_{a_2a_3,a'b'}(\mathbf{q},i\nu_n).$$

This pattern obviously applies to the spin-fluctuation propagator as well. So finally we have together

$$\begin{aligned}
\left[\delta^{ab,a_2a_3} + \chi^{c,0}_{ab,a_1a_4}(\mathbf{q},i\nu_n) U_c^{a_1a_4,a_2a_3}\right] \chi^{c}_{a_2a_3,a'b'}(\mathbf{q},i\nu_n) &= \chi^{c,0}_{ab,a'b'}(\mathbf{q},i\nu_n), \\
\left[\delta^{ab,a_2a_3} - \chi^{s,0}_{ab,a_1a_4}(\mathbf{q},i\nu_n) U_s^{a_1a_4,a_2a_3}\right] \chi^{s}_{a_2a_3,a'b'}(\mathbf{q},i\nu_n) &= \chi^{s,0}_{ab,a'b'}(\mathbf{q},i\nu_n).
\end{aligned} \tag{3.6}$$

In terms of matrix form, they can be written as

$$\begin{aligned}
\tilde{\chi}^{c}(\mathbf{q},i\nu_n) &= \left(\tilde{1} + \tilde{\chi}^{c,0}(\mathbf{q},i\nu_n)\tilde{U}^c\right)^{-1} \tilde{\chi}^{c,0}(\mathbf{q},i\nu_n), \\
\tilde{\chi}^{s}(\mathbf{q},i\nu_n) &= \left(\tilde{1} - \tilde{\chi}^{s,0}(\mathbf{q},i\nu_n)\tilde{U}^s\right)^{-1} \tilde{\chi}^{s,0}(\mathbf{q},i\nu_n).
\end{aligned} \tag{3.7}$$

3.6 Self-energies and Effective Interaction Vertices

In this section we calculate the single-particle self-energy (including normal and anomalous self-energies as shown in Fig. 3.2) in FLEX approximation, which incorporates the contribution of the interaction from the third and higher orders. FLEX formula has double counting problem on the second order, so we need to subtract it in the FLEX formula. We will calculate the first- and second-order diagrams exactly and add them to the interaction vertices later.

Figure 3.2 Diagrammatic illustration of the normal and anomalous self-energies. In FLEX approximation, the internal interaction line (double curved line) is the renormalized fluctuation propagator and the internal particle line is the renormalized/dressed quasiparticle propagator.

Since there are four fluctuations involved in the intermediate interactions, we are working on them separately for G and F.

3.6.1 Normal Self-energy

Using perturbation expansion, the normal Green's function renormalized by charge fluctuation is obtained as

$$
\begin{aligned}
&G^{\sigma}_{ab}(\mathbf{k},\tau) = -\langle T_\tau d_{\mathbf{k}a\sigma}(\tau) d^{\dagger}_{\mathbf{k}b\sigma}(0)\rangle \\
&= -\sum_n \frac{(-1)^n}{n!}\left(\frac{1}{2}\right)^n \int_0^\beta d\tau_1 \cdots d\tau_n \langle T_\tau d_{\mathbf{k}a\sigma}(\tau) \sum_{\mathbf{q}_1,a_i} \left(b_{a_1a_4}(-\mathbf{q}_1,\tau_1) U_c^{a_1a_4,a_2a_3} b_{a_2a_3}(\mathbf{q}_1,\tau_1)\right) \\
&\qquad\qquad \cdots \sum_{\mathbf{q}_n,b_i} \left(b_{b_1b_4}(-\mathbf{q}_n,\tau_n) U_c^{b_1b_4,b_2b_3} b_{b_2b_3}(\mathbf{q}_n,\tau_n)\right) d^{\dagger}_{\mathbf{k}b\sigma}(0)\rangle
\end{aligned}
$$

In terms of FLEX propagator it becomes

$$
\begin{aligned}
G^{\sigma}_{ab}(\mathbf{k},\tau) = -(-1)^2 \int_0^\beta d\tau_1 d\tau_n \sum_{\mathbf{q},a_i,b_i} U_c^{a_1a_4,a_2a_3} U_c^{b_1b_4,b_2b_3} \times \\
\langle T_\tau d_{\mathbf{k}a\sigma}(\tau) b_{a_1a_4}(-\mathbf{q},\tau_1) b_{b_2b_3}(\mathbf{q},\tau_n) d^{\dagger}_{\mathbf{k}b\sigma}(0)\rangle \left[\langle T_\tau b_{a_2a_3}(\mathbf{q},\tau_1) b_{b_1b_4}(-\mathbf{q},\tau_n)\rangle_{FLEX}\right]
\end{aligned}
$$

where

$$
\begin{aligned}
&\langle T_\tau d_{\mathbf{k}a\sigma}(\tau) b_{a_1a_4}(-\mathbf{q},\tau_1) b_{b_2b_3}(\mathbf{q},\tau_n) d^{\dagger}_{\mathbf{k}b\sigma}(0)\rangle \\
&= \frac{1}{2}\langle T_\tau d_{\mathbf{k},a\sigma}(\tau) d^{\dagger}_{\mathbf{k},a_1\sigma}(\tau_1)\rangle \langle T_\tau d_{\mathbf{k}-\mathbf{q},a_4\sigma}(\tau_1) d^{\dagger}_{\mathbf{k}-\mathbf{q},b_2\sigma}(\tau_n)\rangle \langle T_\tau d_{\mathbf{k},b_3\sigma}(\tau_n) d^{\dagger}_{\mathbf{k}b\sigma}(0)\rangle.
\end{aligned}
$$

Thus we have in frequency space the expression

$$
\begin{aligned}
&G^{\sigma}_{ab}(\mathbf{k},i\omega_n) = \\
&\sum_{\mathbf{q},\nu_n,a_i,b_i} G^{\sigma}_{aa_1}(\mathbf{k},i\omega_n)\left[\frac{1}{2} U_c^{a_1a_4,a_2a_3} \chi^c_{a_2a_3,b_1b_4}(\mathbf{q},i\nu_n) U_c^{b_1b_4,b_2b_3} G^{\sigma}_{a_4b_2}(\mathbf{k}-\mathbf{q},i\omega_n - i\nu_n)\right] G^{\sigma}_{b_3b}(\mathbf{k},i\omega_n).
\end{aligned}
$$

In a general notation of indices, it is written as

$$G^{\sigma}_{ab}(\mathbf{k}, i\omega_n) = \sum_{\mathbf{q},\nu_n} G^{\sigma}_{aa'}(\mathbf{k}, i\omega_n) \left[\frac{1}{2} U_c^{a'm,\alpha\beta} \chi^c_{\alpha\beta,\mu\nu}(\mathbf{q}, i\nu_n) U_c^{\mu\nu,nb'} G^{\sigma}_{mn}(\mathbf{k}-\mathbf{q}, i\omega_n - i\nu_n) \right] G^{\sigma}_{b'b}(\mathbf{k}, i\omega_n).$$

We subtract the forms of the self-energy and interaction vertex from it

$$\Sigma_c^{a'b'}(\mathbf{k}, i\omega_n) = \sum_{\mathbf{q},\nu_n} \sum_{m,n} V_{N,c}^{a'm,nb'}(\mathbf{q}, i\nu_n) G_{mn}(\mathbf{k}-\mathbf{q}, i\omega_n - i\nu_n),$$

$$V_{N,c}^{a_1a_4,b_2b_3}(\mathbf{q}, i\nu_n) = \sum_{\alpha\beta,\mu\nu} \frac{1}{2} U_c^{a'm,\alpha\beta} \chi^c_{\alpha\beta,\mu\nu}(\mathbf{q}, i\nu_n) U_c^{\mu\nu,nb'}.$$

Similarly the interaction mediated by the longitudinal spin fluctuation gives

$$G^{\sigma}_{ab}(\mathbf{k}, \tau) = \int_0^{\beta} d\tau_1 \int_0^{\beta} d\tau_n (-1)^3 \left[\langle m^z_{a_2a_3}(\mathbf{q}, \tau_1) m^z_{b_1b_4}(-\mathbf{q}, \tau_n) \rangle_{FLEX} \right] \sum_{\mathbf{q},a_ib_i} U_s^{a_1a_4,a_2a_3} U_s^{b_1b_4,b_2b_3} \langle T_\tau d_{\mathbf{k}a\sigma}(\tau) m^z_{a_1a_4}(-\mathbf{q}, \tau_1) m^z_{b_2b_3}(\mathbf{q}, \tau_n) d^{\dagger}_{\mathbf{k}b\sigma}(0) \rangle$$

where

$$\begin{aligned} & \langle T_\tau d_{\mathbf{k}a\sigma}(\tau) m^z_{a_1a_4}(-\mathbf{q}, \tau_1) m^z_{b_2b_3}(\mathbf{q}, \tau_n) d^{\dagger}_{\mathbf{k}b\sigma}(0) \rangle \\ = \; & \frac{1}{2}\sigma^2 \langle T_\tau d_{\mathbf{k}a\sigma}(\tau) d^{\dagger}_{\mathbf{k},a_1\sigma}(\tau_1) \rangle \langle T_\tau d_{\mathbf{k}-\mathbf{q},a_4\sigma}(\tau_1) d^{\dagger}_{\mathbf{k}-\mathbf{q},b_2\sigma}(\tau_n) \rangle \langle T_\tau d_{\mathbf{k},b_3\sigma}(\tau_n) d^{\dagger}_{\mathbf{k}b\sigma}(0) \rangle \end{aligned}$$

Therefore we have

$$G^{\sigma}_{ab}(\mathbf{k}, i\omega_n) = \sum_{\mathbf{q},\nu_n,a_ib_i} G^{\sigma}_{aa_1}(\mathbf{k}, i\omega_n) \left[\frac{1}{2} U_s^{a_1a_4,a_2a_3} \chi^{m^z}_{a_2a_3,b_1b_4}(\mathbf{q}, i\nu_n) U_s^{b_1b_4,b_2b_3} G^{\sigma}_{a_4b_2}(\mathbf{k}-\mathbf{q}, i\omega_n - i\nu_n) \right] G^{\sigma}_{b_3b}(\mathbf{k}, i\omega_n).$$

It can be shown that the x-transverse fluctuation contribution results in

$$G^{\sigma}_{ab}(\mathbf{k}, i\omega_n) = \sum_{\mathbf{q},\nu_n,a_ib_i} G^{\sigma}_{aa_1}(\mathbf{k}, i\omega_n) \left[\frac{1}{2} U_s^{a_1a_4,a_2a_3} \chi^{m^x}_{a_2a_3,b_1b_4}(\mathbf{q}, i\nu_n) U_s^{b_1b_4,b_2b_3} G^{\bar{\sigma}}_{a_4b_2}(\mathbf{k}-\mathbf{q}, i\omega_n - i\nu_n) \right] G^{\sigma}_{b_3b}(\mathbf{k}, i\omega_n).$$

And for the y-transverse fluctuation

$$G^{\sigma}_{ab}(\mathbf{k}, i\omega_n) = \sum_{\mathbf{q},\nu_n,a_ib_i} G^{\sigma}_{aa_1}(\mathbf{k}, i\omega_n) \left[\frac{1}{2} U_s^{a_1a_4,a_2a_3} \chi^{m^y}_{a_2a_3,b_1b_4}(\mathbf{q}, i\nu_n) U_s^{b_1b_4,b_2b_3} G^{\bar{\sigma}}_{a_4b_2}(\mathbf{k}-\mathbf{q}, i\omega_n - i\nu_n) \right] G^{\sigma}_{b_3b}(\mathbf{k}, i\omega_n).$$

Since $\chi^{m^z} = \chi^{m^x} = \chi^{m^y} \equiv \chi^s$, in a general notation they read

$$G_{ab}(\mathbf{k}, i\omega_n) = \sum_{a'b'} G_{aa'}(\mathbf{k}, i\omega_n)\Sigma^{a'b'}(\mathbf{k}, i\omega_n)G_{b'b}(\mathbf{k}, i\omega_n),$$

with

$$\Sigma^{a'b'}(\mathbf{k}, i\omega_n) = \sum_{\mathbf{q},\nu_n}\sum_{m,n} V_N^{a'm,nb'}(\mathbf{q}, i\nu_n)G_{mn}(\mathbf{k}-\mathbf{q}, i\omega_n - i\nu_n)$$

where the effective interaction vertex contains two terms

$$V_N^{a'm,nb'}(\mathbf{q}, i\nu_n) = V_s^{a'm,nb'}(\mathbf{q}, i\nu_n) + V_c^{a'm,nb'}(\mathbf{q}, i\nu_n),$$

with the charge term

$$V_c^{a'm,nb'}(\mathbf{q}, i\nu_n) = \frac{1}{2}\sum_{\alpha\beta,\mu\nu} U_c^{a'm,\alpha\beta}\left[\chi^c_{\alpha\beta,\mu\nu}(\mathbf{q}, i\nu_n) - \chi^{c,0}_{\alpha\beta,\mu\nu}(\mathbf{q}, i\nu_n)\right] U_c^{\mu\nu,nb'},$$

and the spin term

$$V_s^{a'm,nb'}(\mathbf{q}, i\nu_n) = \frac{3}{2}\sum_{\alpha\beta,\mu\nu} U_s^{a'm,\alpha\beta}\left[\chi^s_{\alpha\beta,\mu\nu}(\mathbf{q}, i\nu_n) - \chi^{s,0}_{\alpha\beta,\mu\nu}(\mathbf{q}, i\nu_n)\right] U_s^{\mu\nu,nb'}.$$

3.6.2 Anomalous Self-energy

Now we evaluate the anomalous self-energy as well as the pairing interaction associated with it. Similar to the above, start with the density-fluctuation contribution

$$\begin{aligned}
&F_{ab}^{\sigma\sigma'}(\mathbf{k}, \tau) = -\langle T_\tau d_{\mathbf{k}a\sigma}(\tau) d_{-\mathbf{k}b\sigma'}(0)\rangle \\
&= -\sum_n \frac{(-1)^n}{n!}\left(\frac{1}{2}\right)^n \int_0^\beta d\tau_1 \cdots d\tau_n \langle T_\tau d_{\mathbf{k}a\sigma}(\tau) \sum_{\mathbf{q}_1, a_i} \left(b_{a_1a_4}(-\mathbf{q}_1, \tau_1) U_c^{a_1a_4,a_2a_3} b_{a_2a_3}(\mathbf{q}_1, \tau_1)\right) \\
&\qquad \cdots \sum_{\mathbf{q}_n, b_i} \left(b_{b_1b_4}(-\mathbf{q}_n, \tau_n) U_c^{b_1b_4,b_2b_3} b_{b_2b_3}(\mathbf{q}_n, \tau_n)\right) d_{-\mathbf{k}b\sigma'}(0)\rangle
\end{aligned}$$

Again in terms of the fluctuation propagators it becomes

$$F_{ab}^{\sigma\sigma'}(\mathbf{k}, \tau) = \int_0^\beta d\tau_1 d\tau_n \sum_{\mathbf{q}, a_i b_i} U_c^{a_1a_4,a_2a_3} \left[\langle b_{a_2a_3}(\mathbf{q}, \tau_1) b_{b_1b_4}(-\mathbf{q}, \tau_n)\rangle_{FLEX}\right] U_c^{b_1b_4,b_2b_3}$$

$$(-1)^3 \langle T_\tau d_{\mathbf{k}a\sigma}(\tau) b_{a_1a_4}(-\mathbf{q}, \tau_1) b_{b_2b_3}(\mathbf{q}, \tau_n) d_{-\mathbf{k}b\sigma'}(0)\rangle$$

where

$$\begin{aligned}
&\langle T_\tau d_{\mathbf{k}a\sigma}(\tau) b_{a_1a_4}(-\mathbf{q}, \tau_1) b_{b_2b_3}(\mathbf{q}, \tau_n) d_{-\mathbf{k}b\sigma'}(0)\rangle \\
&= -\frac{1}{2}\langle T_\tau d_{\mathbf{k}a\sigma}(\tau) d^\dagger_{\mathbf{k},a_1\sigma}(\tau_1)\rangle \langle T_\tau d_{\mathbf{k}-\mathbf{q},a_4\sigma}(\tau_1) d_{-\mathbf{k}+\mathbf{q},b_3\sigma'}(\tau_n)\rangle \langle T_\tau d^\dagger_{-\mathbf{k},b_2\sigma'}(\tau_n) d_{-\mathbf{k}b\sigma'}(0)\rangle
\end{aligned}$$

yields the frequency representation

$$
\begin{aligned}
&F^{\sigma\sigma'}_{ab}(\mathbf{k}, i\omega_n) \\
&= -\sum_{\mathbf{q},\nu_n,a_ib_i} G^{\sigma}_{aa_1}(\mathbf{k}, i\omega_n)\times \\
&\left[-\frac{1}{2}U_c^{a_1a_4,a_2a_3}\chi^{c}_{a_2a_3,b_1b_4}(\mathbf{q}, i\nu_n)U_c^{b_1b_4,b_2b_3}F^{\sigma\sigma'}_{a_4b_3}(\mathbf{k}-\mathbf{q}, i\omega_n - i\nu_n)\right] G^{\sigma'}_{bb_2}(-\mathbf{k}, -i\omega_n).
\end{aligned}
$$

Follow the same procedure we have for the longitudinal-magnetic-fluctuation mediation

$$
\begin{aligned}
&F^{\sigma\sigma'}_{ab}(\mathbf{k}, i\omega_n) \\
&= -\sum_{\mathbf{q},\nu_n,a_ib_i} G^{\sigma}_{aa_1}(\mathbf{k}, i\omega_n)\times \\
&\left[\frac{1}{2}(-\sigma\sigma')U_s^{a_1a_4,a_2a_3}\chi^{m^z}_{a_2a_3,b_1b_4}(\mathbf{q}, i\nu_n)U_s^{b_1b_4,b_2b_3}F^{\sigma\sigma'}_{a_4b_3}(\mathbf{k}-\mathbf{q}, i\omega_n - i\nu_n)\right] G^{\sigma'}_{bb_2}(-\mathbf{k}, -i\omega_n),
\end{aligned}
$$

and the transverse x-fluctuation

$$
\begin{aligned}
&F^{\sigma\sigma'}_{ab}(\mathbf{k}, i\omega_n) = -\sum_{\mathbf{q},\nu_n,a_ib_i} G^{\sigma}_{aa_1}(\mathbf{k}, i\omega_n)\times \\
&\times\left[-\frac{1}{2}U_s^{a_1a_4,a_2a_3}\chi^{m^x}_{a_2a_3,b_1b_4}(\mathbf{q}, i\nu_n)U_s^{b_1b_4,b_2b_3}F^{\overline{\sigma\sigma'}}_{a_4b_3}(\mathbf{k}-\mathbf{q}, i\omega_n - i\nu_n)\right] G^{\sigma'}_{bb_2}(-\mathbf{k}, -i\omega_n).
\end{aligned}
$$

as well as the y-fluctuation part

$$
\begin{aligned}
&F^{\sigma\sigma'}_{ab}(\mathbf{k}, i\omega_n) \\
&= -\sum_{\mathbf{q},\nu_n,a_ib_i} G^{\sigma}_{aa_1}(\mathbf{k}, i\omega_n)\times \\
&\left[\frac{1}{2}(\sigma\sigma')U_s^{a_1a_4,a_2a_3}\chi^{m^y}_{a_2a_3,b_1b_4}(\mathbf{q}, i\nu_n)U_s^{b_1b_4,b_2b_3}F^{\overline{\sigma\sigma'}}_{a_4b_3}(\mathbf{k}-\mathbf{q}, i\omega_n - i\nu_n)\right] G^{\sigma'}_{bb_2}(-\mathbf{k}, -i\omega_n).
\end{aligned}
$$

Again in singlet pairing, $\sigma' = \bar{\sigma}$, we have the charge contribution

$$
\begin{aligned}
&F^{\sigma\bar{\sigma}}_{ab}(\mathbf{k}, i\omega_n) = -\sum_{\mathbf{q},\nu_n,a_ib_i} G^{\sigma}_{aa_1}(\mathbf{k}, i\omega_n)\times \\
&\left[-\frac{1}{2}U_c^{a_1a_4,a_2a_3}\chi^{c}_{a_2a_3,b_1b_4}(\mathbf{q}, i\nu_n)U_c^{b_1b_4,b_2b_3}F^{\sigma\bar{\sigma}}_{a_4b_3}(\mathbf{k}-\mathbf{q}, i\omega_n - i\nu_n)\right] G^{\bar{\sigma}}_{bb_2}(-\mathbf{k}, -i\omega_n),
\end{aligned}
$$

and the longitudinal spin contribution

$$
\begin{aligned}
&F^{\sigma\bar{\sigma}}_{ab}(\mathbf{k}, i\omega_n) = -\sum_{\mathbf{q},\nu_n,a_ib_i} G^{\sigma}_{aa_1}(\mathbf{k}, i\omega_n)\times \\
&\left[\frac{1}{2}U_s^{a_1a_4,a_2a_3}\chi^{m^z}_{a_2a_3,b_1b_4}(\mathbf{q}, i\nu_n)U_s^{b_1b_4,b_2b_3}F^{\sigma\bar{\sigma}}_{a_4b_3}(\mathbf{k}-\mathbf{q}, i\omega_n - i\nu_n)\right] G^{\bar{\sigma}}_{bb_2}(-\mathbf{k}, -i\omega_n),
\end{aligned}
$$

as well as the transverse spin contributions

$$F_{ab}^{\sigma\bar{\sigma}}(\mathbf{k},i\omega_n) = -\sum_{\mathbf{q},\nu_n,a_ib_i} G_{aa_1}^{\sigma}(\mathbf{k},i\omega_n)\times$$
$$\left[-\frac{1}{2}U_s^{a_1a_4,a_2a_3}\chi^{m^x}_{a_2a_3,b_1b_4}(\mathbf{q},i\nu_n)U_s^{b_1b_4,b_2b_3}F^{\bar{\sigma}\sigma}_{a_4b_3}(\mathbf{k}-\mathbf{q},i\omega_n-i\nu_n)\right]G^{\bar{\sigma}}_{bb_2}(-\mathbf{k},-i\omega_n),$$

$$F_{ab}^{\sigma\bar{\sigma}}(\mathbf{k},i\omega_n) = -\sum_{\mathbf{q},\nu_n,a_ib_i} G_{aa_1}^{\sigma}(\mathbf{k},i\omega_n)\times$$
$$\left[-\frac{1}{2}U_s^{a_1a_4,a_2a_3}\chi^{m^y}_{a_2a_3,b_1b_4}(\mathbf{q},i\nu_n)U_s^{b_1b_4,b_2b_3}F^{\bar{\sigma}\sigma}_{a_4b_3}(\mathbf{k}-\mathbf{q},i\omega_n-i\nu_n)\right]G^{\bar{\sigma}}_{bb_2}(-\mathbf{k},-i\omega_n).$$

Since the anomalous Green's function has the property shown before

$$F_{ab}^{\sigma\bar{\sigma}}(\mathbf{k},i\omega_n) = -F_{ab}^{\bar{\sigma}\sigma}(\mathbf{k},i\omega_n)$$

we are left with two types of contributions

$$F_{ab}^{\sigma\bar{\sigma}}(\mathbf{k},i\omega_n) = -\sum_{\mathbf{q},\nu_n,a_ib_i} G_{aa_1}^{\sigma}(\mathbf{k},i\omega_n)\times$$
$$\left[-\frac{1}{2}U_c^{a_1a_4,a_2a_3}\chi^{c}_{a_2a_3,b_1b_4}(\mathbf{q},i\nu_n)U_c^{b_1b_4,b_2b_3}F^{\sigma\bar{\sigma}}_{a_4b_3}(\mathbf{k}-\mathbf{q},i\omega_n-i\nu_n)\right]G^{\bar{\sigma}}_{bb_2}(-\mathbf{k},-i\omega_n),$$

and

$$F_{ab}^{\sigma\bar{\sigma}}(\mathbf{k},i\omega_n) = -\sum_{\mathbf{q},\nu_n,a_ib_i} G_{aa_1}^{\sigma}(\mathbf{k},i\omega_n)\times$$
$$\left[\frac{3}{2}U_s^{a_1a_4,a_2a_3}\chi^{s}_{a_2a_3,b_1b_4}(\mathbf{q},i\nu_n)U_s^{b_1b_4,b_2b_3}F^{\sigma\bar{\sigma}}_{a_4b_3}(\mathbf{k}-\mathbf{q},i\omega_n-i\nu_n)\right]G^{\bar{\sigma}}_{bb_2}(-\mathbf{k},-i\omega_n),$$

from density and spin fluctuation channels, respectively.

Therefore in terms of the general notation of indices it reads

$$F_{ab}^{\sigma\bar{\sigma}}(\mathbf{k},i\omega_n) = -\sum_{a'b'} G_{aa'}^{\sigma}(\mathbf{k},i\omega_n)\Phi^{\sigma\bar{\sigma},a'b'}(\mathbf{k},i\omega_n)G^{\bar{\sigma}}_{bb'}(-\mathbf{k},-i\omega_n),$$

$$\Phi^{\sigma\bar{\sigma},a'b'}(\mathbf{k},i\omega_n) = \sum_{\mathbf{q},\nu_n}\sum_{m,n} V_A^{a'm,b'n}(\mathbf{q},i\nu_n)F^{\sigma\bar{\sigma}}_{mn}(\mathbf{k}-\mathbf{q},i\omega_n-i\nu_n),$$

where the effective pairing interaction contains two contributions

$$V_A^{a'm,b'n}(\mathbf{q},i\nu_n) = V_s^{a'm,b'n}(\mathbf{q},i\nu_n) - V_c^{a'm,b'n}(\mathbf{q},i\nu_n).$$

3.6.3 Self-energies and Higher-order Interaction Vertices

We summarize all the results from the last two sections here for convenience. The expressions for the normal and anomalous self-energies are writen as

$$\Sigma^{a'b'}(\mathbf{k}, i\omega_n) = \frac{T}{N}\sum_{\mathbf{q},\nu_n}\sum_{m,n} V_N^{a'm,nb'}(\mathbf{q}, i\nu_n) G_{mn}(\mathbf{k}-\mathbf{q}, i\omega_n - i\nu_n),$$

$$\Phi^{\sigma\bar{\sigma},a'b'}(\mathbf{k}, i\omega_n) = \frac{T}{N}\sum_{\mathbf{q},\nu_n}\sum_{m,n} V_A^{a'm,b'n}(\mathbf{q}, i\nu_n) F_{mn}^{\sigma\bar{\sigma}}(\mathbf{k}-\mathbf{q}, i\omega_n - i\nu_n),$$

with the following definitions for the effective interaction vertices

$$V_N^{a'm,nb'}(\mathbf{q}, i\nu_n) = V_s^{a'm,nb'}(\mathbf{q}, i\nu_n) + V_c^{a'm,nb'}(\mathbf{q}, i\nu_n),$$

$$V_A^{a'm,b'n}(\mathbf{q}, i\nu_n) = V_s^{a'm,b'n}(\mathbf{q}, i\nu_n) - V_c^{a'm,b'n}(\mathbf{q}, i\nu_n),$$

where the charge and spin interaction vertices are due to exchange of fluctuations

$$V_c^{a'm,nb'}(\mathbf{q}, i\nu_n) = \frac{1}{2}\sum_{\alpha\beta,\mu\nu} U_c^{a'm,\alpha\beta}\left[\chi_{\alpha\beta,\mu\nu}^{c}(\mathbf{q}, i\nu_n) - \chi_{\alpha\beta,\mu\nu}^{c,0}(\mathbf{q}, i\nu_n)\right] U_c^{\mu\nu,nb'},$$

$$V_s^{a'm,nb'}(\mathbf{q}, i\nu_n) = \frac{3}{2}\sum_{\alpha\beta,\mu\nu} U_s^{a'm,\alpha\beta}\left[\chi_{\alpha\beta,\mu\nu}^{s}(\mathbf{q}, i\nu_n) - \chi_{\alpha\beta,\mu\nu}^{s,0}(\mathbf{q}, i\nu_n)\right] U_s^{\mu\nu,nb'}.$$

3.7 Low-order Diagrams

As we mentioned earlier, FLEX formula have double counting problem in the second order and they don't include the first order contribution. Therefore we need to evaluate them by applying the basic perturbation theory. To calculate the lower-order diagrams, it is much easier to employ the following expression of the interaction Hamiltonian

$$H_{int} = \frac{1}{2}\sum_{i,a_i,\sigma\sigma'} U_s^{a_1a_2a_3a_4} d_{i,a_1\sigma}^{\dagger} d_{i,a_3\sigma} d_{i,a_2\sigma'}^{\dagger} d_{i,a_4\sigma'}$$

as we showed before. In momentum space it is nothing but

$$H_{int} = \frac{1}{2}\sum_{\mathbf{k}_i,a_i,\sigma_1\sigma_1'} U_s^{a_1a_2a_3a_4} d_{\mathbf{k}_1,a_1\sigma_1}^{\dagger} d_{\mathbf{k}_3,a_3\sigma_1} d_{\mathbf{k}_2,a_2\sigma_1'}^{\dagger} d_{\mathbf{k}_4,a_4\sigma_1'} \delta_{\mathbf{k}_1+\mathbf{k}_2,\mathbf{k}_3+\mathbf{k}_4}.$$

Due to the lengthy steps, we present the detailed derivation in Appendix A.1 and just show the final results in below.

3.7.1 First Order Contribution — Hartree-Fock Terms

The first order contribution is static without energy-momentum dependence, i.e., Hartree-Fock terms. The Hartree-Fock term in the normal self-energy is obtained as

$$G^{\sigma}_{ab}(\mathbf{k}, i\omega_n) = \sum_{a',b'} G_{aa'}(\mathbf{k}, i\omega_n)\Sigma^{a'b'}_{HF} G_{b'b}(\mathbf{k}, i\omega_n),$$

with

$$\Sigma^{a'b'}_{HF} = \sum_{m,n} V^{a'm,nb'}_{N,HF} \left[\delta_{mn} + \frac{T}{N} \sum_{\mathbf{k}',\omega'_n} G_{mn}(\mathbf{k}', i\omega'_n) \right],$$
$$V^{a'm,nb'}_{N,HF} = \frac{1}{2}(3U_s - U_c)^{a'm,nb'}.$$

And in the anomalous self-energy it is

$$F^{\sigma\sigma'}_{ab}(\mathbf{k}, i\omega_n) = -\sum_{a',b'} G^{\sigma}_{aa'}(\mathbf{k}, i\omega_n)\Phi^{\sigma\sigma',a'b'}_{HF} G^{\sigma'}_{bb'}(-\mathbf{k}, -i\omega_n),$$

with

$$\Phi^{\sigma\sigma',a'b'}_{HF} = \sum_{m,n} V^{a'm,b'n}_{A,HF} \left[\frac{T}{N} \sum_{\mathbf{k}',\omega'_n} F^{\sigma\sigma'}_{mn}(\mathbf{k}', i\omega'_n) \right],$$
$$V^{a'm,b'n}_{A,HF} = \frac{1}{2}(U_s + U_c)^{a'm,b'n}.$$

Note that in the multi-orbital case, Hartree-Fock contributions can not be simply absorbed into chemical potential any more due to their matrix structure in orbital space.

3.7.2 Second Order Diagrams

In the second order contributions, the normal self-energy is obtained as

$$\Sigma^{a'b'}_{(2)}(\mathbf{k}, i\omega_n) = \sum_{\mathbf{q},\nu_n} \sum_{m,n} V^{a'm,nb'}_{N,(2)}(\mathbf{q}, i\nu_n) G_{mn}(\mathbf{k}-\mathbf{q}, i\omega_n - i\nu_n)$$

with

$$V^{a'm,nb'}_{N,(2)}(\mathbf{q}, i\nu_n) = \sum_{\alpha\beta,\mu\nu} [\frac{3}{4} U_s^{a'm,\alpha\beta} \chi^1_{\alpha\beta,\mu\nu}(\mathbf{q}, i\nu_n) U_s^{\mu\nu,nb'} + \frac{1}{4} U_c^{a'm,\alpha\beta} \chi^1_{\alpha\beta,\mu\nu}(\mathbf{q}, i\nu_n) U_c^{\mu\nu,nb'}$$
$$+ \frac{3}{2} U_s^{a'm,\alpha\beta} \chi^2_{\alpha\beta,\mu\nu}(\mathbf{q}, i\nu_n) U_s^{\mu\nu,nb'} - \frac{1}{2} U_c^{a'm,\alpha\beta} \chi^2_{\alpha\beta,\mu\nu}(\mathbf{q}, i\nu_n) U_c^{\mu\nu,nb'}]$$

Gathering the subtracted second-order contributions in the last section, the total second-order contribution to normal interaction vertex is

$$\begin{aligned}
&V_{N,(2)}^{a'm,nb'}(\mathbf{q},i\nu_n)-\frac{3}{2}\tilde{U}_s\tilde{\chi}^{s,0}\tilde{U}_s-\frac{1}{2}\tilde{U}_c\tilde{\chi}^{c,0}\tilde{U}_c\\
&=\sum_{\alpha\beta,\mu\nu}[-\frac{3}{4}U_s^{a'm,\alpha\beta}\chi^1_{\alpha\beta,\mu\nu}(\mathbf{q},i\nu_n)U_s^{\mu\nu,nb'}-\frac{1}{4}U_c^{a'm,\alpha\beta}\chi^1_{\alpha\beta,\mu\nu}(\mathbf{q},i\nu_n)U_c^{\mu\nu,nb'}\\
&=-\frac{3}{4}\tilde{U}_s\tilde{\chi}^1\tilde{U}_s-\frac{1}{4}\tilde{U}_c\tilde{\chi}^1\tilde{U}_c
\end{aligned}$$

where

$$\tilde{\chi}^{s,0}=\tilde{\chi}^1+\tilde{\chi}^2,\quad \tilde{\chi}^{c,0}=\tilde{\chi}^1-\tilde{\chi}^2.$$

And the anomalous self-energy reads

$$\Phi_{(2)}^{\sigma\bar{\sigma},a'b'}(\mathbf{k},i\omega_n)=\sum_{\mathbf{q},\nu_n}\sum_{m,n}V_{A,(2)}^{a'm,b'n}(\mathbf{q},i\nu_n)F_{mn}^{\sigma\bar{\sigma}}(\mathbf{k}-\mathbf{q},i\omega_n-i\nu_n),$$

with

$$\begin{aligned}
V_{A,(2)}^{a'm,b'n}(\mathbf{q},i\nu_n)=\sum_{\alpha\beta,\mu\nu}[&\left(\frac{3}{2}U_s^{a'm,\alpha\beta}\chi^1_{\alpha\beta,\mu\nu}(\mathbf{q},i\nu_n)U_s^{\mu\nu,b'n}-\frac{1}{2}U_c^{a'm,\alpha\beta}\chi^1_{\alpha\beta,\mu\nu}(\mathbf{q},i\nu_n)U_c^{\mu\nu,b'n}\right)\\
&+\frac{3}{4}U_s^{a'm,\alpha\beta}\chi^2_{\alpha\beta,\mu\nu}(\mathbf{q},i\nu_n)U_s^{\mu\nu,b'n}+\frac{1}{4}U_c^{a'm,\alpha\beta}\chi^2_{\alpha\beta,\mu\nu}(\mathbf{q},i\nu_n)U_c^{\mu\nu,b'n}].
\end{aligned}$$

Gathering the subtracted second-order contributions in the last section, the total second-order contribution to the anomalous interaction vertex is

$$\begin{aligned}
&V_{A,(2)}^{a'm,b'n}(\mathbf{q},i\nu_n)-\frac{3}{2}\tilde{U}_s\tilde{\chi}^{s,0}\tilde{U}_s+\frac{1}{2}\tilde{U}_c\tilde{\chi}^{c,0}\tilde{U}_c\\
&=\sum_{\alpha\beta,\mu\nu}-\frac{3}{4}U_s^{a'm,\alpha\beta}\chi^2_{\alpha\beta,\mu\nu}(\mathbf{q},i\nu_n)U_s^{\mu\nu,b'n}-\frac{1}{4}U_c^{a'm,\alpha\beta}\chi^2_{\alpha\beta,\mu\nu}(\mathbf{q},i\nu_n)U_c^{\mu\nu,b'n}\\
&=-\frac{3}{4}\tilde{U}_s\tilde{\chi}^2\tilde{U}_s-\frac{1}{4}\tilde{U}_c\tilde{\chi}^2\tilde{U}_c.
\end{aligned}$$

3.8 FLEX Interaction Vertices

Finally, we can write the expressions for the particle-hole and particle-particle scattering vertices (diagrammatically demonstrated in Fig. 3.3) from second- to infinite-order in FLEX approximation.

Figure 3.3 Diagrammatic demonstration of the effective particle-particle and particle-hole interaction by the exchange of fluctuations. The double curved line refers to the renormalized fluctuation propagator and the single line represents single-particle propagator.

Adding the specific expressions of the low-order diagrams to the FLEX vertices, we find for the particle-hole scattering vertex

$$
\begin{aligned}
&V_N^{a'm,nb'}(\mathbf{q}, i\nu_n) \\
&= \sum_{\alpha\beta,\mu\nu} \left[\frac{3}{2} U_s^{a'm,\alpha\beta} \chi^s_{\alpha\beta,\mu\nu}(\mathbf{q}, i\nu_n) U_s^{\mu\nu,nb'} + \frac{1}{2} U_c^{a'm,\alpha\beta} \chi^c_{\alpha\beta,\mu\nu}(\mathbf{q}, i\nu_n) U_c^{\mu\nu,nb'} \right] \\
&- \sum_{\alpha\beta,\mu\nu} \left[\frac{3}{4} U_s^{a'm,\alpha\beta} \chi^1_{\alpha\beta,\mu\nu}(\mathbf{q}, i\nu_n) U_s^{\mu\nu,nb'} + \frac{1}{4} U_c^{a'm,\alpha\beta} \chi^1_{\alpha\beta,\mu\nu}(\mathbf{q}, i\nu_n) U_c^{\mu\nu,nb'} \right] + \frac{1}{2} (3U_s - U_c)^{a'm,nb'}.
\end{aligned}
$$

and for the particle-particle scattering

$$
\begin{aligned}
&V_A^{a'm,b'n}(\mathbf{q}, i\nu_n) \\
&= \sum_{\alpha\beta,\mu\nu} \left[\frac{3}{2} U_s^{a'm,\alpha\beta} \chi^s_{\alpha\beta,\mu\nu}(\mathbf{q}, i\nu_n) U_s^{\mu\nu,nb'} - \frac{1}{2} U_c^{a'm,\alpha\beta} \chi^c_{\alpha\beta,\mu\nu}(\mathbf{q}, i\nu_n) U_c^{\mu\nu,nb'} \right] \\
&- \sum_{\alpha\beta,\mu\nu} \left[\frac{3}{4} U_s^{a'm,\alpha\beta} \chi^2_{\alpha\beta,\mu\nu}(\mathbf{q}, i\nu_n) U_s^{\mu\nu,nb'} + \frac{1}{4} U_c^{a'm,\alpha\beta} \chi^2_{\alpha\beta,\mu\nu}(\mathbf{q}, i\nu_n) U_c^{\mu\nu,nb'} \right] + \frac{1}{2} (U_s + U_c)^{a'm,b'n}.
\end{aligned}
$$

In matrix form they are written as

$$
\tilde{V}_N(\mathbf{q}, i\nu_n) = \frac{3}{2} \tilde{U}_s \tilde{\chi}^s(\mathbf{q}, i\nu_n) \tilde{U}_s + \frac{1}{2} \tilde{U}_c \tilde{\chi}^c(\mathbf{q}, i\nu_n) \tilde{U}_c - \frac{3}{4} \tilde{U}_s \tilde{\chi}^1 \tilde{U}_s - \frac{1}{4} \tilde{U}_c \tilde{\chi}^1 \tilde{U}_c + \frac{1}{2} \left(3\tilde{U}_s - \tilde{U}_c \right).
$$

$$
\tilde{V}_A(\mathbf{q}, i\nu_n) = \frac{3}{2} \tilde{U}_s \tilde{\chi}^s(\mathbf{q}, i\nu_n) \tilde{U}_s - \frac{1}{2} \tilde{U}_c \tilde{\chi}^c(\mathbf{q}, i\nu_n) \tilde{U}_c - \frac{3}{4} \tilde{U}_s \tilde{\chi}^2 \tilde{U}_s - \frac{1}{4} \tilde{U}_c \tilde{\chi}^2 \tilde{U}_c + \frac{1}{2} \left(\tilde{U}_s + \tilde{U}_c \right).
$$

Meanwhile, the self-energies are given by

$$
\Sigma^{a'b'}(\mathbf{k}, i\omega_n) = \sum_{\mathbf{q},\nu_n} \sum_{m,n} V_N^{a'm,nb'}(\mathbf{q}, i\nu_n) G_{mn}(\mathbf{k} - \mathbf{q}, i\omega_n - i\nu_n),
$$

$$
\Phi^{\sigma\bar{\sigma},a'b'}(\mathbf{k}, i\omega_n) = \sum_{\mathbf{q},\nu_n} \sum_{m,n} V_A^{a'm,b'n}(\mathbf{q}, i\nu_n) F_{mn}^{\sigma\bar{\sigma}}(\mathbf{k} - \mathbf{q}, i\omega_n - i\nu_n).
$$

The building blocks in this formula are the electron Green's functions, $\tilde{G}$ and $\tilde{F}$, and the coupling constants, $\tilde{U}_s$ and $\tilde{U}_c$. We have known the specific form of the coupling constants when we discuss the interaction Hamiltonian. Also the early discussion of the non-interacting Hamiltonian gives the bare matrix Green's function as

$$\tilde{G}_0(\mathbf{k}, i\omega_n)^{-1} = i\omega_n \tilde{\mathbf{1}} - \left(\tilde{\varepsilon}_{\mathbf{k}} - \mu\tilde{\mathbf{1}}\right).$$

3.9 Renormalized Matrix Green's Function

Then when we take into account the effective interaction due to the exchange of fluctuations, the single-particle Green's functions are renormalized and there appear the anomalous components as a consequence of the interaction-driven phase transition to superconducting state.

In Nambu space, the matrix form of the Green's function is given by

$$\begin{aligned}\mathbb{G}(\mathbf{k}, \tau)_{ab} &= -\langle T_\tau \begin{bmatrix} d_{\mathbf{k}a\sigma}(\tau) \\ d^\dagger_{-\mathbf{k}a\bar{\sigma}}(\tau) \end{bmatrix} \begin{bmatrix} d^\dagger_{\mathbf{k}b\sigma}(0) & d_{-\mathbf{k}b\bar{\sigma}}(0) \end{bmatrix} \rangle \\ &= \begin{bmatrix} G^\sigma_{ab}(\mathbf{k}, \tau) & F^{\sigma\bar{\sigma}}_{ab}(\mathbf{k}, \tau) \\ \\ \overline{F}^{\bar{\sigma}\sigma}_{ab}(\mathbf{k}, \tau) & -G^{\bar{\sigma}}_{ba}(-\mathbf{k}, -\tau) \end{bmatrix}.\end{aligned}$$

Transforming to Matsubara frequency it becomes

$$\mathbb{G}(\mathbf{k}, i\omega_n)_{ab} = \begin{bmatrix} G^\sigma_{ab}(\mathbf{k}, i\omega_n) & F^{\sigma\bar{\sigma}}_{ab}(\mathbf{k}, i\omega_n) \\ \\ \overline{F}^{\bar{\sigma}\sigma}_{ab}(\mathbf{k}, i\omega_n) & -G^{\bar{\sigma}}_{ba}(-\mathbf{k}, -i\omega_n) \end{bmatrix}.$$

Since we have the transformation properties for Green's function matrices obtained earlier

$$\tilde{G}(\mathbf{k}, i\omega_n)^T = \tilde{G}(\mathbf{k}, -i\omega_n)^*$$

$$\overline{F}^{\sigma\bar{\sigma}}_{ab}(\mathbf{k}, i\omega_n) = F^{\bar{\sigma}\sigma}_{ab}(-\mathbf{k}, i\omega_n)^*,$$

it holds

$$\mathbb{G}(\mathbf{k}, i\omega_n)_{ab} = \begin{bmatrix} G^\sigma_{ab}(\mathbf{k}, i\omega_n) & F^{\sigma\bar{\sigma}}_{ab}(\mathbf{k}, i\omega_n) \\ \\ F^{\sigma\bar{\sigma}}_{ab}(-\mathbf{k}, i\omega_n)^* & -G^{\bar{\sigma}}_{ab}(-\mathbf{k}, i\omega_n)^* \end{bmatrix}.$$

That is

$$\mathbb{G}(k)_{ab} = \begin{bmatrix} G^{\sigma}(k) & F^{\sigma\bar{\sigma}}(k) \\ \overline{F}^{\bar{\sigma}\sigma}(k) & -G^{\bar{\sigma}}(-k)^T \end{bmatrix}_{ab} = \begin{bmatrix} G^{\sigma}(k) & F^{\sigma\bar{\sigma}}(k) \\ F^{\sigma\bar{\sigma}}(k')^* & -G^{\bar{\sigma}}(k')^* \end{bmatrix}_{ab}$$

where $k \equiv (\mathbf{k}, i\omega_n)$, $k' \equiv (-\mathbf{k}, i\omega_n)$.

The full Green's function is a composite matrix in the sense that it is a 2×2 matrix in the fermion space as shown above, and meanwhile it is an $M \times M$ matrix in the orbital space. The two subspaces are independent of each other. Therefore we can either treat the whole matrix as an $M \times M$ matrix with each matrix element to be a 2×2 matrix with the specific orbital indices as we did above, or treat it as a 2×2 matrix with each element to be an $M \times M$ matrix with the specific type: G or F. For the latter, we write the matrix Green's function as

$$\mathbb{G}(k) = \begin{bmatrix} \tilde{G}(k) & \tilde{F}(k) \\ \tilde{F}(k')^* & -\tilde{G}(k')^* \end{bmatrix}$$

where $\tilde{G}$ and $\tilde{F}$ are $M \times M$ matrices in the orbital space, $k = (\mathbf{k}, i\omega_n)$, $k' \equiv (-\mathbf{k}, i\omega_n)$.

Then the matrix form of the Dyson-Gorkov equation becomes

$$\mathbb{G}(k) = \mathbb{G}_0(k) + \mathbb{G}_0(k)\hat{\Sigma}(k)\mathbb{G}(k)$$

$$\Longrightarrow \left(\hat{1} - \mathbb{G}_0(k)\hat{\Sigma}(k)\right)\mathbb{G}(k) = \mathbb{G}_0(k)$$

$$\Longrightarrow \mathbb{G}(k) = \left[\mathbb{G}_0(k)^{-1} - \hat{\Sigma}(k)\right]^{-1}$$

where

$$\hat{\Sigma}(k) = \begin{bmatrix} \tilde{\Sigma}(k) & \tilde{\Phi}^{\sigma\bar{\sigma}}(k) \\ \tilde{\Phi}^{\sigma\bar{\sigma}}(k')^* & -\tilde{\Sigma}(k')^* \end{bmatrix} \equiv \begin{bmatrix} \tilde{\Sigma}(k) & \tilde{\Phi}(k) \\ \tilde{\Phi}(k')^* & -\tilde{\Sigma}(k')^* \end{bmatrix}$$

and the bare Green's function is diagonal in Nambu space

$$\mathbb{G}_0(k) = \begin{bmatrix} \tilde{G}_0(k) & 0 \\ 0 & -\tilde{G}_0(k')^* \end{bmatrix}$$

since $\tilde{F}(k) = 0$ on the quadratic level.

Solving the matrix equation formally we obtain two independent equations which are coupled matrix Dyson-Gorkov equaitons

$$\tilde{G}(k)\left[\tilde{G}_0(k)^{-1} - \tilde{\Sigma}(k)\right] - \tilde{F}(k)\tilde{\Phi}(k')^* = \tilde{1},$$

$$\tilde{G}(k)\tilde{\Phi}(k) + \tilde{F}(k)\left[\tilde{G}_0(-k)^{-1} - \tilde{\Sigma}(k')\right]^* = \tilde{0}.$$

Which can be diagrammatically demonstrated in Fig. 3.4.

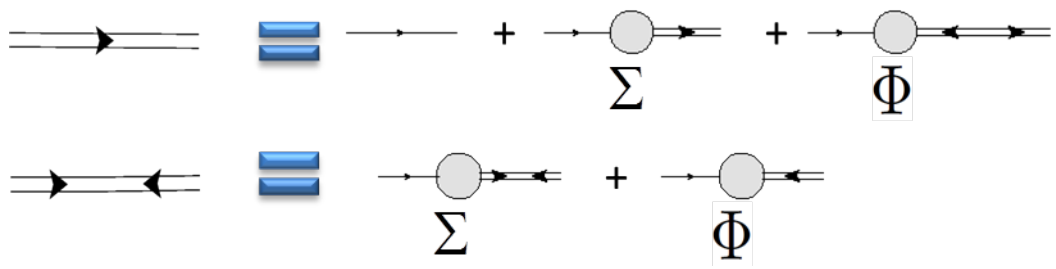

Figure 3.4 Diagrammatic demonstration of the Dyson-Gorkov equations. The double-line refers to the renormalized or dressed single-particle propagator, while the single-line indicates the bare one.

In this way, the $2M \times 2M$ matrix equation is simplified into two $M \times M$ matrix equations. From the second equation we solve for F

$$\tilde{F}(k) = -\tilde{G}(k)\tilde{\Phi}(k)\left[\tilde{G}_0^*(k')^{-1} - \tilde{\Sigma}^*(k')\right]^{-1}$$

substitute it into the first equation

$$\begin{aligned}\tilde{G}(k)\left[\tilde{G}_0(k)^{-1} - \tilde{\Sigma}(k)\right] + \tilde{G}(k)\tilde{\Phi}(k)\left[\tilde{G}_0^*(k')^{-1} - \tilde{\Sigma}^*(k')\right]^{-1}\tilde{\Phi}(k')^* &= \tilde{1} \\ \Longrightarrow \tilde{G}(k)\left[\tilde{G}_0(k)^{-1} - \tilde{\Sigma}(k) + \tilde{\Phi}(k)\left[\tilde{G}_0^*(k')^{-1} - \tilde{\Sigma}^*(k')\right]^{-1}\tilde{\Phi}(k')^*\right] &= \tilde{1}\end{aligned}$$

we find the expression for G

$$\begin{aligned}\tilde{G}(k) &= \left[\tilde{G}_0(k)^{-1} - \tilde{\Sigma}(k) + \tilde{\Phi}(k)\left[\tilde{G}_0^*(k')^{-1} - \tilde{\Sigma}^*(k')\right]^{-1}\tilde{\Phi}(k')^*\right]^{-1} \\ &= \left[i\omega_n\tilde{\mathbf{1}} - \left(\tilde{\varepsilon}_{\mathbf{k}} - \mu\tilde{\mathbf{1}}\right) - \tilde{\Sigma}(k) - \tilde{\Phi}(k)\left[i\omega_n\tilde{\mathbf{1}} + \left(\tilde{\varepsilon}_{\mathbf{k}} - \mu\tilde{\mathbf{1}}\right) + \tilde{\Sigma}^*(k')\right]^{-1}\tilde{\Phi}(k')^*\right]^{-1}\end{aligned}$$

where $k = (\mathbf{k}, i\omega_n)$, $k' = (-\mathbf{k}, i\omega_n)$.

It is easy to check that the above matrix formula can reproduce the expressions in the the single-band case

$$\begin{aligned} G(k) &= \frac{(\varepsilon_{\mathbf{k}} + \mathrm{X}(k)) + (i\omega_n - \mathrm{Y}(k))}{(i\omega_n - \mathrm{Y}(k))^2 - (\varepsilon_{\mathbf{k}} + \mathrm{X}(k))^2 - |\Phi(k)|^2}, \\ F(k) &= \frac{\Phi(k)}{(i\omega_n - \mathrm{Y}(k))^2 - (\varepsilon_{\mathbf{k}} + \mathrm{X}(k))^2 - |\Phi(k)|^2}, \end{aligned}$$

where

$$\mathrm{X}(k) = \frac{1}{2}\left(\Sigma(k) + \Sigma^*(k')\right), \quad \mathrm{Y}(k) = \frac{1}{2}\left(\Sigma(k) - \Sigma^*(k')\right).$$

CHAPTER 4. SELF-CONSISTENT SOLUTION

To perform the calculation for iron-based superconductors, we consider a Hamiltonian described by a 2-orbital tight-binding model and on-site multiorbital electronic interactions,

$$\begin{aligned} H = & \sum_{\mathbf{k},ab,\sigma} \varepsilon_{\mathbf{k}}^{ab} d_{\mathbf{k}a\sigma}^{\dagger} d_{\mathbf{k}b\sigma} + U \sum_{i,a} n_{ia\uparrow} n_{ia\downarrow} + U' \sum_{i,a>b} n_{ia} n_{ib} \\ & + J_H \sum_{i,a>b,\sigma\sigma'} d_{ia\sigma}^{\dagger} d_{ib\sigma'}^{\dagger} d_{ia\sigma'} d_{ib\sigma} \\ & + J' \sum_{i,a\neq b} d_{ia\uparrow}^{\dagger} d_{ia\downarrow}^{\dagger} d_{ib\downarrow} d_{ib\uparrow} \end{aligned} \tag{4.1}$$

where $n_{ia\sigma} = d_{ia\sigma}^{\dagger} d_{ia\sigma}$ is the occupation number of the orbital a with spin σ at site i and $n_{ia} = \sum_{\sigma} n_{ia\sigma}$ with the orbital index $a(b)$ standing for the Fe orbitals d_{xz} and d_{yz}. The tight-binding description [Raghu et al. (2008)] is given by $\varepsilon_{\mathbf{k}}^{xy} = \varepsilon_{\mathbf{k}}^{yx} = -4t_4 \sin k_x \sin k_y$ and $\varepsilon_{\mathbf{k}}^{aa} = -2t_1 \cos k_a - 2t_2 \cos k_b - 4t_3 \cos k_x \cos k_y - \mu$ where $a, b = x(y)$ stand for $d_{xz}(d_{yz})$ orbitals and the momentum components with $a \neq b$. We use the tight-binding parameters $t_1 = -0.33$, $t_2 = 0.385$, $t_3 = -0.234$, and $t_4 = -0.26$. [Sknepnek et al. (2009); Zhang et al. (2009a, 2010)] Near half filling this tight-binding model gives rise to the FS that contains two hole pockets and two electron pockets for which we refer to the hole pockets around $(0, 0)$ and (π, π) as α_1 and α_2 sheets, respectively, and the electron pockets around $(\pi, 0)$ and $(0, \pi)$ as β_1 and β_2 sheets, respectively, in the unfolded (1 Fe per unit cell) Brillouin zone (BZ). As noted by Kuroki *et al.* [Kuroki et al. (2009)] and Kemper *et al.* [Kemper et al. (2010)], the appearance of a hole pocket around the (π, π) point of the unfolded BZ is crucial to the formation of fully gapped $s^{\pm}$ state. The predominant Fe-orbital character distribution on each FS sheet has been analyzed in Ref. [Graser et al. (2009)]. In the 5-orbital tight-binding description, [Kemper et al. (2010)] a third orbital d_{xy} predominantly contributes to the hole pocket at the (π, π) point and

partially to the $(\pi, 0)$ and $(0, \pi)$ electronic pockets. Although the 2-orbital model does not include the third predominant orbital composition on the FS, as we will show later, the intra-orbital nesting configuration of it remains similar to that of the 5-orbital description, which is believed to play an important role for the magnetic fluctuation and the superconductivity in the itinerant picture. Thus this simplified 2-orbital description qualitatively captures the key features of the electronic structure near the Fermi energy, serving as a good starting point for the understanding of the interplay between magnetism and superconductivity in the Fe-based superconductors.

The on-site interactions consist of the intra- and inter-orbital Coulomb repulsion controlled by the coupling constant U and U', the inter-orbital Hund's rule coupling J_H and pair hopping term J'. For the bare Coulomb interaction, due to rotational symmetry, the coupling constants are related by $U = U' + 2J$ and $J = J_H = J'$. However, as discussed in the Ref. [Zhang et al. (2009a)], when they are parameters in an approximate theory such as FLEX which ignores vertex corrections, they are not identical to the bare Coulomb matrix elements but should be considered as low energy coupling parameters that have been renormalized by high energy excitations. Therefore we study cases with various parameter values and present the typical results here.

Within the framework of the self-consistent fluctuation exchange approximation, we search for stable SC solution using the above itinerant model at different coupling constants, doping levels and temperatures. Further we examine the features of the magnetic response for systems that develop superconductivity induced by exchange of short-range fluctuations. In FLEX formalism both spin and charge/orbital fluctuations contribute to the pairing interaction, but the major contribution to the pairing glue comes from spin fluctuations for the parameter regime we are studying. The nested structure of the FS leads to peak in the magnetic susceptibility near the AFM wave vector $\mathbf{Q}_{\mathrm{AFM}} = (0, \pi),\ (\pi, 0)$, which is strongest at half-filling, $n = 2.0$ per site, indicating its correspondence to the parent compound.

The calculations are performed on imaginary frequency axis for a lattice of 64×64 sites with 8192 Matsubara frequencies. When self-consistently solving the FLEX equations, the convergence of iterations is considered achieved when the maximum relative difference between

two consecutive iterations of the self-energy element, $\Sigma^{ab}(\mathbf{k}, i\omega_n)$ or $\Phi^{ab}(\mathbf{k}, i\omega_n)$, is less than 10^{-6}. Please refer to Appendix B.2 for the information of numerical implementation.

It turns out that compared with the single-band case the search for self-consistent solution in multiorbital model is a much more difficult task: (1) it is more sensitive to the Fermi surface configuration and the spin flucutation structure; (2) it takes much longer time to find a stable solution. The iteration number can be on the order of ten thousands before a convergence is reached. Having tested order parameters with different symmetry type, we only found one type of symmetry, the s± state associated with commensurate short-range spin fluctuations, surviving. Below we briefly describe our solution regarding the magnetic structure and the order parameter function in this model.

4.1 Comensurate Antiferromagnetic Correlation

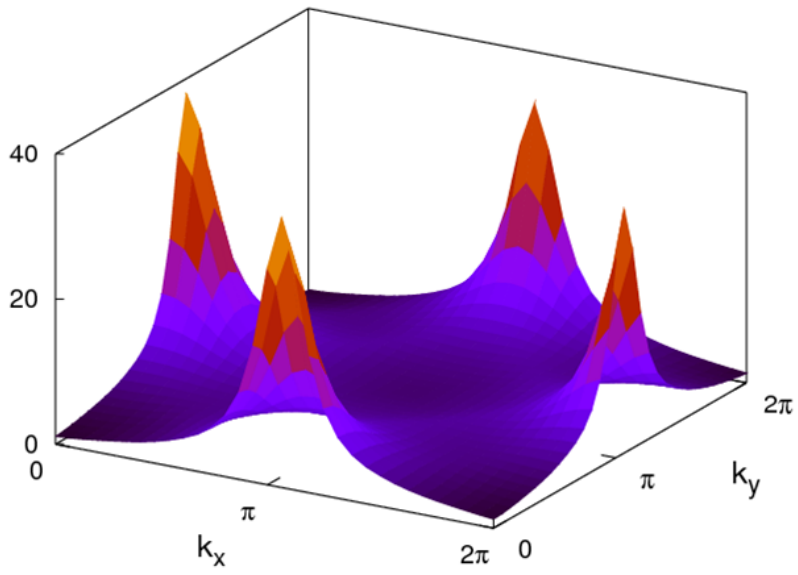

Figure 4.1 Magnetic susceptibility in momentum space. It shows strongly enhanced antiferromagnetic fluctuation.

We find strongly enhanced comensurate antiferromagnetic correlation in this system as shown in Fig. 4.1. Clearly we see that the spin susceptibility is peaked at the antiferromag-

netic wave vector $(\pm\pi, 0)$ and $(0, \pm\pi)$, which is consistent with the experimentally established magnetic structure in 1111 and 122 structures as discussed in Chapter 1.

For certain parameter sets, the system can develop incommensurate magnetic peak. However, the incommensurate spin fluctuation structure does not support superconductivity. In our calculation, this kind of structure can not provide sufficient pairing condition. As we will see later in Fig. 5.1, in the superconducting state Fermi surface is not perfectly nested, commensurate fluctuations match better the pair scattering between hole- and electron-pocket. This is different from the magnetic splitting in the d-wave case where the pair scattering is intraband.

4.2 Superconducting Order Parameter: s± wave

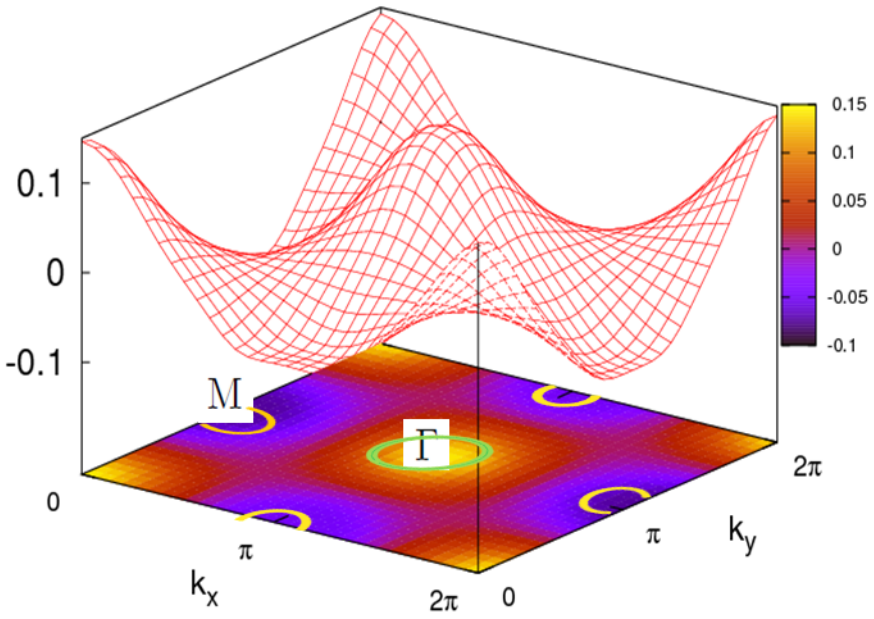

Figure 4.2 Supercoducting order parameter structure in momentum space. It has the sign-reversed s-wave symmetry.

A finite superconducting order parameter develops associated with the antiferromagnetic spin fluctuations, exhibiting sign-reversed s-wave, or say s±-wave, symmetry as shown in Fig. 4.2. This indicates that spin fluctuations are capable to serve as the mediating glue for Cooper

pairing formation in this system. And the antiferromagnetic spin flucatuation structure supports s±-wave symmetry. Based on a systematic study applying different-symmetry order parameters as the initial values, we did not find other symmetry type survive the iterations. Therefore, we suggest that s±-wave state is most favourable in this system.

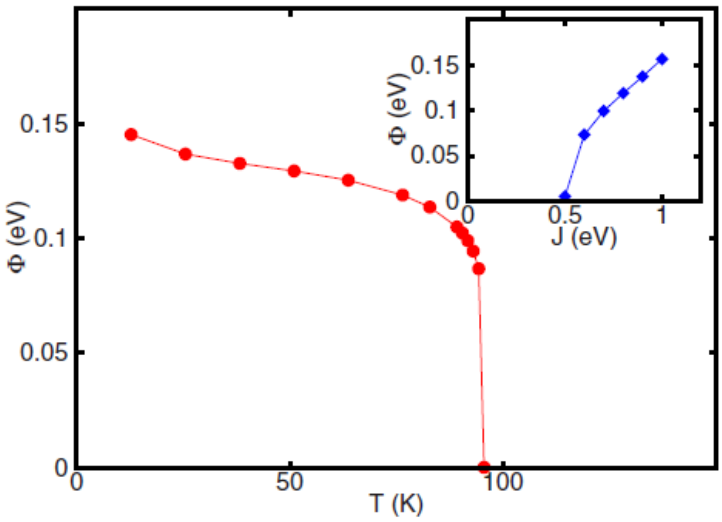

Figure 4.3 The temperature dependence of the superconducting order parameter is shown by the red points. The order parameter is also very sensitive to Hund's coupling and the pair hopping term J as shown in the inset by the blue points.

Besides a temperature dependence of the order parameter as shown in Fig. 4.3 we also find that the superconducting order is sensitive to the Hund's coupling J_H as shown in the inset of the figure. Only when the Hund's coupling is strong enough can superconducting emerge. Since here we take the pair hopping term $J' = J_H$, we suspect that the pairing hopping term might be also important for superconductivity. Both J_H and J' are interorbital couplings, therefore they could enhance superconductivity by increasing interorbital transitions.

4.3 Interorbital Coupling

Indeed, we find that interorbital may help gap formation as can be clearly seen in Fig. 4.4. In this figure, we compare two cases: in case I (the upper row) the system develops huge magnetic peak in the intraorbital channel but a very tiny peak in interorbital channel. In case II (the lower row) the intraorbital peak is much less than that in case one but it develops a similar

interorbital peak. Case II is obviously less magnetic than case I. However, with the assistance of the mild interorbital interaction, case II establishes an order parameter with similar magnitude as that in case I. This might happen in real material given that the system does not have gigantic magnetic fluctuations.

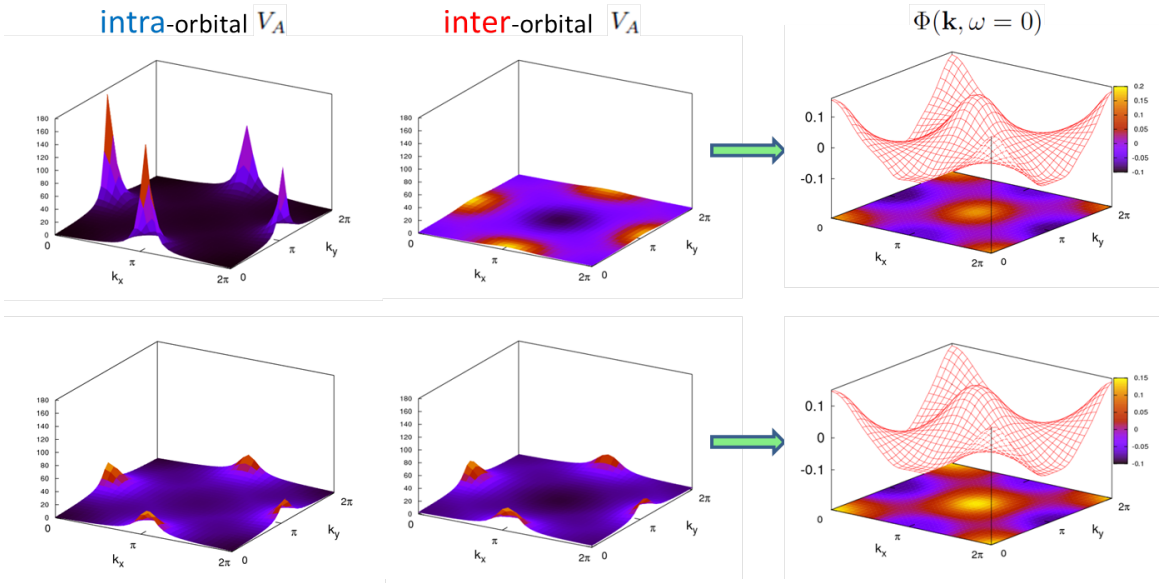

Figure 4.4 We compare two cases: in case I (the upper row) the system develops huge magnetic peak in the intraorbital channel but a very tiny peak in interorbital channel. In case II (the lower row) the intraorbital peak is much less than that in case one but it develops a similar interorbital peak. Case II is obviously less magnetic than case I. However, with the assistance of the mild interorbital interaction, case II establishes an order parameter with similar magnitude as that in case I.

CHAPTER 5. SPECTRAL INFORMATION

5.1 Introduction

The magnetic excitation spectrum carries important information on the nature of magnetism and the characteristics of superconductivity. For the latter, it has been discussed in the context of cuprates that an observation of a sharp quasiparticle-like resonance peak in the spin fluctuation spectrum with the onset of superconductivity may strongly indicate a sign change in the gap structure due to the superconducting coherence factors. And the analogous discussion has been applied to the iron pnictides based on the random phase approximation (RPA) and the mean-field BCS approximation, showing that a strong spin resonance occurs in the $s^{\pm}$-wave SC state. This indicates that the spin resonance phenomenon is compatible with the $s^{\pm}$-wave SC gap. Meanwhile, as a momentum resolved probe of the spin correlation, inelastic neutron scattering (INS) experiments have reported the observation of resonance mode in the superconducting state. Notice that the spin resonance is a consequence of the sign-reversed gap opening in the quasiparticle spectrum not an evidence for the magnetic pairing glue. In order to reveal the relationship between AFM fluctuations and superconductivity in the iron-based materials, more detailed inspections on the structure of the spin fluctuations are needed. Recently, INS measurements observe the same type of anisotropic feature in the magnetic spectrum both in the normal and in the SC state of the 122 system. [Lester et al. (2010); Diallo et al. (2010); Li (2010)] This anisotropy is characterized by larger broadening along the transverse direction with respect to the AFM wave vector $\mathbf{Q}_{\mathrm{AFM}}$ in momentum space. Ref. [Li (2010)] also shows no changes observed in the spatial correlations through T_c, which is consistent with the magnetic scenario in that the onset of superconductivity does not change magnetic correlation length. Early theoretical exploration on the short-range spin-fluctuation induced superconduc-

tivity has argued that magnetic fluctuations throughout an extended momentum region near AFM wave vector $\mathbf{Q}_{\rm AFM}$ are relevant to superconductivity. Thus it raises a question: Is the observed anisotropic feature of the spin fluctuations, i.e., larger broadening along the transverse direction in momentum space, consistent with superconductivity in this system?

On the other hand, as discussed for cuprates, [Abanov and Chubukov (1999); Abanov et al. (2001); Eschrig (2006)] an important identification of the mediating boson, if it exists, is from the fermionic spectrum which can be observed by angle-resolved photoemission spectroscopy (ARPES). Indeed, ARPES has reported the observations of kink feature in the electronic dispersion for the hole-doped 122 system. [Richard et al. (2009); Wray et al. (2008); Koitzsch et al. (2009)] However there is discrepancy in its vanishing temperature among the observations from different groups. If it is unique to the SC state, i.e., vanishing above T_c, and the subtracted bosonic mode energy coincides with the resonance energy, it would be a strong evidence for magnetic pairing mechanism.

Motivated by these experimental facts, we perform a detailed investigation of the spin and charge spectra in the normal and superconducting states, in which the magnetic susceptibility and the SC gap function are determined within the self-consistent fluctuation exchange (FLEX) approximation using a 2-orbital model for iron pnictides. This itinerant model calculation finds a fully gapped $s^{\pm}$-wave SC state driven by the enhanced commensurate AFM correlation. Based on a systematic study on the momentum structure of the short-range spin fluctuations, we find the same type of anisotropy as that observed in INS measurements. To understand the interplay between the fluctuation anisotropy and the $s^{\pm}$ superconductivity, we present a qualitative analysis through the orbital contents and the deviation from perfect nesting of the electronic structure for the 2-orbital and a more complete 5-orbital model. Meanwhile, the calculated dispersion of the magnetic resonance mode exhibits an anisotropic propagating pattern. And the calculated fermionic spectral function shows the fingerprint of electron-mode coupling as observed in ARPES.

The magnetic susceptibility is theoretically calculated using the Matsubara frequency as

$$\chi_s\left(\mathbf{q}, i\nu_n\right) = \sum_{aa,bb} \chi_s^{aa,bb}\left(\mathbf{q}, i\nu_n\right), \tag{5.1}$$

with bosonic Matsubara frequency $\nu_n = 2n\pi T$. Carrying out the analytical continuation from Mastubara frequencies to the real frequencies numerically using Padé approximant, the dynamical spin susceptibility is given by

$$\chi_s(\mathbf{q},\omega) = \chi_s\left(\mathbf{q}, i\nu_n \to \omega + i\delta\right), \tag{5.2}$$

whose imaginary part $\mathrm{Im}\chi_s$ directly relates to INS intensity. Simultaneously the quasiparticle spectral function is obtained as

$$A\left(\mathbf{k},\omega\right) = -\frac{1}{\pi}\mathrm{Im}\left[\sum_a G^{aa}\left(\mathbf{k}, i\omega_n \to \omega + i\delta\right)\right], \tag{5.3}$$

which corresponds to ARPES intensity.

5.2 Superconducting Gap Structure

For the current model we only find stable SC solutions in the hole doped regime, with the particle density $1.85 \leq n \leq 1.90$ per site, driven by short-range spin fluctuations for certain range of coupling constants. The achieved SC states are of $s^{\pm}$-wave symmetry: Fully gapped on each FS sheet with an overall sign change between the α and β sheets. To illustrate the momentum structure of the gap function, we show the results for a typical set of coupling constants $U = 1.5,\ U' = 1.2$ and $J = J' = 0.8$ with particle density $n = 1.88$ at $T = 0.001$. In this case the system exhibits a transition from the paramagnetic normal state to the SC state at $T_c = 0.0075$ and the static spin susceptibility $\chi_s(\mathbf{q}, \omega = 0)$ shows well pronounced peaks at the commensurate wave vector $\mathbf{Q}_{\mathrm{AFM}} = (0,\pi),\ (\pi,0)$ both in the normal and in the SC state. Note that we do not assign specific units to the parameters and quantities: The coupling constants scale with the hopping parameters and all energies scale with the SC gap magnitude while the temperatures scale with T_c. In Fig. 5.1 (a), we show the renormalized FS configuration obtained from the intensity projection of the Cooper-pair wave function $F(\mathbf{k},\omega)$. Taking the small damping parameter $\delta = 0.002$ in the analytical continuation for the $T = 0.001$ solution and subtracting the gap magnitude from the spectral function $A(\omega)$ at the Fermi wave vectors $\mathbf{k}_F$ for each FS sheet, the variation of the gap magnitude on each separated FS sheet is plotted in Fig. 5.1 (b). Clearly in this case the gap is nearly isotropic on each pocket. The ratio $2\Delta/T_c \sim 6 - 8$ implies a strong coupling system.

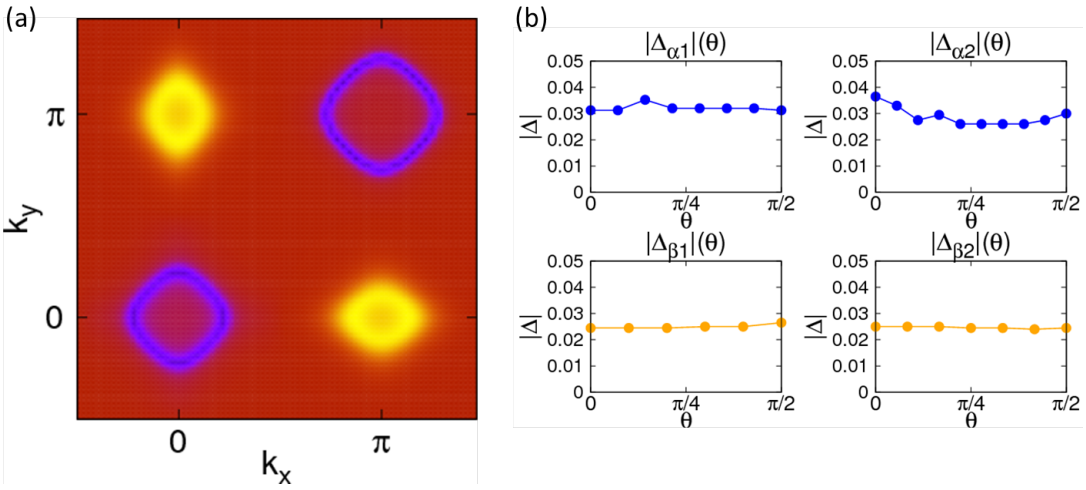

Figure 5.1 (a) The renormalized Fermi surface in the superconducting state. (b) Gap magnitude versus angle around each FS sheet. There is an overall sign change in between the hole and electron pockets.

5.3 Magnetic Spectrum

In this section we investigate the momentum structure of the short-range magnetic fluctuations that mediate superconductivity and make connection with the magnetic response measured in INS experiments. Our main points are as follows:

- The short-range spin fluctuations that are capable of driving the fully gapped $s^{\pm}$ superconductivity generally exhibit an anisotropy in momentum space with **q**-width larger along the direction transverse to $\mathbf{Q}_{\mathrm{AFM}}$ than along the longitudinal direction. This can be understood by examining the intra-orbital scattering processes in systems away from perfect nesting.

- The momentum structure of the spin excitations exhibits the same type of anisotropy, which, in the SC state, gives rise to an elliptical shape of the spin resonance mode. Further, the resonance mode disperses with increasing energy in the pattern broadening more rapidly along the transverse than along the longitudinal direction. This anisotropic dispersion of the resonance mode associated with the intrinsic anisotropy of the mode

leads to more elliptically shaped **q**-image.

- The dispersion of the magnetic resonance shows an upward pattern with increasing energy in the nearly isotropic $s^{\pm}$ state with commensurate magnetic peak. But the weight of the mode decays dramatically and vanishes above the particle-hole threshold.

- In the strong coupling approach, the resonance energy is affected by the SC gap magnitude and the magnetic correlation strength.

To illustrate these points, we present the results for the magnetic susceptibility $\chi_s(\mathbf{q},\omega)$ calculated using the typical set of parameters mentioned in the previous section followed with discussions. As J. T. Park *et al.* [Park et al. (2010)] show that the unfolded BZ description of the magnetic spectrum in the paramagnetic state is justified, our spin-fluctuation spectrum calculated in the BZ with 1 Fe ion is discussed below. The qualitative agreement of the calculated anisotropy with that observed in INS, in turn, suggests that the magnetic spectrum originates predominantly from the Fe-sublattice. In the following we refer to the transverse (TR) or longitudinal (LO) direction as the direction transverse or longitudinal to the corresponding AFM momentum transfer $\mathbf{Q}_{\mathrm{AFM}}$.

5.3.1 Results

To analyze the momentum structure of the spin fluctuations, we begin with the static spin susceptibility $\mathrm{Re}\chi_s(\mathbf{q},\omega=0)$. As shown in Fig. 5.2, besides that the static response achieves strongest enhancement at $\mathbf{Q}_{\mathrm{AFM}}$, spins are correlated spatially in an anisotropic manner with the largest span along the TR direction and smallest along the LO direction in momentum space. This results in an elliptically shaped momentum structure. Our systematic study shows that the degree of anisotropy increases with the deviation from the perfect nesting in the electronic structure. Moreover, the calculation for the temperature right above and right below the transition temperature shows that the spatial correlation does not change through T_c, reflecting the fact that spin-fluctuation induced superconductivity does not modify magnetic correlation length when entering SC phase, although it is the same electrons that contribute to the magnetic and SC properties. This is in agreement with the INS observations. [Li (2010)]

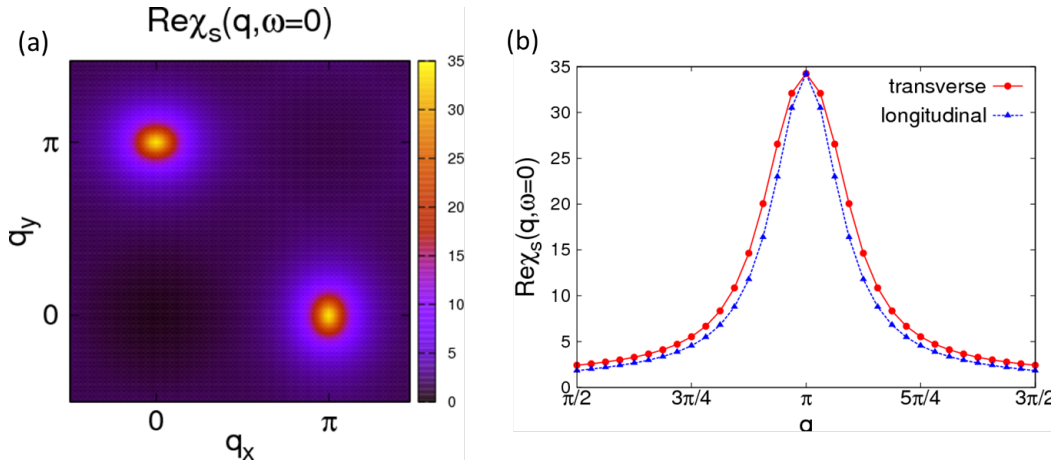

Figure 5.2 The **q**-anisotropy of the static spin susceptibility. (a) is the intensity plot of in the momentum space and (b) shows the scans along the TR (red solid circle) and LO (blue solid triangle) direction, respectively.

The imaginary part of the spin susceptibility $\mathrm{Im}\chi_s(\mathbf{q},\omega)$ contains information on the magnetic excitations. As discussed for a sign-reversed SC gap structure, the most striking feature of the magnetic spectrum is the appearance of a resonance mode at the characteristic momentum transfer $\mathbf{Q}_{\mathrm{AFM}}$ when entering SC phase in spite of no long-range magnetic order. This sharp mode is of spin-excitonic type in our model, originated from the Stoner enhancement factor $\left[\det\left|\hat{1}-\hat{\chi}_{s,0}\left(\mathbf{q},i\nu_n\right)\hat{U}_s\right|\right]^{-1}$. [Abanov and Chubukov (1999); Eschrig (2006)] Indeed, our calculation indicates a well-pronounced quasiparticle-like peak as shown in Fig. 5.3. In this figure, the results for the spin susceptibility $\mathrm{Im}\chi_s(\mathbf{Q}_{\mathrm{AFM}},\omega)$ as a function of frequency at the momentum transfer $\mathbf{Q}_{\mathrm{AFM}}$ for temperatures $T\approx 1.1T_c$, $T\approx 0.9T_c$ and $T\approx 0.1T_c$ are presented. In the normal state the magnetic spectrum exhibits a broad continuum associated with the overdamping feature of the spin fluctuations. The transition to SC state modifies the spectrum by pushing the spectral weight to higher energy and rapidly developing a resonance mode as the temperature decreasing. The fact that this mode is made out of a particle-hole bound state in the excitonic form leads to an energy threshold taking the minimal value of sums of two gap magnitudes on any pair of FS points connected by the momentum transfer $\mathbf{Q}_{\mathrm{AFM}}$. Here we refer to this threshold as $\Omega\equiv\min_{\mathbf{k}}\left(|\Delta_{\mathbf{k}}|+|\Delta_{\mathbf{k}+\mathbf{Q}_{\mathrm{AFM}}}|\right)$. For the parameter set under discussion, the

ratio of the resonance energy to the threshold and to the SC transition temperature are roughly $\omega_{\rm res}/\Omega \approx 0.6$ and $\omega_{\rm res}/k_B T_c \approx 4$, which agrees with the experimental values measured for K- and Co-doped $BaFe_2As_2$. [?Lumsden et al. (2009)]

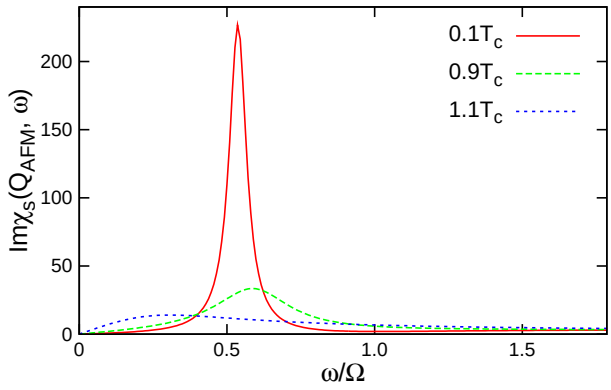

Figure 5.3 Magnetic spectrum at the momentum transfer $\mathbf{Q}_{\rm AFM}$ slightly above ($T = 1.1T_c$) and below ($T = 0.9T_c$) the transition temperature T_c, as well as deep in the superconducting state ($T = 0.1T_c$).

Next we analyze the momentum dependence of the magnetic spectrum at the resonance frequency $\omega_{\rm res}$. Figure 5.4 shows the results for $\mathrm{Im}\chi_s(\mathbf{q}, \omega_{\rm res})$ where a zoom-in $\mathbf{q}$-image of the mode at $(\pi, 0)$ is given in the middle. Similar to the static magnetic response, the $\mathbf{q}$-shape of the resonance mode is also elliptical with maximal broadening along the TR direction and minimal along the LO direction. This is an intrinsic anisotropy of the magnetic spectrum not only in the SC state but also existing in the normal state, which has been observed in the INS measurements. [Lester et al. (2010); Li (2010)]

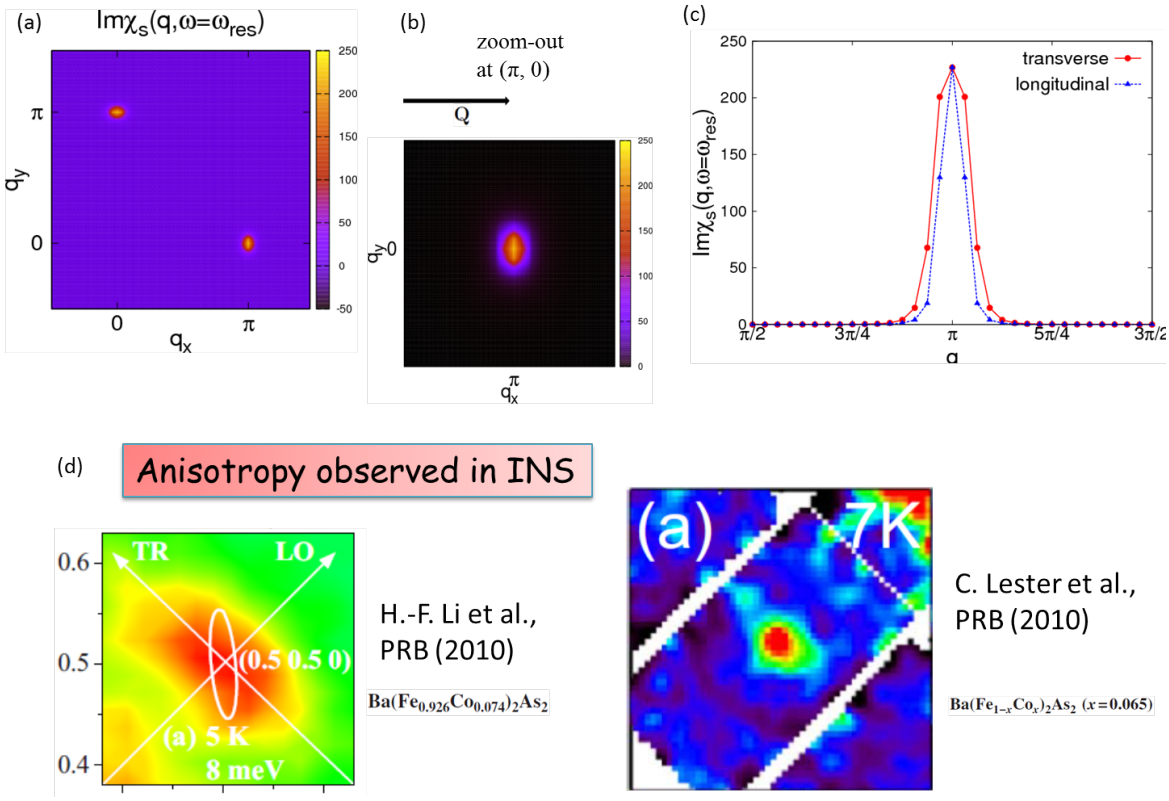

Figure 5.4 The **q**-anisotropy of the spin resonance mode. (a) is the intensity plot of $\mathrm{Im}\chi_s(\mathbf{q}, \omega_{\mathrm{res}})$ at the resonance energy in the momentum space and (b) gives a zoom-out image of the resonance mode at $(\pi, 0)$. (c) shows the scans along the TR (red solid circle) and LO (blue solid triangle) direction, respectively. (d) shows the observed **q**-anisotropy of the spin resonance mode in two inelastic neutron scattering experiments.

More interestingly, the propagation of the resonance mode also exhibits an anisotropic behavior. Figure 5.5 shows the dispersion of the resonance mode along the TR and LO direction at $T \approx 0.1T_c$, deep in the SC state. Two features are associated with the propagating behavior of the quasiparticle-like magnetic excitations in a fully gapped nearly isotropic $s^{\pm}$ state driven by commensurate short-range spin fluctuations: First, the resonance mode disperses with increasing energy in an anisotropic pattern broadening most rapidly along the TR rather than the LO direction as clearly seen in Fig. 5.5 (a) and (c), reminiscent of the anisotropic propagation

of spin waves in the spin density wave state of the 122 parent compound; [Matan et al. (2009)] second, the resonance mode disperses upwards in energy with dramatically decreasing weight and vanishes above the particle-hole threshold Ω as shown in Fig. 5.5 (b) and (d). This upward dispersion is in contrast to the downward pattern in the d-wave cuprate. [Eremin et al. (2005)]

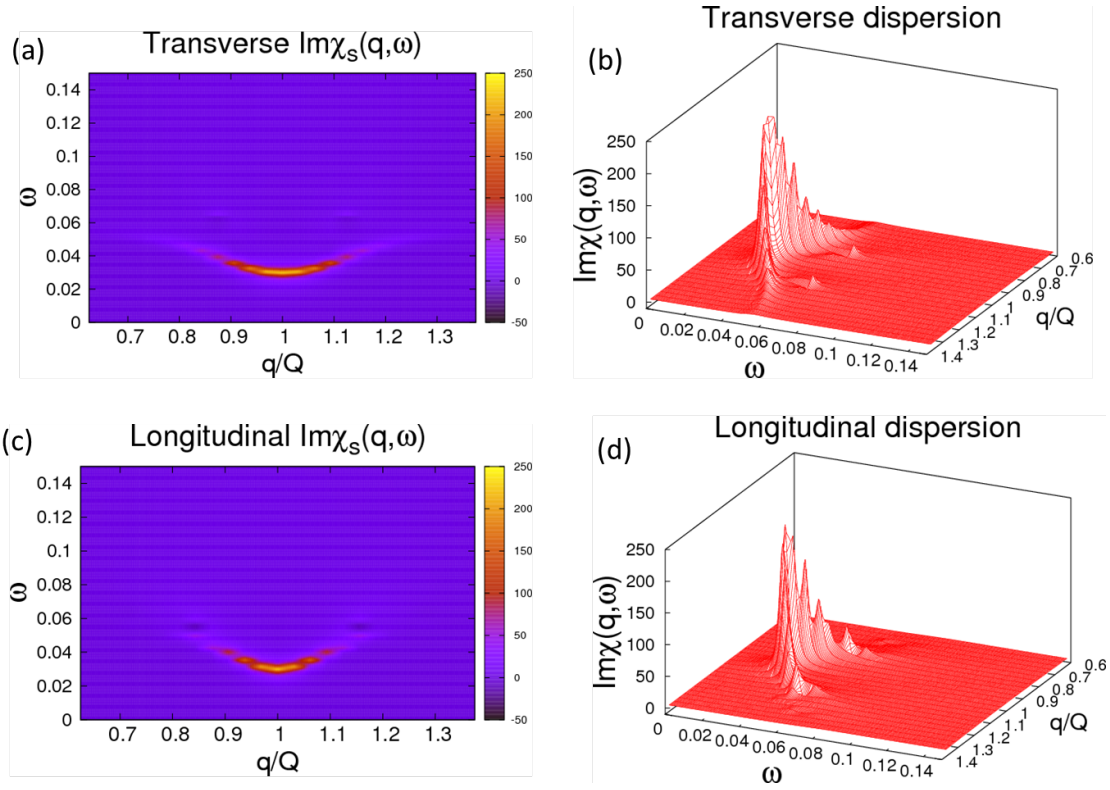

Figure 5.5 The anisotropic dispersive behavior of the resonance mode along the TR and LO direction with respect to $\mathbf{Q}_{\mathrm{AFM}}$. (a) and (c) are the intensity plot along the TR and LO direction, respectively, while (b) and (d) show the weight decay of the propagating mode.

The anisotropy of the dispersion relation enhances the image ellipticity of the measured magnetic response, if we consider a frequency average of the spectrum over a small window through the resonance energy, *i.e.*, $\frac{1}{2\Delta\omega}\int_{\omega_{\mathrm{res}}-\Delta\omega}^{\omega_{\mathrm{res}}+\Delta\omega} \mathrm{d}\omega \mathrm{Im}\chi_s(\mathbf{q},\omega)$, mimic the observation in INS. This enhanced ellipticity due to the combination of the intrinsic and dispersing anisotropy of the resonance mode is shown in Fig. 5.6, where we take $\Delta\omega = \omega_{\mathrm{res}}/4$.

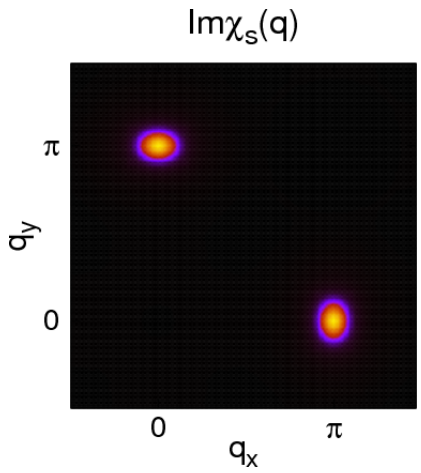

Figure 5.6 The dynamical spin susceptibility averaged over a small frequency window of $\Delta\omega = \omega_{\rm res}/4$ through the resonance energy here.

5.3.2 Discussion of the Spin-fluctuation Anisotropy and the $s^{\pm}$ Superconductivity

A systematic study of the 2- and a 3-orbital [Daghofer et al. (2010)] models, both in hole and in electron doped regions for a variety of coupling constants, draws our attention to the connection between the momentum anisotropy of the magnetic fluctuations and the $s^{\pm}$ superconductivity. Our normal-state calculations show that different anisotropic pattern of the fluctuations occurs at different parameter set in different model system, either transversely or longitudinally lengthened. But the development of short-range spin fluctuations centered at $\mathbf{Q}_{\rm AFM}$ does not necessarily lead to superconductivity. For the various systems we have studied, the establishment of a stable $s^{\pm}$ state is generally associated with the transversely lengthened fluctuations. This is the characteristic momentum structure of the static correlations and of the magnetic spectra both in the normal and in the SC state. It poses a question: Is superconductivity sensitive to the momentum structure of the magnetic glue?

Here we discuss how the specific momentum structure of the spin fluctuations affects the $s^{\pm}$ superconductivity in the magnetic scenario where the same electrons contribute to both the magnetic and the SC properties. We gain the insight by recognizing the important role played by the orbital weight on the FS sheets. As pointed out by Kemper *et al.*, [Kemper et al. (2010)] the dominant pairing processes involve intra-orbital scattering. The intra-orbital

effective pairing interaction vertex $\Gamma_A^{cc,cc}$ is dominated by the processes of exchanging spin-1 fluctuations as

$$\Gamma_A^{cc,cc}\left(\mathbf{k},\mathbf{k}',i\nu_n\right) \sim \frac{3}{2}\sum_{aa,bb} U_s^{cc,aa}\chi_s^{aa,bb}\left(\mathbf{k}-\mathbf{k}',i\nu_n\right)U_s^{bb,cc}$$

where a,b,c are orbital indices and $\Gamma_A^{cc,cc}$ becomes significant when the momentum transfer $\mathbf{k}-\mathbf{k}' \sim \mathbf{Q}_{\mathrm{AFM}}$. It gives rise to the intra-orbital Cooper-pair formation through

$$\Phi^{cc}(\mathbf{k},i\omega_n) = \frac{T}{N}\sum_{\mathbf{k}',\omega_n'} \Gamma_A^{cc,cc}(\mathbf{k},\mathbf{k}',i\omega_n - i\omega_n')F^{cc}(\mathbf{k}',i\omega_n')$$

which scatters a pair of c-orbital electrons on $\alpha(\beta)$ sheets to a pair of c-orbital electrons on $\beta(\alpha)$ sheets, i.e., an inter-band scattering.

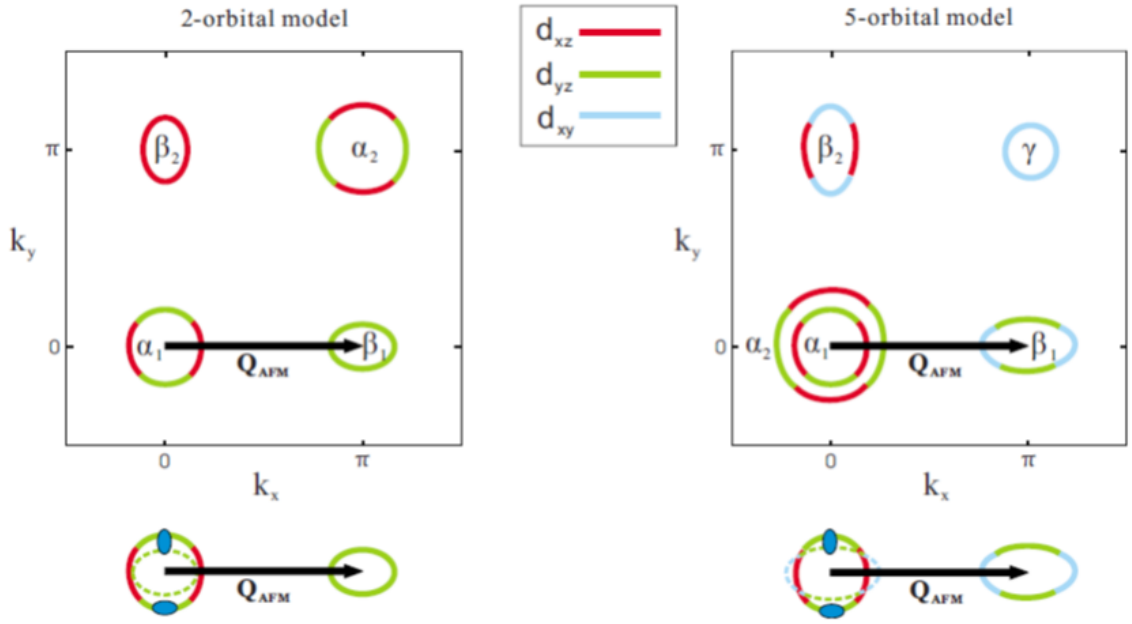

Figure 5.7 Schematic illustration of the intra-orbital pair scattering processes with momentum transfer for the 2-orbital and a more complete 5-orbital model. In the lower part, by translating $\mathbf{Q}$, the β_1-pocket is moved to the position of the α_1-pocket. For intra-orbital, but inter-band, scattering to happen, the effective scattering vertices, depicted by the small dark-blue ellipses, should be able to cover the same orbital pieces on the two deviated FS sheets, i.e., the sheet and the shifted sheet (dashed line). One can perform similar operation for the $\alpha_1(\alpha_2)$ and $\beta_1(\beta_2)$ sheets in the 2-orbital model and for the $\alpha_1(\gamma)$ and $\beta_1(\beta_2)$ sheets in the 5-orbital model. Clearly, the transversely lengthened vertices are more capable of inducing the intra-orbital, but inter-band, pair scattering processes.

A schematic demonstration of the FS configuration, with predominant iron d-orbital distribution indicated, for the current 2-orbital model and for a more complete 5-orbital model are shown in Fig. 5.7, which were analyzed by Graser *et al.* [Graser et al. (2009)] and Kemper *et al.* [Kemper et al. (2010)]. To illustrate the pair scattering between two bands with the typical momentum transfer, β_1 pocket is translated by $\mathbf{Q}_{\mathrm{AFM}}$ to overlap with α_1 pocket. As the electronic structure is away from perfect nesting, the intra-orbital scattering is more supported by the transversely lengthened pairing vertices than the longitudinally lengthened ones which are depicted by the small dark-blue ellipses in the figure. One can perform the same translation for other pairs of pockets separated by $\mathbf{Q}_{\mathrm{AFM}}$ in both models and draw the same conclusion. Therefore, due to the orbital character of the microscopic electronic structure and the deviation from perfect nesting, this type of anisotropic momentum structure of short-range spin fluctuations favor the formation of $s^{\pm}$ SC state, since the intra-orbital pairing processes are made more plausible driven by transversely lengthened fluctuations.

5.3.3 Factors Affecting the Resonance Energy

In the strong coupling approach, the factors affecting the resonance mode energy involve the SC gap magnitude $|\Delta|$ and the magnetic correlation length ξ [Abanov and Chubukov (1999)]. Our systematic study indicates that the resonance energy ω_{res} increases with increasing gap magnitude but decreases with increasing correlation length.

5.4 Fermionic Spectrum

As discussed for cuprates [Abanov and Chubukov (1999); Abanov et al. (2001); Eschrig (2006)], the impact of the mediating bosonic modes on fermions leaves fingerprint in the fermionic spectrum, the SC spectral function, if the bosonic excitations are gapped quasiparticles such as optical phonons in the conventional superconductors. This gives rise to the kink feature in the electronic energy dispersion observed in ARPES measurements. The signature of electron-mode coupling is believed to be linked to the pairing. If short-range spin fluctuations mediate Cooper pairs, with the emergence of the gapped quasiparticle-like spin resonance mode in the superconducting state, large fermionic decay occurs by exchange of the magnetic

resonance mode in scattering processes. This leaves a dip in the electronic spectral function at the energy $\omega_{\rm dip} = |\Delta_{\mathbf{k}+\mathbf{Q}_{\rm AFM}}| + \omega_{\rm res}$ where $|\Delta_{\mathbf{k}+\mathbf{Q}_{\rm AFM}}|$ indicates the SC gap magnitude at the Fermi point connected by the AFM wave vector. Indeed, our calculation does show the dip feature in the electronic spectral function. As shown in Fig. 5.8, the spectral function at a $\mathbf{k}$-point on the α_1 sheet exhibits the characteristic peak-dip-hump behavior in $A_{\mathbf{k}}(\omega)$ with the dip position $\omega_{\rm dip} \approx 0.05$ to be the sum of the resonance energy $\omega_{\rm res} \approx 0.03$ and the gap magnitude $|\Delta_{\mathbf{k}+\mathbf{Q}_{\rm AFM}}| \approx 0.02$ at the point on the other band connected by $\mathbf{Q}_{\rm AFM}$. The normal state data at the same $\mathbf{k}$-point is also plotted in Fig. 5.8 to show the conservation of spectral weight. This calculated dip feature in the quasiparticle spectrum can explain the ARPES observation [Richard et al. (2009)] as shown on the left of Fig. 5.8.

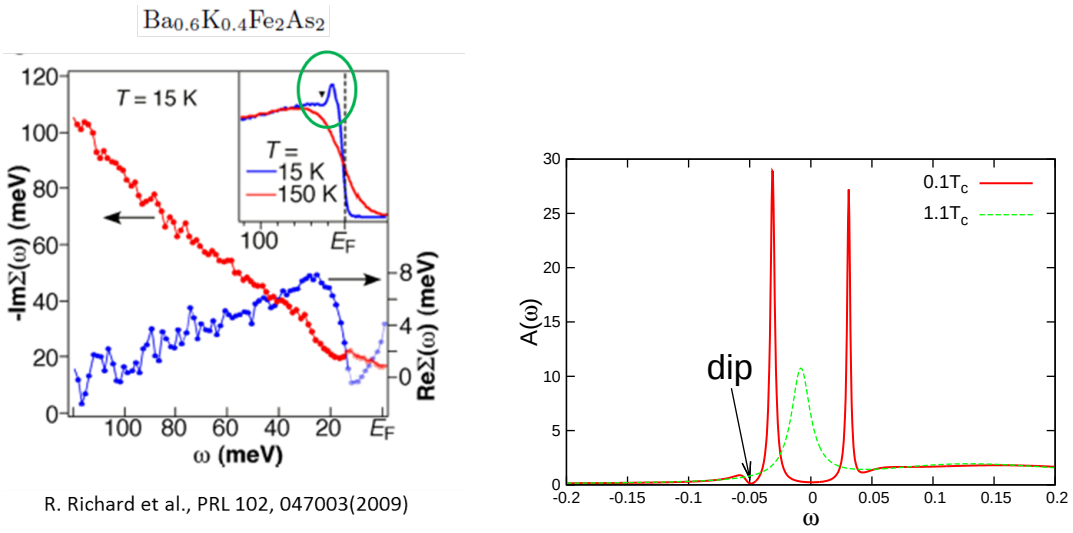

Figure 5.8 (Right part) The fermionic spectral function at a $\mathbf{k}$-point on the sheet in the SC state (red solid line) as well as in the normal state (green dashed line). Notice the peak-dip-hump feature in the negative frequency regime when the system becomes superconducting. Comparing the SC state data with the normal state data, we see that the spectral weight is conserved. And this calculated dip feature can explain the ARPES observation as shown on the left.

5.5 Summary

We have investigated the momentum structure of the short-range magnetic fluctuations that drive the nearly isotropic $s^{\pm}$ superconductivity using a microscopic model for the Fe-based superconductors in the self-consistent fluctuation exchange approximation. The calculated magnetic response exhibits an anisotropic feature with largest momentum span along the direction transverse to the momentum transfer $\mathbf{Q}_{\mathrm{AFM}}$, which gives rise to an elliptical image of the magnetic excitation. The calculated momentum anisotropy of the magnetic spectrum agrees with the INS measurements. An analysis on the orbital character of the electronic structure associated with the deviation from perfect nesting shows that the transversely lengthened short-range spin fluctuations enhance intra-orbital, but inter-band, pair scattering processes that play an important role to the formation of $s^{\pm}$-wave superconductivity in this system. Therefore, this anisotropic momentum structure of the magnetic fluctuations favors the development of the SC phase in the magnetic scenario for the iron-based superconductors.

Our detailed study on the resonance mode in the magnetic spectrum shows that the dispersion of the mode is also anisotropic with larger broadening along the transverse than the longitudinal direction. Meanwhile, the mode propagates upwards with increasing energy in the case of nearly isotropic $s^{\pm}$-state and commensurate spin susceptibility, but vanishes above the particle-hole threshold.

As the feedback from the spin excitations on fermions, the spectral function exhibits the peak-dip-hump feature, which serves as one of the interpretations of the ARPES observation of the kink feature.

CHAPTER 6. FINAL THOUGHTS

In the light of our theoretcial results, we make a few comments at the end of the discussion.

- Combining with the band structure, our systematic study shows that superconductivity is very sensitive to the momentum configuration of the short-range spin fluctuations. Only when it matches the Fermi surface configuration in an efficient way, superconductivity can be induced. Interestingly, it requires the weakening of nesting condition of the Fermi surface, although it does need certain degrees of nesting to develop sufficient dynamical antiferromagnetic correlations. This is also noticed by a recent DFT calculation [Wadati et al. (2010)]. One of the roles played by many experimental tuning parameters is a disruption of the nesting condition such that superconductivity wins over its competing order, the magnetism.

- As we consider the itinerant SDW fluctuations as the superconducting mediating glue, it seems like the itineracy nature of the spin fluctuations has some effect on the superconducting transition temperature. It might be one of the reasons why T_c stops rising so far. Also our model takes account only on-site interactions which could be not enough to explain some properties.

- Fluctuation exchange methods show that when the spin fluctuation structure matches the Fermi surface configuration, the system can be driven from a magnetic state to the superconducting state with its order parameter symmetry determined by them. In distinguishing from RPA calculations, FLEX calculation mainly found stable s±-wave solution, without evidence for d-wave symmetry. Since FLEX is self-consistent in both charge and spin sectors, we suspect d-wave is likely suppressed by the Fermi surface configuration. In distinguishing from numerical RG calculation, FLEX has the advantage of study the

full frequency-momentum structure that reveals the resonance mode and the anisotropic fluctuation configuration.

- FLEX method is cheaper than quantum Monte Carlo, but still it is quite time-consuming when handling multiorbital system. The amount of calculation time and the cost of memory increase significantly when one more orbital added. This is the main restriction for generalizing to 5-orbital model. Especially the computing is hard to be parallelled in MPI in more-orbital model since the calculation is not completely local any more.

- Another disadvantage of FLEX is that it does not take into account vertex correction, which might be important in the non-phonon mechanism as Migdal approximation is not guaranteed in other cases.

- As a future study, FLEX combining with other techniques may give better understanding of the iron-based superconductors.

APPENDIX A. ANALYTICAL DETAILS

A.1 Low-order Diagrams

In this appendix, we give the detailed derivation of the lower-order terms in multiorbital FLEX formalism. To calculate the lower-order diagrams, it is much easier to employ the following expression of the interaction Hamiltonian

$$H_{int} = \frac{1}{2} \sum_{i,a_i,\sigma\sigma'} U_s^{a_1 a_2 a_3 a_4} d^\dagger_{i,a_1\sigma} d_{i,a_3\sigma} d^\dagger_{i,a_2\sigma'} d_{i,a_4\sigma'}$$

as we showed before. In momentum space it is nothing but

$$H_{int} = \frac{1}{2} \sum_{\mathbf{k}_i,a_i,\sigma_1\sigma_1'} U_s^{a_1 a_2 a_3 a_4} d^\dagger_{\mathbf{k}_1,a_1\sigma_1} d_{\mathbf{k}_3,a_3\sigma_1} d^\dagger_{\mathbf{k}_2,a_2\sigma_1'} d_{\mathbf{k}_4,a_4\sigma_1'} \delta_{\mathbf{k}_1+\mathbf{k}_2,\mathbf{k}_3+\mathbf{k}_4}.$$

A.1.1 First Order Contribution — Hartree-Fock Terms

Insert the interaction once into the normal Green's function we have

$$\begin{aligned} G^\sigma_{ab}(\mathbf{k},\tau) &= -\langle T_\tau d_{\mathbf{k}a\sigma}(\tau) d^\dagger_{\mathbf{k}b\sigma}(0)\rangle \\ &= -(-)\int_0^\beta d\tau_1 \langle T_\tau d_{\mathbf{k}a\sigma}(\tau) H_{int}(\tau_1) d^\dagger_{\mathbf{k}b\sigma}(0)\rangle \\ &= \int_0^\beta d\tau_1 \frac{1}{2} \sum_{\mathbf{k}_i,a_i,\sigma_1\sigma_1'} U_s^{a_1 a_2 a_3 a_4} \langle T_\tau d_{\mathbf{k}a\sigma}(\tau) d^\dagger_{\mathbf{k}_1,a_1\sigma_1} d_{\mathbf{k}_3,a_3\sigma_1} d^\dagger_{\mathbf{k}_2,a_2\sigma_1'} d_{\mathbf{k}_4,a_4\sigma_1'}(\tau_1) d^\dagger_{\mathbf{k}b\sigma}(0)\rangle \end{aligned}$$

Applying different contractions we have

$$\begin{aligned} G^\sigma_{ab}(\mathbf{k},\tau) &= \int_0^\beta d\tau_1 \sum U_s^{a_1 a_2 a_3 a_4} [-G_{aa_1}(\mathbf{k},\tau-\tau_1) G_{a_3 a_2}(\mathbf{k}',\tau_1-\tau_1) G_{a_4 b}(\mathbf{k},\tau_1) \\ &\qquad + 2G_{aa_1}(\mathbf{k},\tau-\tau_1) G_{a_4 a_2}(\mathbf{k}',\tau_1-\tau_1) G_{a_3 b}(\mathbf{k},\tau_1)] \\ &= \int_0^\beta d\tau_1 \sum G_{aa'}(\mathbf{k},\tau-\tau_1) \left[\frac{1}{2}(3U_s - U_c)^{a'm,nb'} G_{mn}(\mathbf{k}',0^-)\right] G_{b'b}(\mathbf{k},\tau_1) \end{aligned}$$

with

$$\langle T_\tau d_{\mathbf{k}a\sigma}(\tau) d^\dagger_{\mathbf{k}_1,a_1\sigma_1} d_{\mathbf{k}_3,a_3\sigma_1} d^\dagger_{\mathbf{k}_2,a_2\sigma_1'} d_{\mathbf{k}_4,a_4\sigma_1'}(\tau_1) d^\dagger_{\mathbf{k}b\sigma}(0)\rangle$$
$$= 2\left[-G_{aa_1}(\mathbf{k},\tau-\tau_1)G_{a_3a_2}(\mathbf{k}',\tau_1-\tau_1)G_{a_4b}(\mathbf{k},\tau_1) + 2G_{aa_1}(\mathbf{k},\tau-\tau_1)G_{a_4a_2}(\mathbf{k}',\tau_1-\tau_1)G_{a_3b}(\mathbf{k},\tau_1)\right]$$

where we used $U^{1234} = U^{2143}$ and $2U_s^{1234} - U_s^{1243} = \frac{1}{2}(3U_s - U_c)^{1234}$. Therefore we have

$$G^\sigma_{ab}(\mathbf{k}, i\omega_n) = \sum_{a',b'} G_{aa'}(\mathbf{k}, i\omega_n)\Sigma^{a'b'}_{HF} G_{b'b}(\mathbf{k}, i\omega_n),$$

with

$$\Sigma^{a'b'}_{HF} = \sum_{m,n} V^{a'm,nb'}_{N,HF}\left[\delta_{mn} + \frac{T}{N}\sum_{\mathbf{k}',\omega_n'} G_{mn}(\mathbf{k}', i\omega_n')\right],$$

where

$$V^{a'm,nb'}_{N,HF} = \frac{1}{2}(3U_s - U_c)^{a'm,nb'}.$$

Next insert the interaction once into the anomalous Green's function we have

$$\begin{aligned} F^{\sigma\sigma'}_{ab}(\mathbf{k},\tau) &= -\langle T_\tau d_{\mathbf{k}a\sigma}(\tau) d_{-\mathbf{k}b\sigma'}(0)\rangle \\ &= -(-)\int_0^\beta d\tau_1 \langle T_\tau d_{\mathbf{k}a\sigma}(\tau) H_{int}(\tau_1) d_{-\mathbf{k}b\sigma'}(0)\rangle \\ &= \int_0^\beta d\tau_1 \frac{1}{2}\sum_{\mathbf{k}_i,a_i,\sigma_1\sigma_1'} U_s^{a_1a_2a_3a_4}\langle T_\tau d_{\mathbf{k}a\sigma}(\tau) d^\dagger_{\mathbf{k}_1,a_1\sigma_1} d_{\mathbf{k}_3,a_3\sigma_1} d^\dagger_{\mathbf{k}_2,a_2\sigma_1'} d_{\mathbf{k}_4,a_4\sigma_1'}(\tau_1) d_{-\mathbf{k}b\sigma'}(0)\rangle \end{aligned}$$

Again different contractions give rise to

$$\begin{aligned} F^{\sigma\sigma'}_{ab}(\mathbf{k},\tau) &= -\int_0^\beta d\tau_1 \sum U_s^{a_1a_2a_3a_4} G^\sigma_{aa_1}(\mathbf{k},\tau-\tau_1) F^{\sigma\sigma'}_{a_3a_4}(\mathbf{k}',\tau_1-\tau_1) G^{\sigma'}_{ba_2}(-\mathbf{k},-\tau_1) \\ &= -\int_0^\beta d\tau_1 \sum G^\sigma_{aa'}(\mathbf{k},\tau-\tau_1)\left[\frac{1}{2}(U_s+U_c)^{a'm,b'n} F^{\sigma\sigma'}_{mn}(\mathbf{k}',\tau_1-\tau_1)\right] G^{\sigma'}_{bb'}(-\mathbf{k},-\tau_1), \end{aligned}$$

where

$$\begin{aligned} &\langle T_\tau d_{\mathbf{k}a\sigma}(\tau) d^\dagger_{\mathbf{k}_1,a_1\sigma_1} d_{\mathbf{k}_3,a_3\sigma_1} d^\dagger_{\mathbf{k}_2,a_2\sigma_1'} d_{\mathbf{k}_4,a_4\sigma_1'}(\tau_1) d_{-\mathbf{k}b\sigma'}(0)\rangle \\ &= -2G^\sigma_{aa_1}(\mathbf{k},\tau-\tau_1) F^{\sigma\sigma'}_{a_3a_4}(\mathbf{k}',\tau_1-\tau_1) G^{\sigma'}_{ba_2}(-\mathbf{k},-\tau_1) \end{aligned}$$

where we used $U_s^{1243} = \frac{1}{2}(U_s + U_c)^{1234}$. Therefore we obtain

$$F^{\sigma\sigma'}_{ab}(\mathbf{k}, i\omega_n) = -\sum_{a',b'} G^\sigma_{aa'}(\mathbf{k}, i\omega_n)\Phi^{\sigma\sigma',a'b'}_{HF} G^{\sigma'}_{bb'}(-\mathbf{k}, -i\omega_n),$$

with

$$\Phi_{HF}^{\sigma\sigma',a'b'} = \sum_{m,n} V_{A,HF}^{a'm,b'n} \left[\frac{T}{N} \sum_{\mathbf{k}',\omega_n'} F_{mn}^{\sigma\sigma'}(\mathbf{k}', i\omega_n') \right],$$

where

$$V_{A,HF}^{a'm,b'n} = \frac{1}{2}(U_s + U_c)^{a'm,b'n}.$$

Note that in the multi-orbital case, Hartree-Fock contributions can not be simply absorbed into chemical potential any more due to the matrix structure.

A.1.2 Second Order Diagrams

Using the same strategy as in the first-order case, we honestly evaluate the second-order diagrams. First for normal Green's function we get

$$\begin{aligned}
G_{ab}^{\sigma}(\mathbf{k},\tau) &= -\langle T_\tau d_{\mathbf{k}a\sigma}(\tau) d_{\mathbf{k}b\sigma}^\dagger(0)\rangle \\
&= -\frac{(-1)^2}{2!}\int_0^\beta d\tau_1 \int_0^\beta d\tau_2 \langle T_\tau d_{\mathbf{k}a\sigma}(\tau) H_{int}(\tau_1) H_{int}(\tau_2) d_{\mathbf{k}b\sigma}^\dagger(0)\rangle \\
&= -\int_0^\beta d\tau_1 \int_0^\beta d\tau_2 \frac{1}{2} \sum_{\mathbf{k}_i,a_i,\sigma_1\sigma_1'} U_s^{a_1a_2a_3a_4} \frac{1}{2} \sum_{\mathbf{k}_i',b_i,\sigma_2\sigma_2'} U_s^{b_1b_2b_3b_4} \\
&\quad \langle T_\tau d_{\mathbf{k}a\sigma}(\tau) d_{\mathbf{k}_1,a_1\sigma_1}^\dagger d_{\mathbf{k}_3,a_3\sigma_1} d_{\mathbf{k}_2,a_2\sigma_1'}^\dagger d_{\mathbf{k}_4,a_4\sigma_1'}(\tau_1) d_{\mathbf{k}_1',b_1\sigma_2}^\dagger d_{\mathbf{k}_3',b_3\sigma_2} d_{\mathbf{k}_2',b_2\sigma_2'}^\dagger d_{\mathbf{k}_4',b_4\sigma_2'}(\tau_2) d_{\mathbf{k}b\sigma}^\dagger(0)\rangle
\end{aligned}$$

where

$$\begin{aligned}
&\langle T_\tau d_{\mathbf{k}a\sigma}(\tau) d_{\mathbf{k}_1,a_1\sigma_1}^\dagger d_{\mathbf{k}_3,a_3\sigma_1} d_{\mathbf{k}_2,a_2\sigma_1'}^\dagger d_{\mathbf{k}_4,a_4\sigma_1'}(\tau_1)\ d_{\mathbf{k}_1',b_1\sigma_2}^\dagger d_{\mathbf{k}_3',b_3\sigma_2} d_{\mathbf{k}_2',b_2\sigma_2'}^\dagger d_{\mathbf{k}_4',b_4\sigma_2'}(\tau_2) d_{\mathbf{k}b\sigma}^\dagger(0)\rangle \\
&= 4G_{aa_1}(\mathbf{k},\tau-\tau_1) G_{b_4b}(\mathbf{k},\tau_2)\times \\
&[2G_{a_4b_1}(\mathbf{k}_4,\tau_1-\tau_2) G_{a_3b_2}(\mathbf{k}_3,\tau_1-\tau_2) G_{b_3a_2}(\mathbf{k}_2,\tau_2-\tau_1) \\
&- G_{a_4b_2}(\mathbf{k}_4,\tau_1-\tau_2) G_{a_3b_1}(\mathbf{k}_3,\tau_1-\tau_2) G_{b_3a_2}(\mathbf{k}_2,\tau_2-\tau_1) \\
&- G_{a_3b_2}^{\sigma}(\mathbf{k}_3,\tau_1-\tau_2) F_{a_4b_3}^{\sigma_1\sigma_1'}(\mathbf{k}_4,\tau_1-\tau_2) \overline{F}_{b_1a_2}^{\sigma_1'\sigma_1}(\mathbf{k}_2,\tau_2-\tau_1) \\
&+ G_{a_4b_2}^{\sigma}(\mathbf{k}_4,\tau_1-\tau_2) F_{a_3b_3}^{\sigma\sigma'}(\mathbf{k}_3,\tau_1-\tau_2) \overline{F}_{b_1a_2}^{\sigma'\sigma}(\mathbf{k}_2,\tau_2-\tau_1) \\
&+ G_{a_3b_1}^{\sigma}(\mathbf{k}_3,\tau_1-\tau_2) F_{a_4b_3}^{\sigma'\sigma}(\mathbf{k}_4,\tau_1-\tau_2) \overline{F}_{b_2a_2}^{\sigma\sigma'}(\mathbf{k}_2,\tau_2-\tau_1) \\
&- G_{a_4b_1}^{\sigma'}(\mathbf{k}_4,\tau_1-\tau_2) F_{a_3b_3}^{\sigma\sigma'}(\mathbf{k}_3,\tau_1-\tau_2) \overline{F}_{b_2a_2}^{\sigma\sigma'}(\mathbf{k}_2,\tau_2-\tau_1)]
\end{aligned}$$

Thus we have

$$\begin{aligned}
G^{\sigma}_{ab}(\mathbf{k},i\omega_n) &= \sum U_s^{a_1a_2a_3a_4}U_s^{b_1b_2b_3b_4}G_{aa_1}(\mathbf{k},i\omega_n)G_{b_4b}(\mathbf{k},i\omega_n)\times \\
&[G_{a_4b_1}(\mathbf{k}-\mathbf{q},i\omega_n-i\nu_n)\left(-G_{a_3b_2}(\mathbf{k}'+\mathbf{q},i\omega'_n+i\nu_n)G_{b_3a_2}(\mathbf{k}',i\omega'_n)\right) \\
&+G_{a_3b_2}(\mathbf{k}-\mathbf{q},i\omega_n-i\nu_n)\left(-G_{a_4b_1}(\mathbf{k}'+\mathbf{q},i\omega'_n+i\nu_n)G_{b_3a_2}(\mathbf{k}',i\omega'_n)\right) \\
&-\frac{1}{2}G_{a_4b_2}(\mathbf{k}-\mathbf{q},i\omega_n-i\nu_n)\left(-G_{a_3b_1}(\mathbf{k}'+\mathbf{q},i\omega'_n+i\nu_n)G_{b_3a_2}(\mathbf{k}',i\omega'_n)\right) \\
&-\frac{1}{2}G_{a_3b_1}(\mathbf{k}-\mathbf{q},i\omega_n-i\nu_n)\left(-G_{a_4b_2}(\mathbf{k}'+\mathbf{q},i\omega'_n+i\nu_n)G_{b_3a_2}(\mathbf{k}',i\omega'_n)\right) \\
&-G^{\sigma}_{a_3b_2}(\mathbf{k}-\mathbf{q},i\omega_n-i\nu_n)\left(-F^{\sigma_1\sigma'_1}_{a_4b_3}(\mathbf{k}'+\mathbf{q},i\omega'_n+i\nu_n)\overline{F}^{\sigma'_1\sigma_1}_{b_1a_2}(\mathbf{k}',i\omega'_n)\right) \\
&+G^{\sigma}_{a_4b_2}(\mathbf{k}-\mathbf{q},i\omega_n-i\nu_n)\left(-F^{\sigma\sigma'}_{a_3b_3}(\mathbf{k}'+\mathbf{q},i\omega'_n+i\nu_n)\overline{F}^{\sigma'\sigma}_{b_1a_2}(\mathbf{k}',i\omega'_n)\right) \\
&+G^{\sigma}_{a_3b_1}(\mathbf{k}-\mathbf{q},i\omega_n-i\nu_n)\left(-F^{\sigma'\sigma}_{a_4b_3}(\mathbf{k}'+\mathbf{q},i\omega'_n+i\nu_n)\overline{F}^{\sigma\sigma'}_{b_2a_2}(\mathbf{k}',i\omega'_n)\right) \\
&+G^{\sigma'}_{a_4b_1}(\mathbf{k}-\mathbf{q},i\omega_n-i\nu_n)\left(-F^{\sigma'\sigma}_{a_3b_3}(\mathbf{k}'+\mathbf{q},i\omega'_n+i\nu_n)\overline{F}^{\sigma\sigma'}_{b_2a_2}(\mathbf{k}',i\omega'_n)\right)].
\end{aligned}$$

After some algebra we obtain

$$\begin{aligned}
G^{\sigma}_{ab}(\mathbf{k},i\omega_n) &= \sum G_{aa'}(\mathbf{k},i\omega_n)G_{b'b}(\mathbf{k},i\omega_n)G_{mn}(\mathbf{k}-\mathbf{q},i\omega_n-i\nu_n)\times \\
&[\chi^1_{\alpha\beta,\mu\nu}(\mathbf{q},i\nu_n)\left(\frac{3}{4}U_s^{a'm,\alpha\beta}U_s^{\mu\nu,nb'}+\frac{1}{4}U_c^{a'm,\alpha\beta}U_c^{\mu\nu,nb'}\right) \\
&+\chi^2_{\alpha\beta,\mu\nu}(\mathbf{q},i\nu_n)\left(\frac{3}{2}U_s^{a'm,\alpha\beta}U_s^{\mu\nu,nb'}-\frac{1}{2}U_c^{a'm,\alpha\beta}U_c^{\mu\nu,nb'}\right)].
\end{aligned}$$

Therefore

$$\Sigma^{a'b'}_{(2)}(\mathbf{k},i\omega_n)=\sum_{\mathbf{q},\nu_n}\sum_{m,n}V^{a'm,nb'}_{N,(2)}(\mathbf{q},i\nu_n)G_{mn}(\mathbf{k}-\mathbf{q},i\omega_n-i\nu_n)$$

with

$$\begin{aligned}
V^{a'm,nb'}_{N,(2)}(\mathbf{q},i\nu_n) &= \sum_{\alpha\beta,\mu\nu}[\frac{3}{4}U_s^{a'm,\alpha\beta}\chi^1_{\alpha\beta,\mu\nu}(\mathbf{q},i\nu_n)U_s^{\mu\nu,nb'}+\frac{1}{4}U_c^{a'm,\alpha\beta}\chi^1_{\alpha\beta,\mu\nu}(\mathbf{q},i\nu_n)U_c^{\mu\nu,nb'} \\
&\quad+\frac{3}{2}U_s^{a'm,\alpha\beta}\chi^2_{\alpha\beta,\mu\nu}(\mathbf{q},i\nu_n)U_s^{\mu\nu,nb'}-\frac{1}{2}U_c^{a'm,\alpha\beta}\chi^2_{\alpha\beta,\mu\nu}(\mathbf{q},i\nu_n)U_c^{\mu\nu,nb'}]
\end{aligned}$$

Gathering the subtracted second-order contributions in the last section, the total second-order contribution to normal interaction vertex is

$$\begin{aligned}
&V^{a'm,nb'}_{N,(2)}(\mathbf{q},i\nu_n)-\frac{3}{2}\tilde{U}_s\tilde{\chi}^{s,0}\tilde{U}_s-\frac{1}{2}\tilde{U}_c\tilde{\chi}^{c,0}\tilde{U}_c \\
&=\sum_{\alpha\beta,\mu\nu}[-\frac{3}{4}U_s^{a'm,\alpha\beta}\chi^1_{\alpha\beta,\mu\nu}(\mathbf{q},i\nu_n)U_s^{\mu\nu,nb'}-\frac{1}{4}U_c^{a'm,\alpha\beta}\chi^1_{\alpha\beta,\mu\nu}(\mathbf{q},i\nu_n)U_c^{\mu\nu,nb'} \\
&=-\frac{3}{4}\tilde{U}_s\tilde{\chi}^1\tilde{U}_s-\frac{1}{4}\tilde{U}_c\tilde{\chi}^1\tilde{U}_c
\end{aligned}$$

where

$$\tilde{\chi}^{s,0} = \tilde{\chi}^1 + \tilde{\chi}^2, \quad \tilde{\chi}^{c,0} = \tilde{\chi}^1 - \tilde{\chi}^2.$$

Next we perform the same calculation for the anomalous Green's function

$$\begin{aligned}
&F_{ab}^{\sigma\sigma'}(\mathbf{k},\tau) \\
&= -\langle T_\tau d_{\mathbf{k}a\sigma}(\tau) d_{-\mathbf{k}b\sigma'}(0)\rangle \\
&= -\int_0^\beta d\tau_1 \int_0^\beta d\tau_2 \frac{1}{2} \sum_{\mathbf{k}_i,a_i,\sigma_1\sigma_1'} U_s^{a_1a_2a_3a_4} \frac{1}{2} \sum_{\mathbf{k}_i',b_i,\sigma_2\sigma_2'} U_s^{b_1b_2b_3b_4} \\
&\langle T_\tau d_{\mathbf{k}a\sigma}(\tau) d^\dagger_{\mathbf{k}_1,a_1\sigma_1} d_{\mathbf{k}_3,a_3\sigma_1} d^\dagger_{\mathbf{k}_2,a_2\sigma_1'} d_{\mathbf{k}_4,a_4\sigma_1'}(\tau_1)\, d^\dagger_{\mathbf{k}_1',b_1\sigma_2} d_{\mathbf{k}_3',b_3\sigma_2} d^\dagger_{\mathbf{k}_2',b_2\sigma_2'} d_{\mathbf{k}_4',b_4\sigma_2'}(\tau_2) d_{-\mathbf{k}b\sigma'}(0)\rangle
\end{aligned}$$

where

$$\begin{aligned}
&\langle T_\tau d_{\mathbf{k}a\sigma}(\tau) d^\dagger_{\mathbf{k}_1,a_1\sigma_1} d_{\mathbf{k}_3,a_3\sigma_1} d^\dagger_{\mathbf{k}_2,a_2\sigma_1'} d_{\mathbf{k}_4,a_4\sigma_1'}(\tau_1)\, d^\dagger_{\mathbf{k}_1',b_1\sigma_2} d_{\mathbf{k}_3',b_3\sigma_2} d^\dagger_{\mathbf{k}_2',b_2\sigma_2'} d_{\mathbf{k}_4',b_4\sigma_2'}(\tau_2) d_{-\mathbf{k}b\sigma'}(0)\rangle \\
&= 4G^\sigma_{aa_1}(\mathbf{k},\tau-\tau_1)\overline{G}^{\sigma'}_{b_2b}(-\mathbf{k},\tau_2)\times \\
&[F^{\sigma\sigma'}_{a_3b_3}(\mathbf{k}_3,\tau_1-\tau_2)G_{a_4b_1}(\mathbf{k}_4,\tau_1-\tau_2)G_{b_4a_2}(\mathbf{k}_2,\tau_2-\tau_1) \\
&- 2F^{\sigma\sigma'}_{a_3b_4}(\mathbf{k}_3,\tau_1-\tau_2)G_{a_4b_1}(\mathbf{k}_4,\tau_1-\tau_2)G_{b_3a_2}(\mathbf{k}_2,\tau_2-\tau_1) \\
&- F^{\sigma'\sigma}_{a_4b_3}(\mathbf{k}_4,\tau_1-\tau_2)G_{a_3b_1}(\mathbf{k}_3,\tau_1-\tau_2)G_{b_4a_2}(\mathbf{k}_2,\tau_2-\tau_1) \\
&+ F^{\sigma\sigma'}_{a_4b_4}(\mathbf{k}_4,\tau_1-\tau_2)G_{a_3b_1}(\mathbf{k}_3,\tau_1-\tau_2)G_{b_3a_2}(\mathbf{k}_2,\tau_2-\tau_1) \\
&+ F^{\sigma\sigma'}_{a_3b_4}(\mathbf{k}_3,\tau_1-\tau_2)F^{\sigma_1\sigma_1'}_{a_4b_3}(\mathbf{k}_4,\tau_1-\tau_2)\overline{F}^{\sigma_1'\sigma_1}_{b_1a_2}(\mathbf{k}_2,\tau_2-\tau_1) \\
&- F^{\sigma\sigma_1'}_{a_3b_3}(\mathbf{k}_3,\tau_1-\tau_2)F^{\sigma_1\sigma'}_{a_4b_4}(\mathbf{k}_4,\tau_1-\tau_2)\overline{F}^{\sigma_1'\sigma_1}_{b_1a_2}(\mathbf{k}_2,\tau_2-\tau_1)]
\end{aligned}$$

thus in frequency space it becomes

$$\begin{aligned}
F^{\sigma\sigma'}_{ab}(\mathbf{k},i\omega_n) \;=\; & \sum U_s^{a_1a_2a_3a_4} U_s^{b_1b_2b_3b_4} G^\sigma_{aa_1}(\mathbf{k},i\omega_n)\left(-G^{\sigma'}_{bb_2}(-\mathbf{k},-i\omega_n)\right)\times \\
& [-F^{\sigma\sigma'}_{a_3b_3}(\mathbf{k}-\mathbf{q},i\omega_n-i\nu_n)G_{a_4b_1}(\mathbf{k}'+\mathbf{q},i\omega_n'+i\nu_n)G_{b_4a_2}(\mathbf{k}',i\omega_n') \\
& +2F^{\sigma\sigma'}_{a_3b_4}(\mathbf{k}-\mathbf{q},i\omega_n-i\nu_n)G_{a_4b_1}(\mathbf{k}'+\mathbf{q},i\omega_n'+i\nu_n)G_{b_3a_2}(\mathbf{k}',i\omega_n') \\
& +F^{\sigma'\sigma}_{a_4b_3}(\mathbf{k}-\mathbf{q},i\omega_n-i\nu_n)G_{a_3b_1}(\mathbf{k}'+\mathbf{q},i\omega_n'+i\nu_n)G_{b_4a_2}(\mathbf{k}',i\omega_n') \\
& -F^{\sigma\sigma'}_{a_4b_4}(\mathbf{k}-\mathbf{q},i\omega_n-i\nu_n)G_{a_3b_1}(\mathbf{k}'+\mathbf{q},i\omega_n'+i\nu_n)G_{b_3a_2}(\mathbf{k}',i\omega_n') \\
& -F^{\sigma\sigma'}_{a_3b_4}(\mathbf{k}-\mathbf{q},i\omega_n-i\nu_n)F^{\sigma_1\sigma_1'}_{a_4b_3}(\mathbf{k}'+\mathbf{q},i\omega_n'+i\nu_n)\overline{F}^{\sigma_1'\sigma_1}_{b_1a_2}(\mathbf{k}',i\omega_n') \\
& +F^{\sigma\sigma_1'}_{a_3b_3}(\mathbf{k}-\mathbf{q},i\omega_n-i\nu_n)F^{\sigma_1\sigma'}_{a_4b_4}(\mathbf{k}'+\mathbf{q},i\omega_n'+i\nu_n)\overline{F}^{\sigma_1'\sigma_1}_{b_1a_2}(\mathbf{k}',i\omega_n')]
\end{aligned}$$

After some algebra we obtain

$$\begin{aligned} F_{ab}^{\sigma\bar{\sigma}}(\mathbf{k}, i\omega_n) &= \sum G_{aa_1}^{\sigma}(\mathbf{k}, i\omega_n)\left(-G_{bb_2}^{\bar{\sigma}}(-\mathbf{k}, -i\omega_n)\right) F_{mn}^{\sigma\bar{\sigma}}(\mathbf{k}-\mathbf{q}, i\omega_n - i\nu_n) \times \\ & [\chi^1_{\alpha\beta,\mu\nu}(\mathbf{q}, i\nu_n)\left(\frac{3}{2}U_s^{a'm,\alpha\beta}U_s^{\mu\nu,b'n} - \frac{1}{2}U_c^{a'm,\alpha\beta}U_c^{\mu\nu,b'n}\right) \\ & +\chi^2_{\alpha\beta,\mu\nu}(\mathbf{q}, i\nu_n)\left(\frac{3}{4}U_s^{a'm,\alpha\beta}U_s^{\mu\nu,b'n} + \frac{1}{4}U_c^{a'm,\alpha\beta}U_c^{\mu\nu,b'n}\right)]. \end{aligned}$$

Therefore

$$\Phi_{(2)}^{\sigma\bar{\sigma},a'b'}(\mathbf{k}, i\omega_n) = \sum_{\mathbf{q},\nu_n}\sum_{m,n} V_{A,(2)}^{a'm,b'n}(\mathbf{q}, i\nu_n) F_{mn}^{\sigma\bar{\sigma}}(\mathbf{k}-\mathbf{q}, i\omega_n - i\nu_n),$$

with

$$\begin{aligned} V_{A,(2)}^{a'm,b'n}(\mathbf{q}, i\nu_n) &= \sum_{\alpha\beta,\mu\nu}[\left(\frac{3}{2}U_s^{a'm,\alpha\beta}\chi^1_{\alpha\beta,\mu\nu}(\mathbf{q}, i\nu_n)U_s^{\mu\nu,b'n} - \frac{1}{2}U_c^{a'm,\alpha\beta}\chi^1_{\alpha\beta,\mu\nu}(\mathbf{q}, i\nu_n)U_c^{\mu\nu,b'n}\right) \\ & +\frac{3}{4}U_s^{a'm,\alpha\beta}\chi^2_{\alpha\beta,\mu\nu}(\mathbf{q}, i\nu_n)U_s^{\mu\nu,b'n} + \frac{1}{4}U_c^{a'm,\alpha\beta}\chi^2_{\alpha\beta,\mu\nu}(\mathbf{q}, i\nu_n)U_c^{\mu\nu,b'n}]. \end{aligned}$$

Gathering the subtracted second-order contributions in the last section, the total second-order contribution to the anomalous interaction vertex is

$$\begin{aligned} & V_{A,(2)}^{a'm,b'n}(\mathbf{q}, i\nu_n) - \frac{3}{2}\tilde{U}_s\tilde{\chi}^{s,0}\tilde{U}_s + \frac{1}{2}\tilde{U}_c\tilde{\chi}^{c,0}\tilde{U}_c \\ &= \sum_{\alpha\beta,\mu\nu} -\frac{3}{4}U_s^{a'm,\alpha\beta}\chi^2_{\alpha\beta,\mu\nu}(\mathbf{q}, i\nu_n)U_s^{\mu\nu,b'n} - \frac{1}{4}U_c^{a'm,\alpha\beta}\chi^2_{\alpha\beta,\mu\nu}(\mathbf{q}, i\nu_n)U_c^{\mu\nu,b'n} \\ &= -\frac{3}{4}\tilde{U}_s\tilde{\chi}^2\tilde{U}_s - \frac{1}{4}\tilde{U}_c\tilde{\chi}^2\tilde{U}_c. \end{aligned}$$

APPENDIX B. NUMERICAL DETAILS

B.1 Numerical Tricks

The key part of the numerical implementation is the Fourier transformation between the momentum + frequency domain into the coordinate + time domain. The Fourier transform from momentum space to coordinate space will be done using periodic boundary conditions and are easily implemented. We evaluate

$$f_{\mathbf{i}} = \frac{1}{N^2} \sum_{\mathbf{k}} e^{-i\mathbf{k}\cdot\mathbf{i}} f_{\mathbf{k}} \tag{B.1}$$

which yields explicitly:

$$f_{i_x,i_y} = \frac{1}{N^2} \sum_{n_x=0}^{N-1} \sum_{n_y=0}^{N-1} e^{-i\frac{2\pi}{N}(n_x i_x + n_y i_y)} f_{n_x,n_y}. \tag{B.2}$$

The inverse transform is

$$f_{\mathbf{k}} = \sum_{\mathbf{i}} e^{i\mathbf{k}\cdot\mathbf{i}} f_{\mathbf{i}} \tag{B.3}$$

which is explicitly witten as

$$f_{n_x,n_y} = \sum_{i_x=0}^{N-1} \sum_{i_y=0}^{N-1} e^{i\frac{2\pi}{N}(n_x i_x + n_y i_y)} f_{i_x,i_y}. \tag{B.4}$$

The Fourier transformation from frequency to time and back is more subtle. First, functions in frequency space decay very slowly (in some cases as $1/\omega_n$). Second, important physical information is contained in the values $f_{\mathbf{i}}(\tau = 0^+)$ and $f_{\mathbf{i}}(\tau = \beta^-)$. It turns out that both phenomena are closely related to each other. As shown below, it holds for bosons as well as fermions that

$$f(\omega_n) = -\frac{f(0^+) - f(0^-)}{i\omega_n} - \frac{1}{i\omega_n} \int_0^\beta f'(\tau)\, e^{i\omega_n \tau} d\tau \tag{B.5}$$

Since $\int_0^\beta f'(\tau)\, e^{i\omega_n\tau} d\tau$ must vanishes for $\omega_n \to \pm\infty$ the second term vanishes vaster that $1/\omega_n$, i.e. the dominant large ω_n behavior is due to the discontinuity at $\tau = 0$. In addition, we show

below that a linear interpolation of $f(\tau)$ between the discrete time points $\tau_l = l\Delta = l\beta/N_m$ yields

$$f(\omega_n) = W_n \Delta \sum_{l=0}^{N_m-1} e^{i\omega_n \tau_l} f_l + \left(f\left(0^+\right) - f\left(0^-\right)\right) R_n, \tag{B.6}$$

where

$$\begin{aligned} W_n &= 2\frac{1-\cos(\Delta\omega_n)}{\Delta^2\omega_n^2} \\ R_n &= -\frac{1-i\Delta\omega_n - e^{-i\Delta\omega_n}}{\Delta\omega_n^2}. \end{aligned} \tag{B.7}$$

For the $2+1$-dimensional Fourier transform $f_{i_x,i_y,l} = f_{\mathbf{i}}(\tau_l)$ we need to analyze the following expression

$$f_{\mathbf{i}}(\tau_l) = \frac{T}{N^2} \sum_{\mathbf{k}} \sum_{n=-\frac{N_m}{2}}^{\frac{N_m}{2}-1} e^{-i(\mathbf{k}\cdot\mathbf{i}+\omega_n\tau_l)} f_{\mathbf{k}}(\omega_n) \tag{B.8}$$

Suppose we know the large $|\omega_n|$ behavior for the function $f_{\mathbf{k}}(\omega_n)$:

$$f_{\mathbf{k}}(\omega_n \to \pm\infty) \simeq \frac{f_{\mathbf{k}}^{\infty}}{i\omega_n}. \tag{B.9}$$

This motivates to introduce (ξ is an arbitrary factor):

$$\widetilde{f}_{\mathbf{k}}(\omega_n) = f_{\mathbf{k}}(\omega_n) - \frac{f_{\mathbf{k}}^{\infty}}{i\omega_n - \xi}, \tag{B.10}$$

which decays faster as $1/\omega_n$ and we obtain[1]

$$f_{\mathbf{i}}(\tau_l) = \frac{T}{N^2} \sum_{\mathbf{k}} \sum_{n=-\frac{N_m}{2}}^{\frac{N_m}{2}-1} e^{-i(\mathbf{k}\cdot\mathbf{i}+\omega_n\tau_l)} \widetilde{f}_{\mathbf{k}}(\omega_n) - \frac{e^{(\beta-\tau_l)\xi}}{e^{\beta\xi}+1} \frac{1}{N^2} \sum_{\mathbf{k}} e^{-i\mathbf{k}\cdot\mathbf{i}} f_{\mathbf{k}}^{\infty} \tag{B.11}$$

Shifting frequencies according to $\widetilde{f}^{s}_{n_x,n_y,n} \equiv \widetilde{f}_{\mathbf{k}}(\omega_n - N_m\pi T)$ finally yields for $f_{i_x,i_y,l} = f_{\mathbf{i}}(\tau_l)$ the result

$$\begin{aligned} f_{i_x,i_y,l} &= \frac{T e^{i\left(\frac{N_m-s}{N_m}\right)\pi l}}{N^2} \sum_{n_x=0}^{N-1} \sum_{n_y=0}^{N-1} \sum_{n=0}^{N_m-1} e^{-i2\pi\left(\frac{n_x i_x + n_y i_y}{N} + \frac{nl}{N_m}\right)} \widetilde{f}^{s}_{n_x,n_y,n} \\ &\quad - \frac{e^{(\beta-\tau_l)\xi}}{e^{\beta\xi}+1} \frac{1}{N^2} \sum_{n_x=0}^{N-1} \sum_{n_y=0}^{N-1} e^{-i2\pi\left(\frac{n_x i_x + n_y i_y}{N}\right)} f^{\infty}_{n_x n_y}. \end{aligned} \tag{B.12}$$

This result is valid for fermions ($s=1$) and bosons ($s=0$). We used $\omega_n = (2n+s)\pi T$. It turns out that the second, purely two dimensional Fourier transformation can always be performed analytically.

[1] This result is only valid for fermions. We won't need the result for bosons.

Fourier transformation of $G_{\mathbf{k}}(\omega_n)$ to $G_{\mathbf{i}}(\tau)$ It holds

$$G_{\mathbf{k}}(\omega_n \to \pm\infty) \simeq \frac{1}{i\omega_n} \tag{B.13}$$

i.e. $G^{\infty}_{\mathbf{k}} = 1$. Thus, we introduce[2].

$$\widetilde{G}_{\mathbf{k}}(\omega_n) = G_{\mathbf{k}}(\omega_n) - \frac{1}{i\omega_n - \xi} \tag{B.14}$$

and obtain $G_{i_x i_y l} = G_{\mathbf{i}}(\tau_l)$ via

$$\begin{aligned} G_{i_x,i_y,l} &= \frac{Te^{i\left(\frac{N_m-1}{N_m}\right)\pi l}}{N^2} \sum_{n_x=0}^{N-1}\sum_{n_y=0}^{N-1}\sum_{n=0}^{N_m-1} e^{-i2\pi\left(\frac{n_x i_x + n_y i_y}{N} + \frac{nl}{N_m}\right)} \widetilde{G}^{s}_{n_x,n_y,n} \\ &\quad - \frac{e^{(\beta-\tau_l)\xi}}{e^{\beta\xi}+1}\delta_{i_x,0}\delta_{i_y,0} \end{aligned} \tag{B.15}$$

where

$$\widetilde{G}^{s}_{n_x,n_y,n} = \widetilde{G}_{n_x,n_y}(\omega_n - N_m \pi T). \tag{B.16}$$

The Fourier transform only yields $G_{i_x,i_y,l}$ for $0 \le l \le N_m - 1$. To obtain G_{i_x,i_y,N_m} we take advantage of the fact that $G_{\mathbf{i}}(0^+) - G_{\mathbf{i}}(0^-) = -\delta_{\mathbf{i},\mathbf{0}}$, which yields

$$G_{i_x,i_y,N_m} = -G_{i_x,i_y,0} - \delta_{i_x,0}\delta_{i_y,0}. \tag{B.17}$$

Fourier transformation of $\chi_{\mathbf{i}}(\tau)$ to $\chi_{\mathbf{q}}(\nu_m)$ We determine the particle hole bubble $\chi_{\mathbf{i}}(\tau) = -G_{\mathbf{i}}(\tau)\, G_{\mathbf{i}}(-\tau)$. It holds $\chi_{\mathbf{i}}(\tau) = G_{\mathbf{i}}(\tau)\, G_{\mathbf{i}}(\beta - \tau)$ which yields with $\chi_{i_x i_y l} = \chi_{\mathbf{i}}(\tau_l)$:

$$\chi_{i_x i_y l} = G_{i_x,i_y,l} G_{i_x,i_y,N_m - l} \tag{B.18}$$

In order to determine $\chi_{i_x i_y l}$ for $l = 0$ use G_{i_x,i_y,N_m} determined above. It holds $\chi_{\mathbf{i}}(0^+) = \chi_{\mathbf{i}}(0^-)$, implying that $\chi_{n_x n_y n} = \chi_{\mathbf{q}}(\nu_n)$ will always decay faster than $1/\nu_n$. Thus, it follows

$$\chi_{n_x n_y n} = W_n \Delta \widehat{\chi}_{n_x n_y n} \tag{B.19}$$

where

$$\widehat{\chi}_{n_x n_y n} = \sum_{n_x=0}^{N-1}\sum_{n_y=0}^{N-1}\sum_{l=0}^{N_m-1} e^{i2\pi\left(\frac{n_x i_x + n_y i_y}{N} + \frac{nl}{N_m}\right)} \chi_{i_x i_y l} \tag{B.20}$$

[2]Below we show that $\xi = T\log\left(\frac{1-n}{n}\right)$ is a convenient choice for the arbitrary parameter ξ.

and $W_n = 2\frac{1-\cos(\Delta\nu_n)}{\Delta^2\nu_n^2}$ with $\Delta = \beta/N_m$ and $\nu_n = 2\pi nT$, i.e.

$$W_n = 2\left(\frac{N_m}{2\pi n}\right)^2\left(1-\cos\left(\frac{2\pi n}{N_m}\right)\right) \tag{B.21}$$

An FFT evaluation of the above sum will only provide results for $0 \leq n \leq N_m - 1$. Because of the implicit periodicity of $\widehat{\chi}_{n_x n_y n}$, negative frequencies can be obtained via:

$$\chi_{n_x n_y}(\nu_n) = \begin{cases} W_n \Delta \widehat{\chi}_{n_x n_y n} & \text{if } \nu_n > 0 \\ W_n \Delta \widehat{\chi}_{n_x n_y N_m + n} & \text{if } \nu_n < 0 \end{cases} \tag{B.22}$$

Eventually we need to determine the shifted frequency expression

$$\chi^s_{n_x,n_y,n} = \chi(\nu_n - N_m \pi T) = \chi\left(\nu_{n-\frac{N_m}{2}}\right) \tag{B.23}$$

This yields

$$\chi^s_{n_x,n_y,n} = \begin{cases} W_{n-\frac{N_m}{2}} \Delta \widehat{\chi}_{n_x n_y \frac{N_m}{2}+n} & \text{if } 0 \leq\ n < \frac{N_m}{2} \\ W_{n-\frac{N_m}{2}} \Delta \widehat{\chi}_{n_x n_y n-\frac{N_m}{2}} & \text{if } \frac{N_m}{2} \leq n \leq N_m - 1 \end{cases} \tag{B.24}$$

Fourier transformation of $V_{\mathbf{q}}(\nu_n)$ to $V_{\mathbf{i}}(\tau)$. Once the particle hole bubble $\chi_{n_x n_y n} = \chi_{\mathbf{q}}(\nu_n)$ is known, $V_{\mathbf{q}}(\nu_n)$ follows from the above equation. Since $\chi_{\mathbf{q}}(\nu_n)$ decays faster than $1/\nu_n$, the same is true for $V_{\mathbf{q}}(\nu_n)$. We shift the frequency as usual:

$$V^s_{n_x,n_y,n} = V(\nu_n - N_m \pi T) \tag{B.25}$$

and the Fourier transform is

$$V_{i_x,i_y,l} = \frac{Te^{i\pi l}}{N^2}\sum_{n_x=0}^{N-1}\sum_{n_y=0}^{N-1}\sum_{n=0}^{N_m-1} e^{-i2\pi\left(\frac{n_x i_x + n_y i_y}{N} + \frac{nl}{N_m}\right)} V^s_{n_x,n_y,n}. \tag{B.26}$$

The Fourier transformation only yields $V_{i_x,i_y,l}$ for $0 \leq l \leq N_m - 1$. It holds however that $V_{i_x,i_y,N} = V_{i_x,i_y,0}$: since $V_{\mathbf{q}}(\nu_n)$ decays faster than $1/\nu_n$ it is continuous for $\tau = 0$, i.e. $V_{\mathbf{i}}(\beta^-) = V_{\mathbf{i}}(0^-) = V_{\mathbf{i}}(0^+)$ which corresponds to the above result for $V_{i_x,i_y,N}$.

Fourier transformation of $\Sigma_{\mathbf{i}}(\tau)$ to $\Sigma_{\mathbf{k}}(\omega_n)$ The self energy is given as $\Sigma_{\mathbf{i}}(\tau) = V_{\mathbf{i}}(\tau) G_{\mathbf{i}}(\tau)$. It holds $\Sigma_{\mathbf{i}}(0^+) = V_{\mathbf{i}}(0^+) G_{\mathbf{i}}(0^+)$ and $\Sigma_{\mathbf{i}}(0^-) = V_{\mathbf{i}}(0^-) G_{\mathbf{i}}(0^-) = V_{\mathbf{i}}(0^+)(G_{\mathbf{i}}(0^+) + \delta_{\mathbf{i},\mathbf{0}})$. Thus, it follows

$$\Sigma_{\mathbf{i}}\left(0^+\right) - \Sigma_{\mathbf{i}}\left(0^-\right) = -V_{\mathbf{i}}\left(0^+\right)\delta_{\mathbf{i},\mathbf{0}} \tag{B.27}$$

This allows to write for the Fourier transform $\Sigma_{n_x n_y n} = \Sigma_{\mathbf{k}}(\omega_n)$:

$$\Sigma_{n_x n_y n} = W_n \Delta \widehat{\Sigma}_{n_x n_y n} - V_{0,0,0} R_n \tag{B.28}$$

with

$$\widehat{\Sigma}_{n_x n_y n} = \sum_{i_x=0}^{N-1} \sum_{i_y=0}^{N-1} \sum_{l=0}^{N_m-1} e^{i2\pi\left(\frac{n_x i_x + n_y i_y}{N} + \frac{nl}{N_m}\right)} e^{i\frac{\pi l}{N_m}} \Sigma_{i_x i_y l} \tag{B.29}$$

As before, the notation used is $\Sigma_{i_x i_y l} = \Sigma_{\mathbf{i}}(\tau_l)$. In addition holds that $V_{0,0,0} = V_{\mathbf{i=0}}(0^+)$ is the effective interaction at $\tau = 0$ at the origin. Finally it holds:

$$\begin{aligned} W_n &= 2\frac{1-\cos(\Delta\omega_n)}{\Delta^2\omega_n^2} \\ R_n &= -\frac{1 - i\Delta\omega_n - e^{-i\Delta\omega_n}}{\Delta\omega_n^2}. \end{aligned} \tag{B.30}$$

with $\Delta = \beta/N_m$ and $\omega_n = (2n+1)\pi T$.

Once again, an FFT evaluation of the above sum will only provide results for $0 \leq n \leq N_m - 1$. Because of the implicit periodicity of $\widehat{\Sigma}_{n_x n_y n}$, negative frequencies can be obtained via:

$$\Sigma_{n_x n_y}(\omega_n) = \begin{cases} W_n \Delta \widehat{\Sigma}_{n_x n_y n} + V_{0,0,0} R_n & \text{if } \omega_n > 0 \\ W_n \Delta \widehat{\Sigma}_{n_x n_y N_m + n} + V_{0,0,0} R_n & \text{if } \omega_n < 0 \end{cases} \tag{B.31}$$

Eventually we need to determine the shifted frequency expression

$$\Sigma^s_{n_x, n_y, n} = \Sigma_{n_x n_y}(\omega_n - N_m \pi T) = \chi\left(\nu_{n - \frac{N_m}{2}}\right) \tag{B.32}$$

B.1.0.1 particle number calculation

The particle number is determined via

$$n = 1 + \frac{1}{N^2} \sum_{\mathbf{k}} G_{\mathbf{k}}(\tau^+) = 1 + \frac{T}{N^2} \sum_{\mathbf{k},n} G_{\mathbf{k}}(\omega_n) \tag{B.33}$$

The sum over Matsubara frequencies is formally divergent and requires regularization. We introduce again

$$\widetilde{G}_{\mathbf{k}}(\omega_n) = G_{\mathbf{k}}(\omega_n) - \frac{1}{i\omega_n - \xi} \tag{B.34}$$

which decays fast enough to ensure convergence. The sum $T\sum_n \frac{1}{i\omega_n - \xi}$ is the performed using the usual regularization of Matsubara functions

$$T \sum_n \frac{1}{i\omega_n - \xi} = n_\xi - 1 \tag{B.35}$$

where

$$n_\xi = \frac{1}{e^{\beta\xi}+1}. \tag{B.36}$$

This yields

$$n = n_\xi + \frac{T}{N^2}\sum_{\mathbf{k},n}\widetilde{G}_{\mathbf{k}}\left(\omega_n\right) \tag{B.37}$$

If we chose

$$\xi = T\log\left(\frac{1-n}{n}\right) \tag{B.38}$$

it holds $n = n_\xi$ and the condition for the chemical potential becomes

$$\frac{T}{N^2}\sum_{\mathbf{k},n}\widetilde{G}_{\mathbf{k}}\left(\omega_n\right) = 0 \tag{B.39}$$

which is numerically well behaved.

Supression of aliasing We only know the time dependent functions $f\left(\tau\right)$ for a finite number of discrete points $\tau_l = l\Delta$, with $\Delta = \beta/N_m$ and $l = 0, ..., N_m - 1$. For τ between two points ($\tau_l < \tau < \tau_{l+1} = \tau_l + \Delta$) we interpolate linearly, i.e.

$$f\left(\tau_l < \tau < \tau_{l+1}\right) = f_l + \frac{f_{l+1} - f_l}{\Delta}\left(\tau - \tau_l\right)$$

Thus it holds for arbitrary τ:

$$f\left(\tau\right) = \sum_{l=0}^{N_m-1}\theta\left(\tau-\tau_l\right)\theta\left(\Delta-\tau+\tau_l\right)\left[f_l + \frac{f_{l+1}-f_l}{\Delta}\left(\tau-\tau_l\right)\right]$$

Here, we implicitly assumed that we know $f_{N_m} = f\left(\beta^-\right)$, even though the last point we have available is f_{N_m-1}. We address this issue later. This is necessary to be able to interpolate in the regime $\beta - \Delta < \tau < \beta$. Fourier transformation yields

$$\begin{aligned} f\left(\omega_n\right) &= \sum_{l=0}^{N_m-1}\int_{\tau_l}^{\tau_l+\Delta} e^{i\omega_n\tau}\left[f_l + \frac{f_{l+1}-f_l}{\Delta}\left(\tau-\tau_l\right)\right]d\tau \\ &= \sum_{l=0}^{N_m-1} e^{i\omega_n\tau_l}\int_0^\Delta e^{i\omega_l x}\left[f_l + \frac{f_{l+1}-f_l}{\Delta}x\right]dx \\ &= \sum_{l=0}^{N_m-1} e^{i\omega_n\tau_l}\left[f_l\,\frac{1+i\Delta\omega_n - e^{i\Delta\omega_n}}{\Delta\omega_n^2} + f_{l+1}\frac{e^{i\Delta\omega_n}\left(1-i\Delta\omega_n\right)-1}{\Delta\omega_n^2}\right] \end{aligned} \tag{B.40}$$

we introduce $l' = l + 1$ in the second term and use $\tau_l = \tau_{l'-1} = \tau_{l'} - \Delta$.

$$
\begin{aligned}
f(\omega_n) &= \sum_{l=0}^{N_m-1} e^{i\omega_n\tau_l} f_l \frac{1+i\Delta\omega_n - e^{i\Delta\omega_n}}{\Delta\omega_n^2} + \sum_{l=1}^{N_m} e^{i\omega_n\tau_l} f_l \frac{1-i\Delta\omega_n - e^{-i\Delta\omega_n}}{\Delta\omega_n^2} \\
&= \sum_{l=0}^{N_m-1} e^{i\omega_n\tau_l} \left(\frac{2-2\cos(\Delta\omega_n)}{\Delta\omega_n^2}\right) f_l \\
&\quad + e^{i\omega_n\beta} f\left(\beta^-\right) \frac{1-i\Delta\omega_n - e^{-i\Delta\omega_n}}{\Delta\omega_n^2} - f\left(0^+\right) \frac{1-i\Delta\omega_n - e^{-i\Delta\omega_n}}{\Delta\omega_n^2}
\end{aligned} \tag{B.41}
$$

It holds $e^{i\omega_n\beta} = \eta$ where $\eta = 1$ for bosons and $\eta = -1$ for fermions, respectively. In addition it holds $\eta f(\beta^-) = f(0^-)$ such that

$$
f(\omega_n) = W_n \Delta \sum_{l=0}^{N_m-1} e^{i\omega_n\tau_l} f_l + \left(f\left(0^+\right) - f\left(0^-\right)\right) R_n \tag{B.42}
$$

where

$$
\begin{aligned}
W_n &= 2\frac{1-\cos(\Delta\omega_n)}{\Delta^2\omega_n^2} \\
R_n &= -\frac{1-i\Delta\omega_n - e^{-i\Delta\omega_n}}{\Delta\omega_n^2}
\end{aligned} \tag{B.43}
$$

Thus, multiplying the Fourier sum by W_n and including the value of the discontinuity at $\tau = \pm 0$ yields a significant increase in the accuracy of the calculation.

B.2 Numerical Implementation for the Multiorbital FLEX

In this section, we show the numerical steps to implement the Multiorbital FLEX calculation. More complicated than the single-band case, we introduce all the parameters and quantities and list the numerical steps as follows.

1. Choose the parameters U, U', J_H, J', t_1, t_2, t_3, t_4, T, n.

2. Generate $\tilde{U}_s$, $\tilde{U}_c$, $\tilde{\varepsilon}_{\mathbf{k}}$. Here the dispersion relation is given by

$$
\tilde{\varepsilon}_{\mathbf{k}} = \begin{bmatrix} \varepsilon_{\mathbf{k}}^{11} & \varepsilon_{\mathbf{k}}^{12} \\ \varepsilon_{\mathbf{k}}^{21} & \varepsilon_{\mathbf{k}}^{22} \end{bmatrix}
$$

with

$$\begin{aligned}
\varepsilon_{\mathbf{k}}^{11} &= -2t_1\cos k_x - 2t_2\cos k_y - 4t_3\cos k_x\cos k_y, \\
\varepsilon_{\mathbf{k}}^{22} &= -2t_2\cos k_x - 2t_1\cos k_y - 4t_3\cos k_x\cos k_y, \\
\varepsilon_{\mathbf{k}}^{12} &= \varepsilon_{\mathbf{k}}^{21} = -4t_4\sin k_x\sin k_y.
\end{aligned}$$

And initialize self-energy $\Sigma^{ab}(\mathbf{k}, i\omega_n)$ and $\Phi^{ab}(\mathbf{k}, i\omega_n)$ or input self-energy from external files with the self-energy data from another run.

3. Using $\Sigma^{ab}(\mathbf{k}, i\omega_n)$, $\Phi^{ab}(\mathbf{k}, i\omega_n)$ and $\varepsilon^{ab}(\mathbf{k})$ to initialize $G^{ab}(\mathbf{k}, i\omega_n)$ and $F^{ab}(\mathbf{k}, i\omega_n)$ to find chemical potential. Σ^{ab} is symmetric in orbital indices so we only need to store half of it, and $\Phi^{ba} = \left(\Phi^{ab}\right)^*$ then we also store half of it

$$\begin{aligned}
\tilde{G}(k) &= \left[(i\omega_n+\mu)\,\tilde{\mathbf{1}} - \tilde{\varepsilon}_{\mathbf{k}} - \tilde{\Sigma}(k) - \tilde{\Phi}(k)\left[(i\omega_n-\mu)\,\tilde{\mathbf{1}} + \tilde{\varepsilon}_{\mathbf{k}} + \tilde{\Sigma}^*(k)\right]^{-1}\tilde{\Phi}^*(k)\right]^{-1}, \\
\tilde{F}(k) &= \tilde{G}(k)\tilde{\Phi}(k)\left[(i\omega_n-\mu)\,\tilde{\mathbf{1}} + \tilde{\varepsilon}_{\mathbf{k}} + \tilde{\Sigma}^*(k)\right]^{-1}.
\end{aligned}$$

Note that they are all matrix munipulations in orbital space. For each (k_x, k_y, ω_n) we need a few temperary $M\times M$ matrices to store $\tilde{\Phi}(k)\left[(i\omega_n-\mu)\,\tilde{\mathbf{1}} + \tilde{\varepsilon}_{\mathbf{k}} + \tilde{\Sigma}(-k)\right]^{-1}$, $\tilde{\Phi}(k)$, $\tilde{G}(k)$ and $\tilde{F}(k)$ etc, where M is the number of orbitals. And they are all in the shifted frequency scheme, i.e., $\omega_n - N_m\pi T$. We find chemical potential and initialize $\tilde{G}$ and $\tilde{F}$ together to save computation cost. The total particle number is determined via

$$n = \frac{1}{N^2}\sum_{\mathbf{k},a} G^{aa}(\mathbf{k}, 0^-) = M + \frac{1}{N^2}\sum_{\mathbf{k},a} G^{aa}(\mathbf{k}, 0^+) = M + \frac{T}{N^2}\sum_{\mathbf{k},n,a} G^{aa}(\mathbf{k}, i\omega_n).$$

The sum over Matsubara frequencies is formally divergent and requires regularization. We introduce again

$$\check{G}^{ab}(\mathbf{k}, i\omega_n) = G^{ab}(\mathbf{k}, i\omega_n) - \frac{\delta^{ab}}{i\omega_n - \xi}$$

which decays fast enough to ensure convergence. The sum $T\sum_n \frac{1}{i\omega_n-\xi}$ is performed using the usual regulariztion of Mastubara functions

$$T\sum_n \frac{1}{i\omega_n - \xi} = n_\xi - 1$$

where $n_\xi = \frac{1}{e^{\beta\xi}+1}$. This yields

$$n = Mn_\xi + \frac{T}{N^2}\sum_{\mathbf{k},n,a} \check{G}^{aa}(\mathbf{k}, i\omega_n).$$

If we choose $n_\xi = n/M$, i.e.

$$\xi = T\ln\left(\frac{M}{n} - 1\right)$$

the condition for the chemical potentical becomes

$$\frac{T}{N^2}\sum_{\mathbf{k},n,a} \check{G}^{aa}(\mathbf{k}, i\omega_n) = 0$$

which is numerically well behaved. Meanwhile we initialize $\check{G}^{ab}(\mathbf{k}, i\omega_n)$ and $F^{ab}(\mathbf{k}, i\omega_n)$ for later use.

4. Determine the Hartree-Fock contribution to the self-energy. Calculate the Hartree-Fock terms Σ^{ab}_{HF} and Φ^{ab}_{HF}

$$\Sigma^{ab}_{HF} = \sum_{m,n}\left(\frac{3}{2}\tilde{U}_s - \frac{1}{2}\tilde{U}_c\right)^{am,bn}\left[\delta_{mn} + \frac{T}{N^2}\sum_{\mathbf{k},\omega_n} G_{mn}(\mathbf{k}, i\omega_n)\right]$$

i.e.

$$\Sigma^{ab}_{HF} = \sum_{m}\left(\frac{3}{2}\tilde{U}_s - \frac{1}{2}\tilde{U}_c\right)^{am,bm} + \sum_{m,n}\left(\frac{3}{2}\tilde{U}_s - \frac{1}{2}\tilde{U}_c\right)^{am,bn}\left[\frac{T}{N^2}\sum_{\mathbf{k},\omega_n} G_{mn}(\mathbf{k}, i\omega_n)\right].$$

Since the Hartree energy always enters in the combination $\mu\delta^{ab} - \Sigma^{ab}_{HF}$, we can absorb the mean Hartree shift into a redefinition of the chemical potential: $\mu' = \mu - \frac{1}{M}\sum_c \Sigma^{cc}_{HF}$. Thus we only need to include the modified Hartree term

$$\Sigma^{ab}_{HF,mod} = \Sigma^{ab}_{HF} - \delta^{ab}\frac{\mathrm{Tr}\left[\tilde{\Sigma}_{HF}\right]}{M} = \Sigma^{ab}_{HF} - \delta^{ab}\frac{\sum_c \Sigma^{cc}_{HF}}{M},$$

$$\Phi^{ab}_{HF} = \sum_{m,n}\left(\frac{1}{2}\tilde{U}_s + \frac{1}{2}\tilde{U}_c\right)^{am,nb}\left[\frac{T}{N^2}\sum_{\mathbf{k},\omega_n} F_{mn}(\mathbf{k}, i\omega_n)\right].$$

5. Forward Fourier transform $\check{G}^{ab}(\mathbf{k}, i\omega_n)$ and $F^{ab}(\mathbf{k}, i\omega_n)$ to coordinate and imaginary time demain to obtain $\check{G}^{ab}(\mathbf{i}, \tau)$ and $F^{ab}(\mathbf{i}, \tau)$. Next we should fix them according to

$$G^{ab}_{i_x,i_y,l} = \frac{Te^{i\left(\frac{N_m-1}{N_m}\right)\pi l}}{N^2} \sum_{n_x=0}^{N-1}\sum_{n_y=0}^{N-1}\sum_{n=0}^{N_m-1} e^{-i2\pi\left(\frac{n_x i_x + n_y i_y}{N} + \frac{nl}{N_m}\right)} \check{G}^{S;ab}_{n_x,n_y,n} - \frac{e^{(\beta-\tau_l)\xi}}{e^{\beta\xi}+1}\delta_{i_x,0}\delta_{i_y,0}\delta_{a,b}$$

$$F^{ab}_{i_x,i_y,l} = \frac{Te^{i\left(\frac{N_m-1}{N_m}\right)\pi l}}{N^2} \sum_{n_x=0}^{N-1}\sum_{n_y=0}^{N-1}\sum_{n=0}^{N_m-1} e^{-i2\pi\left(\frac{n_x i_x + n_y i_y}{N} + \frac{nl}{N_m}\right)} F^{S;ab}_{n_x,n_y,n}$$

where $\tau_l = \Delta l$ and $\check{G}^s_{n_x,n_y,n} = \check{G}_{n_x,n_y}(\omega_n - N_m\pi T)$, and the same for F^s_n. The Fourier transform only yields $G^{ab}_{i_x,i_y,l}$, $F^{ab}_{i_x,i_y,l}$ for $0 \le l \le N_m - 1$. To obtain them at $l = N_m$ we take advantage of the fact that $G^{ab}_{\mathbf{i}}(0^+) - G^{ab}_{\mathbf{i}}(0^-) = -\delta_{i_x,0}\delta_{i_y,0}\delta^{ab}$, $F^{ab}_{\mathbf{i}}(0^+) - F^{ab}_{\mathbf{i}}(0^-) = 0$, which yields

$$\begin{aligned} G^{ab}_{i_x,i_y,N_m} &= -G^{ab}_{i_x,i_y,0} - \delta_{i_x,0}\delta_{i_y,0}\delta^{ab}, \\ F^{ab}_{i_x,i_y,N_m} &= -F^{ab}_{i_x,i_y,0}. \end{aligned}$$

6. Now using G and F in real space we calculate $\chi^s_{ab,a'b'}(\mathbf{i}, \tau)$ and $\chi^c_{ab,a'b'}(\mathbf{i}, \tau)$ via

$$\begin{aligned} &\chi^s_{ab,a'b'}(\mathbf{q}, i\Omega_n) \\ &= -\frac{T}{N}\sum_{\mathbf{k},i\omega_n} \left[G_{ba'}(\mathbf{k}+\mathbf{q}, i\omega_n + i\Omega_n)G_{b'a}(\mathbf{k}, i\omega_n) + F_{bb'}(\mathbf{k}+\mathbf{q}, i\omega_n + i\Omega_n)F_{a'a}(\mathbf{k}, -i\omega_n)\right], \end{aligned}$$

$$\begin{aligned} &\chi^c_{ab,a'b'}(\mathbf{q}, i\Omega_n) \\ &= -\frac{T}{N}\sum_{\mathbf{k},i\omega_n} \left[G_{ba'}(\mathbf{k}+\mathbf{q}, i\omega_n + i\Omega_n)G_{b'a}(\mathbf{k}, i\omega_n) - F_{bb'}(\mathbf{k}+\mathbf{q}, i\omega_n + i\Omega_n)F_{a'a}(\mathbf{k}, -i\omega_n)\right]. \end{aligned}$$

In order to simplify the programming by using the symmetry property, we switch the first two indices in $\chi^{s,c}$, accordingly switch the last two indices in $U_{s,c}$.

$$\begin{aligned} \Longrightarrow \chi^s_{ba,a'b'}(\mathbf{i}, \tau) &= -G_{ba'}(\mathbf{i}, \tau)G_{b'a}(\mathbf{i}, -\tau) - F_{bb'}(\mathbf{i}, \tau)F_{a'a}(\mathbf{i}, \tau) \\ \chi^c_{ba,a'b'}(\mathbf{i}, \tau) &= -G_{ba'}(\mathbf{i}, \tau)G_{b'a}(\mathbf{i}, -\tau) + F_{bb'}(\mathbf{i}, \tau)F_{a'a}(\mathbf{i}, \tau) \end{aligned}$$

where we have switched the first two indices in χ for convenience. Since $G_{ab} = G_{ba}$, we have

$$\begin{aligned}\chi^{s,c}_{a'b',ba}(\mathbf{i},\tau) &= -G_{a'b}(\mathbf{i},\tau)G_{ab'}(\mathbf{i},-\tau) \mp F_{a'a}(\mathbf{i},\tau)F_{bb'}(\mathbf{i},\tau) \\ &= -G_{ba'}(\mathbf{i},\tau)G_{b'a}(\mathbf{i},-\tau) \mp F_{bb'}(\mathbf{i},\tau)F_{a'a}(\mathbf{i},\tau) = \chi^{s,c;0}_{ba,a'b'}(\mathbf{i},\tau)\end{aligned}$$

That is, $\chi^{s,c}_{A,B} = \chi^{s,c}_{B,A}$ are symmetric matrices in the composite orbital indices, which can be stored in half. The fermionic Green's function has the property that $-f(-\tau) = f(\beta-\tau)$, anti-periodic property in imaginary time. Then it holds

$$\begin{aligned}\chi^{s}_{ba,a'b'}(\mathbf{i},\tau) &= G_{ba'}(\mathbf{i},\tau)G_{b'a}(\mathbf{i},\beta-\tau) - F_{bb'}(\mathbf{i},\tau)F_{a'a}(\mathbf{i},\tau) \\ \chi^{c}_{ba,a'b'}(\mathbf{i},\tau) &= G_{ba'}(\mathbf{i},\tau)G_{b'a}(\mathbf{i},\beta-\tau) + F_{bb'}(\mathbf{i},\tau)F_{a'a}(\mathbf{i},\tau)\end{aligned}$$

which yields

$$\chi^{s}_{ba,a'b'}(i_x,i_y,l) = G_{ba'}(i_x,i_y,l)G_{b'a}(i_x,i_y,N_m-l) - F_{bb'}(i_x,i_y,l)F_{a'a}(i_x,i_y,l),$$

$$\chi^{c}_{ba,a'b'}(i_x,i_y,l) = G_{ba'}(i_x,i_y,l)G_{b'a}(i_x,i_y,N_m-l) + F_{bb'}(i_x,i_y,l)F_{a'a}(i_x,i_y,l),$$

for $l = 0$

$$\begin{aligned}&\chi^{s}_{ba,a'b'}(i_x,i_y,0) \\ &= -G_{ba'}(i_x,i_y,0)G_{b'a}(i_x,i_y,0) - G_{ba'}(0,0,0)\delta_{i_x,0}\delta_{i_y,0}\delta_{b',a} - F_{bb'}(i_x,i_y,0)F_{a'a}(i_x,i_y,0),\end{aligned}$$

$$\begin{aligned}&\chi^{c}_{ba,a'b'}(i_x,i_y,0) \\ &= -G_{ba'}(i_x,i_y,0)G_{b'a}(i_x,i_y,0) - G_{ba'}(0,0,0)\delta_{i_x,0}\delta_{i_y,0}\delta_{b',a} + F_{bb'}(i_x,i_y,0)F_{a'a}(i_x,i_y,0).\end{aligned}$$

Now consider the discontinuity of $\chi^{s,c}$ at $\tau = 0$. Since

$$\begin{aligned}G^{ab}_{\mathbf{i}}(0^+) - G^{ab}_{\mathbf{i}}(0^-) &= -\delta_{\mathbf{i},\mathbf{0}}\delta^{ab} \\ F^{ab}_{\mathbf{i}}(0^+) - F^{ab}_{\mathbf{i}}(0^-) &= 0\end{aligned}$$

then

$$\begin{aligned}&\chi^{s}_{ba,a'b'}(i_x,i_y,0^+) - \chi^{s}_{ba,a'b'}(i_x,i_y,0^-) \\ =\ & -G_{ba'}(i_x,i_y,0^+)G_{b'a}(i_x,i_y,0^-) - F_{bb'}(i_x,i_y,0^+)F_{a'a}(i_x,i_y,0^+) \\ & +G_{ba'}(i_x,i_y,0^-)G_{b'a}(i_x,i_y,0^+) + F_{bb'}(i_x,i_y,0^-)F_{a'a}(i_x,i_y,0^-) \\ =\ & \left[-G_{ba'}(0,0,0)\delta_{b',a} + G_{b'a}(0,0,0)\delta_{b,a'}\right]\delta_{i_x,0}\delta_{i_y,0}\end{aligned}$$

Therefore we have

$$\chi^s_{ba,a'b'}(\mathbf{i},0^+) - \chi^s_{ba,a'b'}(\mathbf{i},0^-) = \Upsilon_{ba,a'b'}\delta_{\mathbf{i},\mathbf{0}}$$

$$\chi^c_{ba,a'b'}(\mathbf{i},0^+) - \chi^c_{ba,a'b'}(\mathbf{i},0^-) = \Upsilon_{ba,a'b'}\delta_{\mathbf{i},\mathbf{0}}$$

where we define a matrix as

$$\Upsilon_{ba,a'b'} \equiv \left[-G_{ba'}(\mathbf{0},0)\delta_{b',a} + G_{b'a}(\mathbf{0},0)\delta_{b,a'}\right]$$

which represent the discontinuous jump at $\tau = 0$ in both χ^s and χ^c that is entering the aliasing correction when transforming χ's from imaginary time to Matsubara frequency space.

7. Backward Fourier transform $\chi^{c,s}(i_x, i_y, l)$ to momentum-Mastubara-frequency domain $\hat{\chi}^{c,s}(n_x, n_y, n)$, then we perform the aliasing correction and shuffle the frequency due to the fact that FFT only provides the results for $0 \leq n \leq N_m - 1$ and the implicit periodicity of $\hat{\chi}$, $\hat{\chi}(-\tau) = \hat{\chi}(\beta - \tau) \Longrightarrow$, negative frequencies can still be obtained. Eventually we need to determine the shifted frequency expressions

$$\chi^{c,s;S}_{ba,a'b'}(n_x, n_y, n)$$
$$= \begin{cases} W(n - \frac{N_m}{2})\Delta\hat{\chi}^{c,s}_{ba,a'b'}(n_x, n_y, n + \frac{N_m}{2}) + \Upsilon_{ba,a'b'}R(n - \frac{N_m}{2}) & 0 \leq n < \frac{N_m}{2}, \\ W(n - \frac{N_m}{2})\Delta\hat{\chi}^{c,s}_{ba,a'b'}(n_x, n_y, n - \frac{N_m}{2}) + \Upsilon_{ba,a'b'}R(n - \frac{N_m}{2}) & \frac{N_m}{2} \leq n \leq N_m - 1. \end{cases}$$

Here the aliasing correction is

$$f(\Omega_n) = W_n\Delta \sum_{l=0}^{N_m-1} e^{i\Omega_n\tau_l} f_l + \left(f(0^+) - f(0^-)\right) R_n$$

with

$$\begin{aligned} W_n &= 2\frac{1-\cos(\Omega_n\Delta)}{\Omega_n^2\Delta^2} \\ R_n &= -\frac{1 - i\Omega_n\Delta - e^{-i\Omega_n\Delta}}{\Omega_n^2\Delta} \end{aligned}$$

where $\Omega_n = 2n\pi T$ is the bosonic Matsubara frequency. At $n = 0$, $W_{n=0} = 1$ and $R_{n=0} = -\frac{\Delta}{2}$.

8. Now $\chi^{c,s}$ are in momentum-frequency domain, we calculate $V_N^{A,B}(\mathbf{q}, i\nu_n)$ and $V_A^{A,B}(\mathbf{q}, i\nu_n)$ via

$$\begin{aligned}
&\tilde{V}_N^{Shift}(\mathbf{q}, i\nu_n) \\
=&\frac{3}{2}\tilde{U}_s\Big(\tilde{1} - \tilde{\chi}^s(\mathbf{q}, i\nu_n)\tilde{U}^s\Big)^{-1}\tilde{\chi}^s(\mathbf{q}, i\nu_n)\tilde{U}_s + \frac{1}{2}\tilde{U}_c\Big(\tilde{1} + \tilde{\chi}^c(\mathbf{q}, i\nu_n)\tilde{U}^c\Big)^{-1}\tilde{\chi}^c(\mathbf{q}, i\nu_n)\tilde{U}_c \\
&-\frac{3}{8}\tilde{U}_s[\tilde{\chi}^s(\mathbf{q}, i\nu_n) + \tilde{\chi}^c(\mathbf{q}, i\nu_n)]\tilde{U}_s - \frac{1}{8}\tilde{U}_c[\tilde{\chi}^s(\mathbf{q}, i\nu_n) + \tilde{\chi}^c(\mathbf{q}, i\nu_n)]\tilde{U}_c \\
&+ \tilde{V}_N^{HF}
\end{aligned}$$

where

$$\tilde{V}_N^{HF} = \frac{1}{2}\left(3\tilde{U}_s - \tilde{U}_c\right).$$

$$\begin{aligned}
&\tilde{V}_A^{Shift}(\mathbf{q}, i\nu_n) \\
=&\frac{3}{2}\tilde{U}_s\Big(\tilde{1} - \tilde{\chi}^s(\mathbf{q}, i\nu_n)\tilde{U}^s\Big)^{-1}\tilde{\chi}^s(\mathbf{q}, i\nu_n)\tilde{U}_s - \frac{1}{2}\tilde{U}_c\Big(\tilde{1} + \tilde{\chi}^c(\mathbf{q}, i\nu_n)\tilde{U}^c\Big)^{-1}\tilde{\chi}^c(\mathbf{q}, i\nu_n)\tilde{U}_c \\
&-\frac{3}{8}\tilde{U}_s[\tilde{\chi}^s(\mathbf{q}, i\nu_n) - \tilde{\chi}^c(\mathbf{q}, i\nu_n)]\tilde{U}_s - \frac{1}{8}\tilde{U}_c[\tilde{\chi}^s(\mathbf{q}, i\nu_n) - \tilde{\chi}^c(\mathbf{q}, i\nu_n)]\tilde{U}_c \\
&+\tilde{V}_A^{HF}
\end{aligned}$$

where

$$\tilde{V}_A^{HF} = \frac{1}{2}\left(\tilde{U}_s + \tilde{U}_c\right).$$

Since we switched the the first two indices in χ, we need to switch the last two indices in $U^{s,c}$. The corresponding matrix form of the coupling constants become

$$\tilde{U}_s = \begin{pmatrix} U & 0 & 0 & J_H \\ 0 & U' & J' & 0 \\ 0 & J' & U' & 0 \\ J_H & 0 & 0 & U \end{pmatrix}, \quad \tilde{U}_c = \begin{pmatrix} U & 0 & 0 & 2U' - J_H \\ 0 & -U' + 2J_H & J' & 0 \\ 0 & J' & -U' + 2J_H & 0 \\ 2U' - J_H & 0 & 0 & U \end{pmatrix}$$

We calculate the $(\mathbf{q}, i\nu_n)$-dependant parts of $\tilde{V}_N$ and $\tilde{V}_A$ only here. Since $U_{s,c}^{A,B}$ are symmetric matrices in A, B, $\chi_{A,B}^{s,c}$ are also symmetric matrices, $V_N^{A,B}$ and $V_A^{A,B}$ are therefore symmetric matrices, which means we can calculate and store half of them.

9. Forward Fourier transform $V_{N,A}^{A,B}(\mathbf{q}, i\nu_n)$ to real space for $A \leq B$ and fix the transformed functions

$$V_{N,A}^{A,B}(i_x, i_y, l) = \frac{Te^{i\pi l}}{N^2} \sum_{n_x=0}^{N-1} \sum_{n_y=0}^{N-1} \sum_{n=0}^{N_m-1} e^{-i2\pi\left(\frac{n_x i_x + n_y i_y}{N} + \frac{nl}{N_m}\right)} V_{N,A}^{S;A,B}(n_x, n_y, n).$$

10. Calculate self-energy in real space using

$$\Sigma^{ab}(\mathbf{k}, i\omega_n) = \frac{T}{N} \sum_{\mathbf{q},\nu_n} \sum_{m,n} V_N^{am,bn}(\mathbf{q}, i\nu_n) G_{mn}(\mathbf{k}-\mathbf{q}, i\omega_n - i\nu_n),$$

$$\Phi^{ab}(\mathbf{k}, i\omega_n) = \frac{T}{N} \sum_{\mathbf{q},\nu_n} \sum_{m,n} V_A^{am,nb}(\mathbf{q}, i\nu_n) F_{mn}(\mathbf{k}-\mathbf{q}, i\omega_n - i\nu_n).$$

Notice that we have switched the last two indices in $V_{N,A}$ to accorperate with the change of indices in U and χ. Then in real space

$$\Sigma^{ab}(\mathbf{i}, \tau) = \sum_{m,n} V_N^{am,bn}(\mathbf{i}, \tau) G_{mn}(\mathbf{i}, \tau),$$

$$\Phi^{ab}(\mathbf{i}, \tau) = \sum_{m,n} V_A^{am,nb}(\mathbf{i}, \tau) F_{mn}(\mathbf{i}, \tau).$$

Since $G_{\mathbf{i}}^{ab}(0^+) - G_{\mathbf{i}}^{ab}(0^-) = -\delta_{i_x,0}\delta_{i_y,0}\delta^{ab}$, $F_{\mathbf{i}}^{ab}(0^+) - F_{\mathbf{i}}^{ab}(0^-) = 0$ and $V_{N,A}$ is continuous at $\tau = 0$,

$$\begin{aligned} \Sigma^{ab}(\mathbf{i}, 0^+) &= \sum_{m,n} V_N^{am,bn}(\mathbf{i}, 0^+) G_{mn}(\mathbf{i}, 0^+) \\ \Sigma^{ab}(\mathbf{i}, 0^-) &= \sum_{m,n} V_N^{am,bn}(\mathbf{i}, 0^+) \left[G_{mn}(\mathbf{i}, 0^+) + \delta_{i_x,0}\delta_{i_y,0}\delta_{m,n}\right]. \end{aligned}$$

It follows that

$$\Sigma^{ab}(\mathbf{i}, 0^+) - \Sigma^{ab}(\mathbf{i}, 0^-) = -\delta_{i_x,0}\delta_{i_y,0} V^{ab}$$

where

$$V^{ab} = \sum_m V_N^{am,bm}(\mathbf{0}, 0) = V^{ba}.$$

Clearly $\Sigma^{ab} = \Sigma^{ba}$, Σ is a symmetric matrix as we expected. And it can be checked that $\Phi^{ba} = (\Phi^{ab})^*$, i.e., Φ should be hermitian matrix.

11. Backward Fourier transform $\Sigma^{ab}(\mathbf{i},\tau)$ and $\Phi^{ab}(\mathbf{i},\tau)$ to momentum-frequency space

$$\hat{\Sigma}^{ab}_{n_x,n_y,n} = \sum_{i_x=0}^{N-1}\sum_{i_y=0}^{N-1}\sum_{l=0}^{N_m-1} e^{i2\pi\left(\frac{n_x i_x+n_y i_y}{N}+\frac{nl}{N_m}\right)}\left[e^{i\frac{\pi l}{N_m}}\Sigma^{ab}_{i_x,i_y,l}\right],$$

$$\hat{\Phi}^{ab}_{n_x,n_y,n} = \sum_{i_x=0}^{N-1}\sum_{i_y=0}^{N-1}\sum_{l=0}^{N_m-1} e^{i2\pi\left(\frac{n_x i_x+n_y i_y}{N}+\frac{nl}{N_m}\right)}\left[e^{i\frac{\pi l}{N_m}}\Phi^{ab}_{i_x,i_y,l}\right].$$

and perform aliasing correction and frequency-shuffle

$$\Sigma^{S;ab}_{n_x,n_y,n} = \begin{cases} W_{n-\frac{N_m}{2}}\Delta\hat{\Sigma}^{ab}_{n_x,n_y,n+\frac{N_m}{2}} - V^{ab}R_{n-\frac{N_m}{2}} & 0\le n<\frac{N_m}{2}, \\ W_{n-\frac{N_m}{2}}\Delta\hat{\Sigma}^{ab}_{n_x,n_y,n-\frac{N_m}{2}} - V^{ab}R_{n-\frac{N_m}{2}} & \frac{N_m}{2}\le n\le N_m-1. \end{cases}$$

$$\Phi^{S;ab}_{n_x,n_y,n} = \begin{cases} W_{n-\frac{N_m}{2}}\Delta\hat{\Phi}^{ab}_{n_x,n_y,n+\frac{N_m}{2}} & 0\le n<\frac{N_m}{2}, \\ W_{n-\frac{N_m}{2}}\Delta\hat{\Phi}^{ab}_{n_x,n_y,n-\frac{N_m}{2}} & \frac{N_m}{2}\le n\le N_m-1. \end{cases}$$

Here the aliasing correction is

$$f(\omega_n) = W_n\Delta\sum_{l=0}^{N_m-1} e^{i\omega_n\tau_l}f_l + \left(f(0^+)-f(0^-)\right)R_n$$

with

$$\begin{aligned} W_n &= 2\frac{1-\cos(\omega_n\Delta)}{\omega_n^2\Delta^2}, \\ R_n &= -\frac{1-i\omega_n\Delta-e^{-i\omega_n\Delta}}{\omega_n^2\Delta}, \end{aligned}$$

where $\omega_n=(2n+1)\pi T$ is the fermionic Matsubara frequency.

12. Add the Hartree-Fock terms calculated earlier to the self-energy

$$\begin{aligned} \Sigma^{S;ab}_{n_x,n_y,n} &\to \Sigma^{S;ab}_{n_x,n_y,n}+\Sigma^{ab}_{HF}, \\ \Phi^{S;ab}_{n_x,n_y,n} &\to \Phi^{S;ab}_{n_x,n_y,n}+\Phi^{ab}_{HF}. \end{aligned}$$

Compare them with the old self-energy. If not the same, go to step 3.

BIBLIOGRAPHY

Abanov, A. and Chubukov, A. (1999). A relation between the resonance neutron peak and arpes data in cuprates. *Phys. Rev. Lett.*, 83:1652. 71, 75, 81

Abanov, A., Chubukov, A., and Schmalian, J. (2001). Fingerprints of spin mediated pairing in cuprates. *Journal of Electron Spectroscopy and Related Phenomena*, 117:129. 71, 81

Bao, W., Qiu, Y., Huang, Q., Green, M. A., Zajdel, P., Fitzsimmons, M. R., Zhernenkov, M., Chang, S., Fang, M., Qian, B., Vehstedt, E. K., Yang, J., Pham, H. M., Spinu, L., and Mao, Z. Q. (2009). Tunable $(\delta\pi, \delta\pi)$-type antiferromagnetic order in α-fe(te,se) superconductors. *Phys. Rev. Lett.*, 102:247001. 9

Bardeen, J., Cooper, L. N., and Schrieffer, J. R. (1957). Theory of superconductivity. *Phys. Rev.*, 108:1175. 1, 2

Baym, G. (1962). Self-consistent approximations in many-body systems. *Phys. Rev.*, 127:1391. 13

Baym, G. and Kadanoff, L. P. (1961). Conservation laws and correlation functions. *Phys. Rev.*, 124:287. 13

Bednorz, J. G. and Muller, K. A. (1986). Possible high t_c superconductivity in the ba-la-cu-o system. *Z. Phys. B*, 64:189. 1

Berk, N. F. and Schrieffer, J. R. (1966). Effect of ferromagnetic spin correlations on superconductivity. *Phys. Rev. Lett.*, 17:433–435. 2, 20

Bickers, N. E. and Scalapino, D. J. (1989). Conserving approximations for strongly fluctuating

electron systems. i. formalism and calculational approach. *Annals of Physics*, 193:206–251. 13, 14

Bickers, N. E., Scalapino, D. J., and White, S. R. (1988). Conserving approximations for strongly correlated electron systems: Bethe-salpeter equation and dynamics for the two-dimensional hubbard model. *Physical Review Letters*, 62(8):961–964. 13

Boeri, L., Calandra, M., Mazin, I. I., Dolgov, O. V., and Mauri, F. (2010). Effects of magnetism and doping on the electron-phonon coupling in $BaFe_2As_2$. *Phys. Rev. B*, 82:020506. 11

Boeri, L., Dolgov, O. V., and Golubov, A. A. (2008). Is $LaFeAsO_{1-x}F_x$ an electron-phonon superconductor? *Phys. Rev. Lett.*, 101:026403. 11

Brinkman, W. F., Serene, J. W., and Anderson, P. W. (1974). Spin-fluctuation stabilization of anisotropic superfluid states. *Phys. Rev. A*, 10:2386–2394. 13

Brouet, V., Marsi, M., Mansart, B., Nicolaou, A., Taleb-Ibrahimi, A., Fevre, P. L., Bertran, F., Rullier-Albenque, F., Forget, A., , and Colson, D. (2009). Nesting between hole and electron pockets in $Ba(Fe_{1x}Co_x)_2As_2(x = 00.3)$ observed with angle-resolved photoemission. *Phys. Rev. B*, 80:165115. 7

Canfield, P. C. and Bud'ko, S. L. (2010). Feas-based superconductivity: a case study of the effects of transition metal doping on $BaFe_2As_2$. *Annu. Rev. Condens. Matter Phys.*, 1:27–50. 3, 6

Chen, C.-T., Tsuei, C. C., Ketchen, M., Ren, Z.-A., and Zhao, Z. X. (2010). Integer and half-integer flux-quantum transitions in a niobium-iron pnictide loop. *Nat. Phys.*, 6:260. 10

Cheng, P., Shen, B., Mu, G., Zhu, X., Han, F., Zeng, B., and Wen, H.-H. (2009). High-t_c superconductivity induced by doping rare-earth elements into cafeasf. *Europhys. Lett.*, 85:67003. 3

Chi, S., Schneidewind, A., Zhao, J., Harriger, L. W., Li, L., Luo, Y., Cao, G., Xu, Z., Loewenhaupt, M., Hu, J., and Dai, P. (2009). Inelastic neutron-scattering measurements of a three-

dimensional spin resonance in the feas-based $BaFe_{1.9}Ni_{0.1}As_2$ superconductor. *Phys. Rev. Lett.*, 102:107006. 11

Choi, H. J., Roundy, D., Sun, H., Cohen, M. L., and Louie, S. G. (2001). First-principles calculation of the superconducting transition in MgB_2 within the anisotropic eliashberg formalism. *Phys. Rev. B*, 66:020513(R). 2

Choi, H. J., Roundy, D., Sun, H., Cohen, M. L., and Louie, S. G. (2002). The origin of the anomalous superconducting properties of MgB_2. *Nature*, 418:758. 2

Christianson, A. D., Parshall, D., Stone, M. B., Nagler, S. E., MacDougall, G. J., Mook, H. A., Lokshin, K., Egami, T., Abernathy, D. L., Goremychkin, E. A., Osborn, R., McGuire, M. A., Sefat, A. S., Jin, R., Sales, B. C., and Mandrus, D. (2008). Unconventional superconductivity in $Ba_{0.6}K_{0.4}Fe_2As_2$ from inelastic neutron scattering. *Nature*, 456:930. 11

Chubukov, A. V., Efremov, D. V., and Eremin, I. (2008). Magnetism, superconductivity, and pairing symmetry in iron-based superconductors. *Phys. Rev. B*, 78:134512. 12

Cooper, L. N. (1956). Bound electron pairs in a degenerate fermi gas. *Phys. Rev.*, 104:1189. 1

Daghofer, M., Nicholson, A., Moreo, A., and Dagotto, E. (2010). Three orbital model for the iron-based superconductors. *Phys. Rev. B*, 81:014511. 79

Dagotto, E. (1994). Correlated electrons in high-temperature superconductors. *Rev. Mod. Phys.*, 66:763. 3

de la Cruz, C., Huang, Q., Lynn, J. W., Li, J., II, W. R., Zarestky, J. L., Mook, H. A., Chen, G. F., Luo, J. L., Wang, N. L., and Dai, P. (2008). Magnetic order close to superconductivity in the iron-based layered $LaO_{1-x}F_xFeAs$ systems. *Nature*, 453:899. 8

Diallo, S. O., Pratt, D. K., Fernandes, R. M., Tian, W., Zarestky, J. L., Lumsden, M., Perring, T. G., Broholm, C. L., Ni, N., BudâĂŹko, S. L., Canfield, P. C., Li, H.-F., Vaknin, D., Kreyssig, A., Goldman, A. I., and McQueeney, R. J. (2010). Paramagnetic spin correlations in $CaFe_2As_2$ single crystals. *Phys. Rev. B*, 81:214407. 70

Ding, H., Richard, P., Nakayama, K., Sugawara, K., Arakane, T., Sekiba, Y., Takayama, A., Souma, S., Sato, T., Takahashi, T., Wang, Z., Dai, X., Fang, Z., Chen, G. F., Luo, J. L., and Wang, N. L. (2008). Observation of fermi-surface-dependent nodeless superconducting gaps in $Ba_{0.6}K_{0.4}Fe_2As_2$. *Europhys. Lett.*, 83:47001. 7

Drew, A. J., Niedermayer, C., Baker, P. J., Pratt, F. L., Blundell, S. J., Lancaster, T., Liu, R. H., Wu, G., Chen, X. H., Watanabe, I., Malik, V. K., Dubroka, A., Rossle, M., Kim, K. W., Baines, C., and Bernhard, C. (2009). Coexistence of static magnetism and superconductivity in $SmFeAsO_{1-x}F_x$ as revealed by muon spin rotation. *Nat. Mat.*, 8:310. 6

Eliashberg, G. M. (1960). Interactions between electrons and lattice vibrations in a superconductor. *Sov. Phys. JETP*, 11:696. 1

Eremin, I., Morr, D. K., Chubukov, A. V., Bennemann, K. H., and Norman, M. R. (2005). Novel neutron resonance mode in $d_{x^2-y^2}$-wave superconductors. *Phys. Rev. Lett.*, 94:147001. 78

Eschrig, M. (2006). The effect of collective spin-1 exciation on electronic spectra in high-t_c superconductors. *Adv. Phys.*, 55:47. 71, 75, 81

Fay, D. and Appel, J. (1980). Coexistence of p-state superconductivity and itinerant ferromagnetism. *Phys. Rev. B*, 22:3173–3182. 13

Goko, T., Aczel, A. A., Baggio-Saitovitch, E., Bud'ko, S. L., Canfield, P. C., Carlo, J. P., Chen, G. F., Dai, P., Hamann, A. C., Hu, W. Z., Kageyama, H., Luck, G. M., Luo, J. L., Nachumi, B., Ni, N., Reznik, D., Sanchez-Candela, D. R., Savici, A. T., Sikes, K. J., Wang, N. L., Wiebe, C. R., Williams, T. J., Yamamoto, T., Yu, W., and Uemura, Y. J. (2009). Superconducting state coexisting with a phase-separated static magnetic order in $(Ba, K)Fe_2As_2$, $(Sr, Na)Fe_2As_2$, and $CaFe_2As_2$. *Phys. Rev. B*, 80:024508. 6

Gordon, R. T., Kim, H., Salovich, N., Giannetta, R. W., Fernandes, R. M., Kogan, V. G., Prozorov, T., BudâĂŹko, S. L., Canfield, P. C., Tanatar, M. A., and Prozorov, R. (2010). Doping evolution of the absolute value of the london penetration depth and superfluid density in single crystals of $Ba(Fe_{1x}Co_x)_2As_2$. *Phys. Rev. B*, 82:054507. 9

Grafe, H.-J., Paar, D., Lang, G., Curro, N. J., Behr, G., Werner, J., Hamann-Borrero, J., Hess, C., Leps, N., Klingeler, R., and Buchner, B. (2008). 75as nmr studies of superconducting $LaFeAsO_{0.9}F_{0.1}$. *Phys. Rev. Lett.*, 101:047003. 9

Graser, S., Maier, T. A., Hirschfeld, P. J., and Scalapino, D. J. (2009). Near-degeneracy of several pairing channels in multiorbital models for the fe pnictides. *N. J. Phys.*, 11:025016. 12, 64, 81

Guo, J., Jin, S., Wang, G., Wang, S., Zhu, K., Zhou, T., He, M., and Chen, X. (2010). Superconductivity in the iron selenide $K_xFe_2Se_2$ ($0 \leq x \leq 1.0$). *Phys. Rev. B*, 82:180520(R). 6

Hanaguri, T., Niitaka, S., Kuroki, K., and Takagi, H. (2010). Unconventional s-wave superconductivity in fe(se,te). *Science*, 328:474. 10

Harlingen, D. J. V. (1995). Phase-sensitive tests of the symmetry of the pairing state in the high-temperature superconductors – evidence for $d_{x^2-y^2}$ symmetry. *Rev. Mod. Phys.*, 67:515. 3

Hebel, L. C. and Slichter, C. P. (1959). Nuclear spin relaxation in normal and superconducting aluminum. *Phys. Rev.*, 113:1504. 9

Hicks, C. W., Lippman, T. M., Huber, M. E., Ren, Z.-A., Yang, J., Zhao, Z.-X., and Moler, K. A. (2009). Limits on the superonducting order parameter in $NdFeAsO_{1-x}F_y$ from scanning squid miscroscopy. *J. Phys. Soc. Jpn.*, 78:013708. 10

Hoffman, J. E. (2010). Sign flips and spin fluctuations in iron high-t_c superconductors. *Science*, 328:441. 10

Hu, W. Z., Dong, J., Li, G., Li, Z., Zheng, P., Chen, G. F., Luo, J. L., and Wang, N. L. (2008). Origin of the spin density wave instability in $AFe_2As_2(A = Ba, Sr)$ as revealed by optical spectroscopy. *Phys. Rev. Lett.*, 101:257005. 8

Ishida, K., Nakai, Y., and Hosono, H. (2009). To what extent iron-pnictide new superconductors have been clarified: a progress report. *J. Phys. Soc. Jap.*, 78:062001. 3

Jerome, D. (1994). *Organic conductors*. Dekker, New York. 1, 13

Jerome, D., Mazaud, A., and Ribault, M. (1980). Superconductivity in a synthetic organic conductor $(TMTSF)_2PF_6$. *J. Phys. (Paris) Lett.*, 41:L95. 1, 13

Jiang, S., Xing, H., Xuan, G., Wang, C., Ren, Z., Feng, C., Dai, J., Xu, Z., and Cao, G. (2009). Superconductivity up to 30 k in the vicinity of the quantum critical point in $BaFe_2(As_{1-x}P_x)_2$. *J. Phys.: Condens. Matter*, 21:382203. 6

Johnston, D. C. (2010). The puzzle of high temperature superconductivity in layered iron pnictides and chalcogenides. *Advances in Physics*, 59:803–1061. 3, 11

Kamihara, Y., Watanabe, T., Hirano, M., and Hosono, H. (2008). Iron-based layered superconductor la[of]feas ($x = 0.05 - 0.12$) with $t = 26k$. *J. Am. Chem. Soc.*, 130:3296. 1, 3

Kemper, A. F., Maier, T. A., Graser, S., Cheng, H.-P., Hirschfeld, P. J., and Scalapino, D. J. (2010). Sensitivity of the superconducting state and magnetic susceptibility to key aspects of electronic stucture in ferropnictides. *New J. Phys.*, 12:073030. 64, 79, 81

Khasanov, R., Bendele, M., Amato, A., Babkevich, P., Boothroyd, A. T., Cervellino, A., Conder, K., Gvasaliya, S. N., Keller, H., Klauss, H.-H., Luetkens, H., Pomjakushin, V., Pomjakushina, E., and Roessli, B. (2009). Coexistence of incommensurate magnetism and superconductivity in $Fe_{1+y}Se_xTe_{1-x}$. *Phys. Rev. B*, 80:140511(R). 6

Koitzsch, A., Inosov, D. S., Evtushinsky, D. V., Zabolotnyy, V. B., Kordyuk, A. A., Kondrat, A., Hess, C., Knupfer, M., BÃijchner, B., Sun, G. L., Hinkov, V., Lin, C. T., Varykhalov, A., and Borisenko, S. V. (2009). Temperature and doping-dependent renormalization effects of the low energy electronic structure of $Ba_{1-x}K_xFe_2As_2$ single crystals. *Phys. Rev. Lett.*, 102:167001. 71

Kondo, T., Santander-Syro, A. F., Copie, O., Liu, C., Tillman, M. E., Mun, E. D., Schmalian, J., BudâĂŹko, S. L., Tanatar, M. A., Canfield, P. C., and Kaminski, A. (2008). Momentum dependence of the superconducting gap in $NdFeAsO_{0.9}F_{0.1}$ single crystals measured by angle resolved photoemission spectroscopy. *Phys. Rev. Lett.*, 101:147003. 7

Kortus, J., Mazin, I. I., Belashchenko, K. D., Antropov, V. P., and Boyer, L. L. (2001). Superconductivity of metallic boron in MgB_2. *Phys. Rev. Lett.*, 86:4656. 2

Kuroki, K., Onari, S., Arita, R., Usui, H., Tanaka, Y., Kontani, H., and Aoki, H. (2008). Unconventional pairing originating from the disconnected fermi surfaces of superconducting $LaFeAsO_{1-x}F_x$. *Phys. Rev. Lett*, 101:087004. 6, 12

Kuroki, K., Usui, H., Onari, S., Arita, R., and Aoki, H. (2009). Pnictogen height as a possible switch between high- tc nodeless and low-tc nodal pairings in the iron-based superconductors. *Phys. Rev. B*, 79:224511. 64

Laplace, Y., Bobroff, J., Rullier-Albenque, F., Colson, D., and Forget, A. (2009). Atomic coexistence of superconductivity and incommensurate magnetic order in the pnictide $Ba(Fe_{1-x}Co_x)_2As_2$. *Phys. Rev. B*, 80:140501. 6

Leggett, A. J. (1975). A theoretical description of the new phases of liquid ^{3}he. *Rev. Mod. Phys.*, 47:331–414. 13

Lester, C., Chu, J.-H., Analytis, J. G., Perring, T. G., Fisher, I. R., and Hayden, S. M. (2010). Dispersive spin fluctuations in the nearly optimally doped superconductor $Ba(Fe_{1x}Co_x)_2As_2(x = 0.065)$. *Phys. Rev. B*, 81:064505. 70, 76

Li, H.-F. (2010). Anisotropic and quasipropagating spin excitations in superconducting $Ba(Fe_{0.926}Co_{0.074})_2As_2$. *Phys. Rev. B*, 82:140503(R). 70, 74, 76

Lu, D. H., Yi, M., Mo, S.-K., Erickson, A. S., Analytis, J., Chu, J.-H., Singh, D. J., Hussain, Z., Geballe, T. H., Fisher, I. R., and Shen, Z.-X. (2008). Electronic structure of the iron-based superconductor laofep. *Nature*, 455:81. 7

Luetkens, H., Klauss, H.-H., Kraken, M., Litterst, F. J., Dellmann, T., Klingeler, R., Hess, C., Khasanov, R., Amato, A., Baines, C., Kosmala, M., Schumann, O. J., Braden, M., Hamann-Borrero, J., Leps, N., Kondrat, A., Behr, G., Werner, J., and Buchner, B. (2009). The electronic phase diagram of the $LaO_{1-x}F_xFeAs$ superconductor. *Nat. Mat.*, 8:305. 4

Lumsden, M. D. and Christianson, A. D. (2010). Magnetism in fe-based superconductors. *J. Phys.: Condens. Matter*, 22:203203. 8

Lumsden, M. D., Christianson, A. D., Parshall, D., Stone, M. B., Nagler, S. E., MacDougall, G. J., Mook, H. A., Lokshin, K., Egami, T., Abernathy, D. L., Goremychkin, E. A., Osborn, R., McGuire, M. A., Sefat, A. S., Jin, R., Sales, B. C., and Mandrus, D. (2009). Two-dimensional resonant magnetic excitation in $BaFe_{1.84}Co_{0.16}As_2$. *Phys. Rev. Lett.*, 102:107005. 11, 76

Matan, K., Morinaga, R., Iida, K., and Sato, T. J. (2009). Anisotropic itinerant magnetism and spin fluctuations in $BaFe_2As_2$: A neutron scattering study. *Phys. Rev. B*, 79:054526. 78

Matano, K., Ren, Z. A., Dong, X. L., Sun, L. L., Zhao, Z. X., and Zheng, G. (2008). Spin-singlet superconductivity with multiple gaps in $PrFeAsO_{0.89}F_{0.11}$. *Europhys. Lett.*, 83:57001. 9

Mazin, I. I. (2010). Superconductivity gets an iron boost. *Nature*, 464:183. 3

Mazin, I. I. and Schmalian, J. (2009). Pairing symmetry and pairing state in ferropnictides: theoretical overview. *Physica C*, 469:614. 3, 7

Mazin, I. I., Singh, D. J., Johannes, M. D., and Du, M. H. (2008). Unconventional superconductivity with a sign reversal in the order parameter of $LaFeAsO_{1-x}F_x$. *Phys. Rev. Lett.*, 101:057003. 6, 11

Mermin, N. D. and Wagner, H. (1966). Absence of ferromagnetism or antiferromagnetism in one- or two-dimeansional isotropic heisenberg models. *Phys. Rev. Lett.*, 17:1133. 7

Monthoux, P., Pines, D., and Lonzarich, G. G. (2007). Superconductivity without phonons. *Nature*, 450:1177. 11

Monthoux, P. and Scalapino, D. J. (1994). Self-consistent $d_{x^2-y^2}$ pairing in a two-dimensional hubbard model. *Phys. Rev. Lett.*, 72:1874–1877. 13

Nagamatsu, J., Nakagawa, N., Muranaka, T., Zenitani, Y., and Akimitsu, J. (2001). Superconductivity at 39 k in magnesium diboride. *Nature*, 410:63–64. 1

Nakajima, S. (1973). Paramagnon effect on the bcs transition in ^{3}he. *Prog. Theor. Phys.*, 50:1101–1109. 13

Nelson, K. D., Mao, Z. Q., Maeno, Y., and Liu, Y. (2004). Odd-parity superconductivity in Sr_2RuO_4. *Science*, 306:1151. 2

Ning, F., Ahilan, K., Imai, T., Sefat, A. S., Jin, R., McGuire, M. A., Sales, B. C., and Mandrus, D. (2008). 59co and 75as nmr investigation of electron-doped high tc superconductor $BaFe_{1.8}Co_{0.2}As_2$ (tc=22âĂĽk). *J. Phys. Soc. Jpn*, 77:103705. 9

Ning, F. L., Ahilan, K., Imai, T., Sefat, A. S., McGuire, M. A., Sales, B. C., Mandrus, D., Cheng, P., Shen, B., and Wen, H.-H. (2010). Contrasting spin dynamics between underdoped and overdoped $Ba(Fe_{1-x}Co_x as_2$. *Phys. Rev. Lett.*, 104:037001. 11

Onnes, H. K. (1911). The resistance of pure mercury at helium temperatures. *Commun. Phys. Lab. Univ. Leiden*, 12:120. 1

Paglione, J. and Greene, R. L. (2010). High-temperature superconductivity in iron-based materials. *Nat. Phys.*, 6:645. 3

Pao, C. H. and Bickers, N. E. (1994). Anisotropic superconductivity in the 2d hubbard model: gap function and interaction weight. *Phys. Rev. Lett.*, 72:1870–1873. 13

Park, J. T., Inosov, D. S., Yaresko, A., Graser, S., Sun, D. L., Bourges, P., Sidis, Y., Li, Y., Kim, J.-H., Haug, D., Ivanov, A., Hradil, K., Schneidewind, A., Link, P., Faulhaber, E., Glavatskyy, I., Lin, C. T., Keimer, B., and Hinkov, V. (2010). Symmetry of spin excitation spectra in the tetragonal paramagnetic and superconducting phases of 122-ferropnictides. *Phys. Rev. B*, 82:134503. 74

Pratt, D. K., Tian, W., Kreyssig, A., Zarestky, J. L., Nandi, S., Ni, N., Bud'ko, S. L., Canfield, P. C., Goldman, A. I., and McQueeney, R. J. (2009). Coexistence of competing antiferromagnetic and superconducting phases in the underdoped $Ba(Fe_{0.953}Co_{0.047})_2As_2$ compound using x-ray and neutron scattering techniques. *Phys. Rev. Lett.*, 103:087001. 6

Qiu, Y., Bao, W., Zhao, Y., Broholm, C., Stanev, V., Tesanovic, Z., Gasparovic, Y. C., Chang, S., Hu, J., Qian, B., Fang, M., and Mao, Z. (2009). Spin gap and resonance at the nesting wave vector in superconducting $FeSe_{0.4}Te_{0.6}$. *Phys. Rev. Lett.*, 103:067008. 9, 11

Raghu, S., Qi, X.-L., Liu, C.-X., Scalapino, D. J., and Zhang, S.-C. (2008). Minimal two-band model of the superconducting iron oxypnictides. *Phys. Rev. B*, 77:220503. 64

Ren, Z.-A., Lu, W., Yang, J., Shen, X.-L., Zheng, C., Chen, G.-C., Dong, X.-L., Sun, L.-L., Zhou, F., and Zhao, Z.-X. (2008). Superconductivity at 55 k in iron-based f-doped layered quaternary compound $Sm[O_{1-x}F_x]FeAs$. *Chin. Phys. Lett.*, 25:2215. 3

Richard, P., Sato, T., Nakayama, K., Souma, S., Takahashi, T., Xu, Y.-M., Chen, G. F., Luo, J. L., Wang, N. L., and Ding, H. (2009). Angle-resolved photoemission spectroscopy of the fe-based $Ba_{0.6}K_{0.4}Fe_2As_2$ high temperature superconductor: Evidence for an orbital selective electron-mode coupling. *Phys. Rev. Lett.*, 102:047003. 71, 82

Schrieffer, J. R., Scalapino, D. J., and Wilkins, J. W. (1963). Effective tunneling density of states in superconductors. *Phys. Rev. Lett.*, 10:336. 1

Shamoto, S., Ishikado, M., Christianson, A. D., Lumsden, M. D., Wakimoto, S., Kodama, K., Iyo, A., and Arai, M. (2010). Inelastic neutron scattering study on the resonance mode in an optimally doped superconductor $LaFeAsO_{0.92}F_{0.08}$. *arXiv*, page 1006.4640. 11

Shimizu, Y., Yamada, T., Takami, T., Niitaka, S., Takagi, H., and Itoh, M. (2009). Pressure-induced antiferromagnetic fluctuations in the pnictide superconductor $FeSe_{0.5}Te_{0.5}$: 125te nmr study. *J. Phys. Soc. Jpn*, 78:123709. 9

Shishido, H., Bangura, A. F., Coldea, A. I., Tonegawa, S., Hashimoto, K., Kasahara, S., Rourke, P. M. C., Ikeda, H., Terashima, T., Settai, R., ÅŇnuki, Y., Vignolles, D., Proust, C., Vignolle, B., McCollam, A., Matsuda, Y., Shibauchi, T., and Carrington, A. (2010). Evolution of the fermi surface of $BaFe_2(As_{1x}P_x)_2$ on entering the superconducting dome. *Phys. Rev. Lett.*, 104:057008. 7

Sigrist, M. and Ueda, K. (1991). Phenomenological theory of unconventional superconductivity. *Rev. Mod. Phys.*, 63:239. 3

Singh, D. J. and Du, M.-H. (2008). Density functional study of $LaFeAsO_{1-x}F_x$: A low carrier density superconductor near itinerant magnetism. *Phys. Rev. Lett.*, 100:237003. 6, 7

Sknepnek, R., Samolyuk, G., Lee, Y.-B., and Schmalian, J. (2009). Anisotropy of the pairing gap of feas-based superconductors induced by spin fluctuations. *Phys. Rev. B*, 79:054511. 12, 64

Steglich, F., Aarts, J., Bredl, C. D., Lieke, W., Meschede, D., Franz, W., and Schafer, H. (1979). Superconductivity in the presence of strong pauli paramagnetism: $CeCu_2Si_2$. *Phys. Rev. Lett.*, 43:1892. 1, 13

Strand, J. D., Bahr, D. J., Harlingen, D. J. V., Davis, J. P., Gannon, W. J., and Halperin, W. P. (2010). The transition between real and complex superconducting order parameter phases in UPt_3. *Science*, 328:1368. 2

Takimoto, T., Hotta, T., and Ueda, K. (2004). Strong-coupling theory of superconductivity in a degenerate hubbard model. *Phys. Rev. B*, 69:104504. 13

Terashima, K., Sekiba, Y., Bowen, J. H., Nakayama, K., Kawahara, T., Sato, T., Richard, P., Xu, Y.-M., Li, L. J., Cao, G. H., Xu, Z.-A., Ding, H., and Takahashi, T. (2010). Fermi surface nesting induced strong pairing in iron-based superconductors. *Proc. Natl Acad. Sci. USA*, 106:7330. 7

Tinkham, M. (1996). *Introduction to Superconductivity*. Dover. 9

Wadati, H., Elfimov, I., and Sawatzky, G. A. (2010). Where are the extra d electrons in transition-metal substituted fe pnictides. *arXiv*, page 1003.2663. 84

Wang, C., Li, L., Chi, S., Zhu, Z., Ren, Z., Li, Y., Wang, Y., Lin, X., Luo, Y., Jiang, S., Xu, X., Cao, G., and Xu, Z. (2008). Thorium-doping-induced superconductivity up to 56 k in $Gd_{1-x}Th_xFeAsO$. *Europhys. Lett*, 83:67006. 3

Wang, F. and Lee, D.-H. (2011). The electron-pairing mechanism of iron-based superconductors. *Science*, 332:200. 3

Wang, F., Zhai, H., Ran, Y., Vishwanath, A., and Lee, D.-H. (2009). Functional renormalization-group study of the pairing symmetry and pairing mechanism of the feas-based high-temperature superconductor. *Phys. Rev. Lett.*, 102:047005. 12

Wen, H.-H. and Li, S. (2011). Materials and novel superconductivity in iron pnictide superconductors. *Annu. Rev. Condens. Matter Phys.*, 2:121–140. 3, 6

Wen, J., Xu, G., Xu, Z., Lin, Z., Li, Q., Chen, Y., Chi, S., Gu, G., and Tranquada, J. M. (2010). Effect of magnetic field on the spin resonance in fete0.5se0.5 as seen via inelastic neutron scattering $FeSe_{0.4}Te0.6$. *Phys. Rev. B*, 81:100513. 9, 11

Wray, L., Qian, D., Hsieh, D., Xia, Y., Li, L., Checkelsky, J. G., Pasupathy, A., Gomes, K. K., Parker, C. V., Fedorov, A. V., Chen, G. F., Luo, J. L., Yazdani, A., Ong, N. P., Wang, N. L., and Hasan, M. Z. (2008). Momentum dependence of superconducting gap, strong-coupling dispersion kink, and tightly bound cooper pairs in the high- tc $(Sr, Ba)_{1x}(K, Na)_xFe_2As_2$ superconductors. *Phys. Rev. B*, 78:184508. 71

Xu, Y.-M., Huang, Y.-B., Cui, X.-Y., Razzoli, E., Radovic, M., Shi, M., Chen, G.-F., Zheng, P., Wang, N.-L., Zhang, C.-L., Dai, P.-C., Hu, J.-P., Wang, Z., and Ding, H. (2011). Observation of a ubiquitous three-dimensional superconducting gap function in optimally doped $Ba_{0.6}K_{0.4}Fe_2As_2$. *Nat. Phys.*, 7:198. 11

Yang, F., Zhai, H., Wang, F., and Lee, D.-H. (2011). The electronic instabilities of the iron-based superconductors: A variational monte-carlo study. *Phys. Rev. B*, 83:134502. 12

Yao, Z.-J., Li, J.-X., and Wang, Z. D. (2009). Spin fluctuations, interband coupling, and unconventional pairing in iron-based superconductors. *New J. Phys.*, 11:025009. 12

Yin, Y., Zech, M., Williams, T. L., Wang, X. F., Wu, G., Chen, X. H., and Hoffman, J. E. (2009). Scanning tunneling spectroscopy and vortex imaging in the iron pnictide superconductor $BaFe_{1.8}Co_{0.2}As_2$. *Phys. Rev. Lett.*, 102:097002. 9

Yin, Z. P., Haule, K., and Kotliar, G. (2011). Magnetism and charge dynamics in iron pnictides. *Nat. Phys.*, 7:294. 9

Zeng, B., Mu, G., Luo, H. Q., Xiang, T., Mazin, I. I., Yang, H., Shan, L., Ren, C., Dai, P. C., and Wen, H.-H. (2010). Anisotropic structure of the order parameter in $FeSe_{0.45}Te_{0.55}$ revealed by angle-resolved specific heat. *Nat. Commun.*, 1:112. 10

Zhang, J., Sknepnek, R., Fernandes, R. M., and Schmalian, J. (2009a). Orbital coupling and superconductivity in the iron pnictides. *Phys. Rev. B*, 79:220502(R). 12, 64, 65

Zhang, J., Sknepnek, R., and Schmalian, J. (2010). Spectral analysis for the iron-based superconductors: anisotropic spin fluctuations and fully gapped $s^{\pm}$-wave superconductivity. *Phys. Rev. B*, 82:134527. 12, 64

Zhang, X., Oh, Y. S., Liu, Y., Yan, L., Kim, K. H., Greene, R. L., and Takeuchi, I. (2009b). Observation of the josephson effect in $Pb/Ba_{1-x}K_xFe_2As_2$ single crystal junctions. *Phys. Rev. Lett.*, 102:147002. 10

Zhao, J., Huang, Q., Cruz, C. D., Li, S., Lynn, J. W., Chen, Y., Green, M. A., Chen, G. F., Li, G., Li, Z., Luo, J. L., Wang, N. L., and Dai, P. (2008). Structural and magnetic phase diagram of $CeFeAsO_{1-x}F_x$ and its relation to high-temperature superconductivity. *Nat. Mat.*, 7:953. 6